UiT

THE ARCTIC
UNIVERSITY
OF NORWAY

Faculty of Science and Technology

Department of Geology

Analyses of Paleozoic and Mesozoic brittle fractures in West-Finnmark.

Geometry, kinematics and relations to structures on the Finnmark Platform in the southwestern Barents Sea
—

Espen Bergø
GEO-3900 Master thesis in Geology
June 2016

UNIVERSITY OF TROMSØ

Abstract

This study focuses on Paleozoic and Mesozoic brittle faults and fractures found onshore and offshore in the northwestern areas of Finnmark, the Finnmark Platform, and the southwestern Barents Sea Margin. These structures have been mapped using software for mapping (ArcGIS 10.5 & Petrel 2013) and analyzing fault-fracture lineaments and faults from bathymetry, digital elevation models, satellite images, aerial images, seismic data, and magnetic anomaly data. The main offshore features studied are the Troms Finnmark Fault Complex (TFFC), the Måsøy Fault Complex, Gjesvær Low, southern parts of Nordkapp Basin and the northern parts of Hammerfest basin. These record Mesozoic and Paleozoic faults, offsetting from the Mesozoic to the Precambrian strata. The Hammerfest- and Nordkapp Basins are bounded by NE-SW and NW-SE oriented faults. The onshore areas of the study area comprises Precambrian basement rocks and Caledonian allochthons occurring as a NE-SW trending belt extending from Magerøya in the northeast to the southwest into Troms County. The foliation and basements rocks are visible affected by brittle faults and fractures. Dominant strike directions on northwestern Porsanger Peninsula are NE-SW, NW-SE and E-W, while Magerøy records dominantly E-W. Directions are related to the TFFC directions. These faults and fractures manifest in outcrops, lineaments on aerial photos, DEM and bathymetry. The lineaments can be traced onshore to offshore. The landscape displays lineaments, fjords and sounds localized in high-density fracture zones, or in the core zones of major faults. The landscape indicates that there are several larger faults hidden in western Finnmark. The onshore NE-SW and E-W lineaments, faults and fractures can be compared with the offshore NE-SW to E-W faults. These NE-SW to E-W oriented faults, fractures and lineaments are related to the tensional stress from the opening of the Atlantic Ocean Margin. NW-SE oriented lineaments are presumed to be related to the Trollfjord Komagelv Fault Zone (TKFZ), which resulted in strike-slip to oblique-slip faults. The NW-SE oriented leg of TFFC is seen in the extension of TKFZ, there is debate to whether this is a segment of TKFZ, but the listric geometry of TFFC makes this impossible to figure out, as this might overprint TKFZ if it is there. The Hammerfest Basin and Nordkapp Basin in the southwest Barents Sea and the smaller rhombic pull-apart basins on the strandflat and coastal areas are both bounded by similar trending NE-SW and NW-SE trending faults and lineaments, indicating that these are related. The onshore and offshore data show a high degree of similarity, where the NE-SW to E-W striking faults both offshore and onshore exhibits dip-slip to oblique-slip shear. The NW-SE faults and lineaments with strike-slip to oblique-slip shear are related to the TKFZ.

Acknowledgments

Table of Contents

1 Introduction

1.1 Background and framework for the study

This master's thesis is part of an ongoing research program at the Artic University of Norway (UiT), studying the land-shelf and offshore-onshore tectonic relationship from Lofoten to northwest Finnmark, in order to further understand the Barents Sea margin tectonic evolution (Gernigon, Laurent et al., 2012; Gernigon, L. et al., 2014; Osmundsen et al., 2011). The focus of this thesis is on brittle faults and fractures found onshore and offshore in the North Western part of Finnmark, the Finnmark platform, and the south-western parts of the Barents Sea margin (fig. 1.1) with special emphasis on their role in generating Paleozoic (Devonian-carboniferous) basins. This research project is a part of the Research Centre for Artic Petroleum Exploration, ARCEx, which is a cooperation between UiT, University of Oslo (UiO), Statoil, and Norwegian University of Science and Technology (NTNU) and is a continuation of earlier research at the UiT, Department of Geology (IG), (eg. Indrevær et al. (2014); Indrevær et al. (2013)), focusing on the onshore-offshore tectonics in Lofoten-Vesterålen and western Troms. In order to realize the main objectives of the thesis (chap. 1.2), a high degree of cross subject and interdisciplinary methods and tools were used in order to gather, process and analyze available data. The most important methods used were modern structural field techniques, seismic interpretation, aerial surveys, and geomatic surveys onshore and offshore (chap. 1.8).

1.2 Objectives of the thesis

The main goal of this thesis is to map, describe, and analyze onshore fractures, faults, and lineaments found in the study area in West-Finnmark (fig. 1.1), and to compare these with faults and major basin-boundary faults offshore on the nearby Finnmark Platform and the southwestern parts of the Barents Sea. Structural fieldwork, available bathymetric data, topographic Digital Elevation Models (DEM), selected 2D seismic profiles, and a 3D seismic survey are all used to map structures onshore and offshore and to compare this new data with structures previously described in earlier studies.
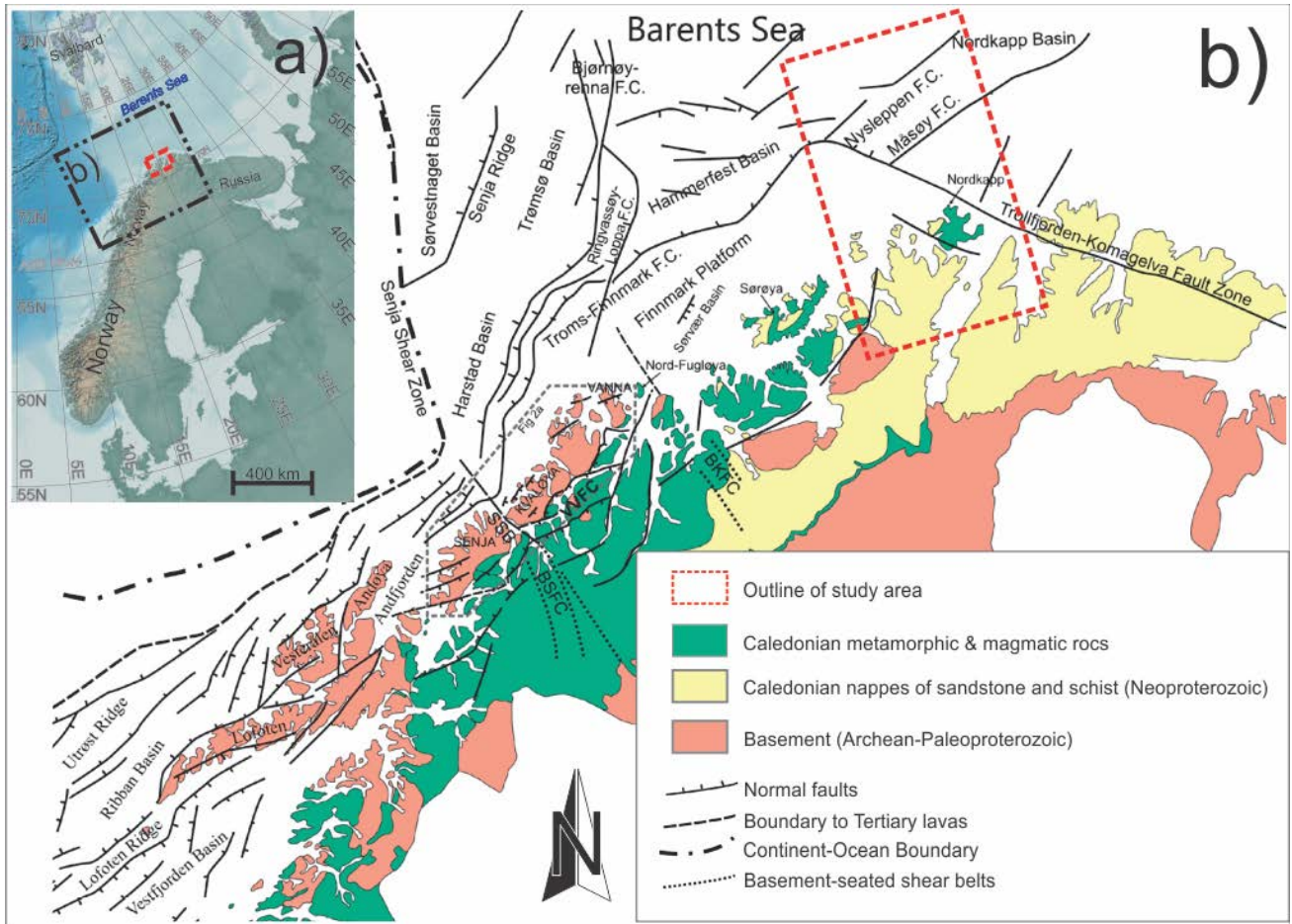
*Fig. 1.1 **a)** Large-scale bathymetric and topographic map of the Artic, the study area is enclosed in dashed* red *square. Modified from Jakobsson et al. (2012) **b)** Regional offshore-onshore tectonic map and setting from Lofoten-Vesterålen to the southwest Barents Sea, study area highlighted with dashed* red *square. Modified from (Indrevær et al., 2013; Jakobsson et al., 2012)*

1.3   Regional geology

1.3.1   Geology of Finnmark

The geology of Finnmark consists of Precambrian basement rocks in tectonic windows in the Caledonides and as autochthonous Neoproterozoic units on the eastern side of the Caledonides. The main Caledonian allochthons occur as a NE-SW trending belt extending from Magerøya in the northeast to the southwest into Troms County (fig. 1.1 & 1.2). The Precambrian basements rocks range in age from Archean to Paleoproterozoic (3.0-1.7 Ga) (Kirkland et al., 2008; Rice, 1990) and represent some of the oldest exposed rocks in Norway (Bryhni et al., 2006). The dominant lithologies are high-grade metamorphic gneisses and granulites, granites and granodiorites, and various meta-volcanic and sedimentary rocks in characteristic greenstone belts (Bryhni et al., 2006; Ramsay et al., 1985; Roberts, R. et al., 2010).
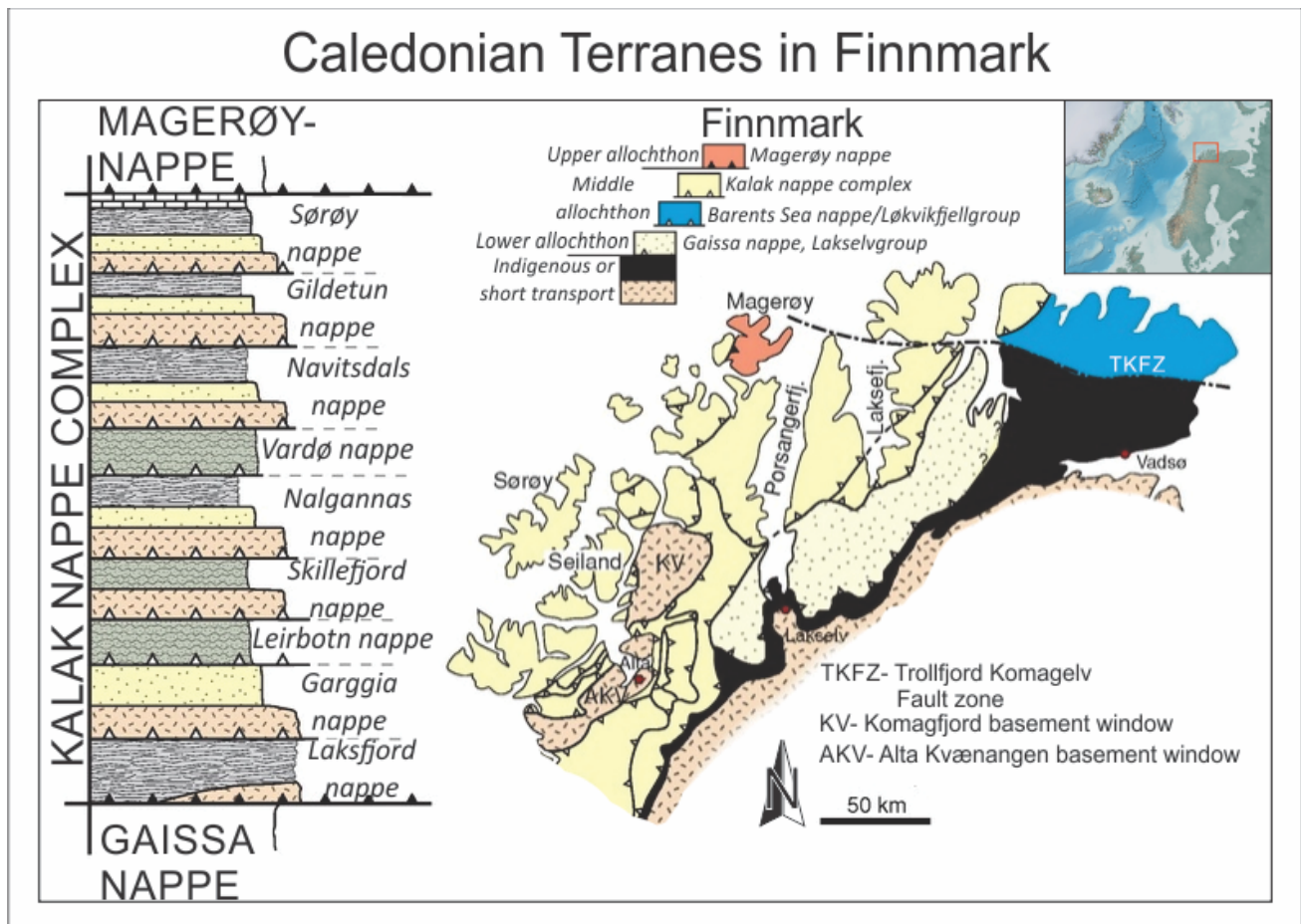
Fig. 1.2 Caledonian terranes in Finnmark, as well as the buildup of the Kalak nappe complex, modified from (Bryhni et al. 2006)

Introduction

The Caledonian allochthons of Finnmark define a sequence of metasedimentary rocks that were thrusted on top of the autochthonous Neoproterozoic cover rocks and the pre-Caledonian basement. The most widespread allocthonous unit in Finnmark is the Middle Nappe sequence, termed the Kalak Nappe Complex (KNC) (fig. 1.2). Comprising internal slivers of the Precambrian bedrock (Rice, 1990), overlying Neoproterozoic (1030 -730 Ma) meta-sedimentary rocks (Kirkland et al., 2008; Ramsay et al., 1985; Sturt et al., 1978) as well as a collection of Neoproterozoic (570-560 Ma) plutons belonging to the Seiland province (Gernigon, L. et al., 2014; Ramsay et al., 1985; Roberts, R. et al., 2010; Sundvoll et al., 2003).

The Caledonian nappes consist of quartz-feldspar gneisses, schists, meta-sandstone, quartzites, amphibolites, and marbles with a general NE-SW strike and NW dip of the main foliation. The type area for these rocks is located on Sørøya (the Sørøy-sequence), where a classical stratigraphy was established by (Ramsay et al., 1985). Today the sequence is interpreted as multiple thrust-sheets of metasedimentary rocks of differing Neoproterozoic ages, as well as 980-600 Ma felsic and mafic plutonic intrusions (Kirkland et al., 2008; Roberts, R. et al., 2010). The magmatic rocks of the Sørøya sequence and the Seiland-province are more massive and have locally well-developed foliation (Sturt et al., 1975), which enables important identification of younger brittle fractures and fracture zones. Magerøy, the northernmost island in Finnmark, contains rocks belonging to the upper allochthon (Magerøy Nappe) consisting of low-metamorphic shales, sandstones and conglomerates, similar to those found in the Lyngen Nappe in Troms. In addition, Magerøy nappe record intrusive complex of Silurian age (Andersen, 1981), as well as Carboniferous mafic intrusive dykes (Magerøy dykes) (Lippard et al., 1997; Roberts, D. et al., 1991).

1.3.2   Study area

The study area is located along the SW Barents Sea margin (fig. 1.1 & 1.3) and includes: (1) the Porsanger Peninsula and Magerøya onshore, (2) the shallow shelf (strandflat) areas off the nearby coast, and (3) the offshore areas of the Finnmark Platform (fig. 1.3), adjacent boundary faults (Troms-Finnmark Fault Complex) and basins to the northwest (Hammerfest and Nordkapp Basins). Where Magerøy mostly consists of the Magerøy nappe, the northwestern areas of Magerøy record lithologies from the KNC. Northwest Porsanger Peninsula comprises rocks from the KNC. The geology of these areas will be described successively in chapter 3.
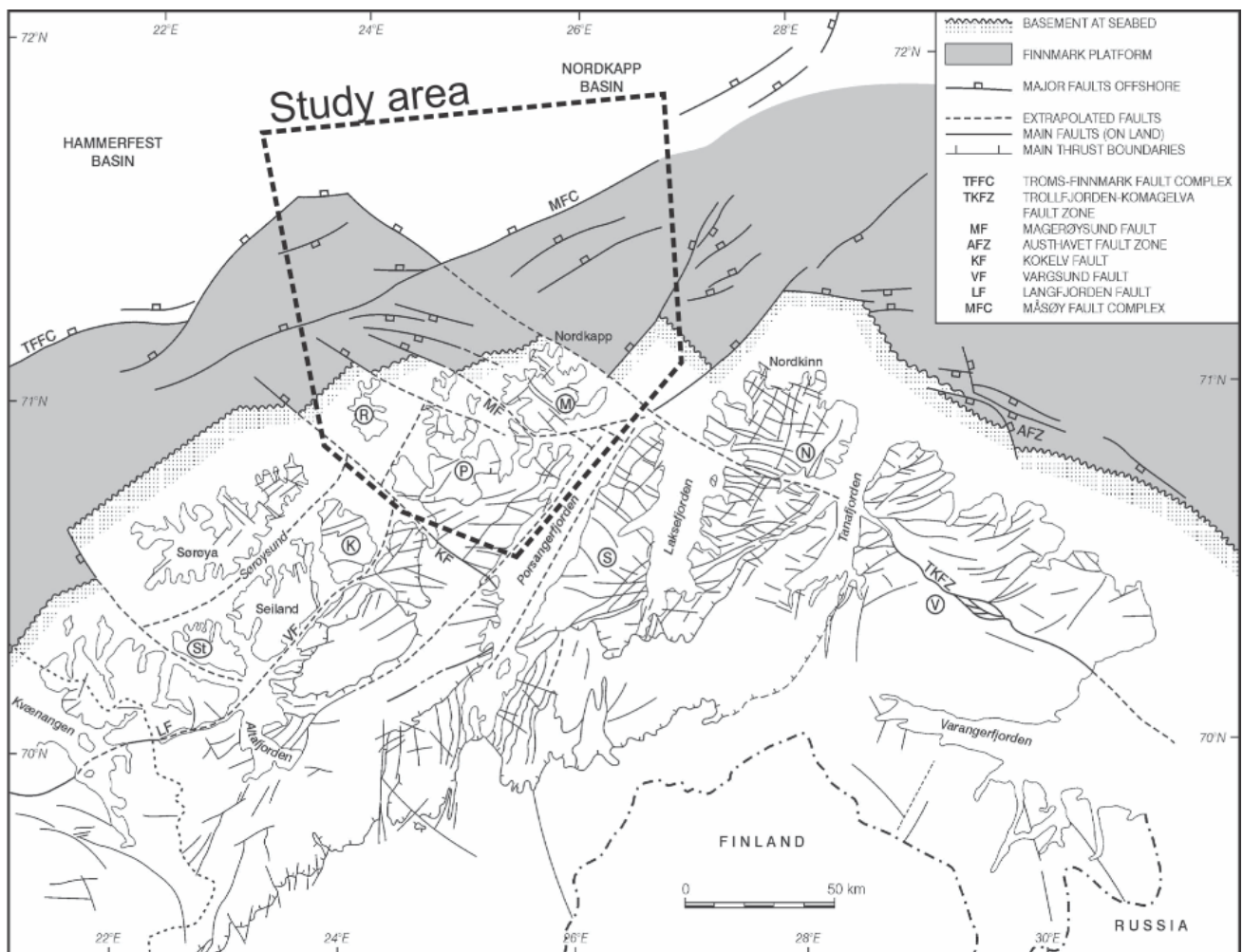
Fig. 1.3, Regional structural map of Northwest Finnmark and the southwestern Barents Sea, from Roberts, D. et al. (2005).

1.3.3   The Barents Sea margin offshore western Finnmark and margin evolution

The southwestern Barents Sea margin offshore western Finnmark was subjected to multiple periods of rifting during the Paleozoic and Mesozoic; these rifting episodes have been linked to the break-up of Pangea (Indrevær et al., 2013). The evolution resulted in different strain regimes that influenced the formation of the basins and the general shape of the Barents Sea. The larger Cretaceous basins found on the Norwegian shelf and Barents Sea are linked to a Jurassic-Early Cretaceous rifting event (Faleide et al., 2008). The sedimentary cycles in the SW Barents Sea since the Late Devonian (Larssen et al., 2002). Rifting and basin creation in SW Barents Sea reflects tectonism since the Jurassic. The most notable rift structures in the west SW Barents Sea are the mid-Cretaceous rift basins and fault zones. These are some of the deepest basins found on Earth (Skogseid et al., 2000) (Skogseid et al., 2000), and contain sedimentary deposits ranging in age from upper Devonian to Eocene-Oligocene in the upper strata of the basins (Larssen et al., 2002).

The Hammerfest basin is located north of Hammerfest/Sørøya, in the SW Barents Sea. As a wide E-W trending basin it is bounded by the Finnmark Platform/TFFC to the south, the Loppa High and the Bjarmeland Platform to the north and the Ringvassøy/Loppa FC to the west (fig 1.1) (Indrevær et al., 2013). This basin was most likely formed in the Early Carboniferous, with the main subsidence occuring during the Triassic and the Early Cretaceous (Gabrielsen et al., 1990). To the northwest, the basin merges via the Nysleppen Fault Complex (NFC) into the Nordkapp Basin. There is no evidence of Paleoproterozoic evaporites or subsequent diapirism in the Hammerfest Basin as there is in other basins found in the SW Barents Sea, including the Nordkapp Basin. The internal structure of the basin is characterized by a complex pattern of faults dominantly striking W-E and WNW-ESE, reflecting Late Jurassic tectonism (Gabrielsen et al., 1990).

The Nordkapp Basin is located to the north of Magerøy and is a narrow, NE-SW trending sub-basin 150 km long and 25-50 km wide (fig. 1.1 & 1.3). The basin is bounded by several NE-SW and NW-SE striking and NW- and SE dipping major normal faults complexes, such as the Nysleppen Fault complex (NFC) and the Måsøy Fault Complex (MFC) (Smelror et al., 2009). These fault complexes become narrower and merge into the Hammerfest Basin in the southwest, making a rhombic-shaped basin geometry. The basin record a sedimentary buildup of Carboniferous through Cenozoic strata, and these strata are heavily affected by salt-doming located along the basin's axis (fig. 1.1) (Koyi et al., 1993).

1.3.4   Post-Caledonian faults of Western Finnmark

Figs. 1.1 and 1.3 illustrate the major and regional faults along the mid-Norwegian shelf that continue northward to the southwest Barents Sea shelf area, including the study onshore-offshore area. Some of the major faults illustrated in these figures can be traced into the study area, where the most important features are the TFFC, TKFZ, MFC and the NFC, where the TFFC, MCF and NFC follow the same NE-SW strike, as opposed to the TKFZ, which strikes NW-SE. Caused by different tectonic events (Gabrielsen et al., 2002). The NE-SW striking faults may have formed synchronous with the early stages of rifting of the North-Atlantic margin in the Carboniferous (Smelror et al., 2009), and subsequent tectonism. The TKFZ, however, is a Neoproterozoic (Vendian) to Early Ordovician dextral strike-slip fault (Gabrielsen et al., 1990; Herrevold et al., 2009; Johnson et al., 1978; Roberts, D. et al., 2005), that has multiple reactivations during post-Caledonian times and possibly also in the Early Carboniferous (Beckinsale et al., 1976).

Brittle faults-fracture lineaments are visible on aerial images and in the Digital Elevation Model (DEM) in the areas from Fugløya in the south, through Loppa/Øksfjordhalvøya, Sørøya, the Porsanger Peninsula and to Magerøy in the north (fig. 1.2). These structures are assumed to be of Mesozoic to Cenozoic age and tie the rifting and creation to Paleozoic-Mesozoic basins in the Barents Sea (Faleide et al., 2008; Gabrielsen et al., 2002; Gabrielsen et al., 1990; Smelror et al., 2009).

Onshore and offshore Lofoten, Vesterålen and western Troms (fig. 1.2) structures have a characteristic rhombic pattern, with NNE-SSE and NE-SW trends that are parallel to the Ribban-, Harstad- and Tromsø-Basins (Bergh et al., 2007; Eig et al., 2011). Further north, in the SW Barents Sea, these trends can be traced along the TFFC, which limits the Hammerfest Basin from the Finnmark Platform, including the Sørvær-Basin (fig. 1.1). There is also a dominant NW-SE trend, parallel with assumed transfer zones, e.g. the Fugløya transfer zone (Indrevær et al., 2013) and Trollfjord-Komagelv fault zone (TKFZ). Together with the NE-SW trending segments, the margin creates a regional stepping pattern and a rhombic fault pattern (Johansen et al., 1994), especially in the areas between Sørøya and Magerøya (fig. 1.1).

1.3.5   Quaternary geology of western Finnmark and the Finnmark Platform

During the last Ice Age vast masses of sediments were transported and deposited along the Norwegian coast (Winsborrow et al., 2010) by a continental ice-sheet that covered northwest Finnmark and the SW Barents Sea from the interior of the continent to the shelf break during the Weichselian (Vorren et al., 1978). As the ice sheet advanced to and persisted at its maximum position, sediments and bedrock blocks were eroded and redeposited elsewhere, creating the fjords, cross-shelf troughs glacial landforms and sedimentary deposits we associate today with coastal Northern Norway (Winsborrow et al., 2010). Offshore in the southwestern Barents Sea, some of the prominent features associated with this period of increased glacial activity are the Upper Regional Unconformity (URU), which reflects the lowermost surface of glacial erosion and the beginning of glacial deposits and tectonism (Andreassen et al., 2008). From the shelf break and passive margin to the onshore areas of the study area, the submarine landscape in the study area includes the same deep fjords, rocky outcrops, strandflat, glacial moraines, beaches and other marine deposits that can be found onshore along most of the Norwegian coastline (Faleide et al., 2008). The overall geomorphology of the seafloor is influenced by glacial activity, and the glacial deposits and erosional patterns result in landforms that record the directions of past ice flow. Abrasion, scouring and plucking of large pieces of the bedrock are the most common methods by which material is removed during glacial erosion (Nichols, 2009).

1.3.6   Strandflat and near-costal submarine geomorphology

The strandflat along the Norwegian coast were first described by Hans Reusch (1894). His description was followed closely by other geologists and scientists with who questioned his proposed origin of the strandflat (Hans, 1924; Nansen, 1922). Presently, a common consensus is that Norwegian coastal strandflat are the result of the Quaternary re-excavation of pre-Cretaceous weathered plains, as easily erodible pre-weathered bedrock is removed by frost-weathering, wave abrasion and sea-ice erosion (Holtedahl, 1998; Nansen, 1922; Olesen, Odleiv et al., 2013; Reusch, 1894). Recently, the strandflat have garnered attention from structural geologists hoping to use them in interpretations of structural features, e.g. tectonic lineaments; bedding, faults and fractures. The strandflat fill the "geologic gaps" between onshore and offshore geology mapped from seismic data and exploration wells. High resolution bathymetric data is used to map lineaments and extend lithology from onshore localities (Indrevær et al., 2014). In the study area (fig. 1.1), the strandflat are extension of onshore landforms, reaching out towards the Finnmark platform.

2 Methods

Fieldwork for this thesis was carried out in June to August 2015. The results of this fieldwork have been combined with observations and interpretations from remote sensing and interpretation of seismic data. The data have been collected and interpreted with the aim of enabling the comparison of structural data collected from various sources. However, due to the nature, specifically the spatial resolution, of some of the remotely sensed data, there is some uncertainty in accuracy and detail.

Due to limited access sections of the study area were not available for field observations. In these cases the landscape's macro-scale structural features were mapped from the interpretation of remote sensing data, satellite images and aerial photographs. A suite of software programs was used to process this data: CorrelDRAW X6, were used to make and modify figures, ArcMAP 10.5 (ESRI) were used to compile maps of DEM, bathymetry and aerial images. Global Mapper 17, where used for bathymetric and magnetic anomaly data. Petrel 2013 (Schlumberger) were used for seismic interpretation, and Orient 3.4 (Vollmer, 2015) was employed to create stereo plots and rose plots.

2.1 Field work

The study area has very low vegetation cover and excellent exposed rock and road-cuts give a good opportunity for good quality fieldwork. The focus during the fieldwork was to collect structural data, in the form of strike, dip and slicken lineament orientations. This data was collected using a Suunto compass, and every measurement site was located with a GPS as well as on topographic maps and aerial images for to ensure proper placement of data points. The structural data will be presented later in chapter 3.

2.2 Data analysis of DEM, bathymetry and aerial images

Aerial photographs have long been used to obtain overviews of landscapes, and as tools in interpreting geological features. Digital Elevation Models (DEM) created from point clouds of remotely sensed elevation data are a newer tool geologists are starting to use in geological and geomorphological studies (Indrevær et al., 2014).

Multiple computer geoscientific software packages were used to process the great variety of data in this study. The analysis of DEM, bathymetry and aerial images were undertaken using the ESRI ArcGIS software

suite. The software gives a possibility to create a streamlined workflow that can handle all the different tasks and multiple file systems involved in interpreting DEM, aerial images, satellite images and bathymetric surveys, as well as in the production of maps and figures. By using ArcMap 10.5, (one component of the ESRI ArcGIS software suite), the DEM data from Statens Kartverk (The Norwegian Mapping Authority) was converted from a raster-file to a more suitable format for integration with the bathymetry files' format. This allows for creation of a complete topographic model of the study area incorporating both marine and terrestrial data. ArcGIS was also used to create a combined DEM and bathymetric model of the available data. This model was exported to Petrel 2013 and is used in the visualization of the study area (e.g. fig. 3.1). It also enabled the mapping of lineaments from onshore to offshore in the same topographic model.

The incorporation of seismic data in this thesis has been important, since 2D and 3D seismic data give the possibility to map and model geological structures in non-exposed rock. However, there are no seismic surveys in close proximity to terrestrial ("onshore") portion of the study area - covering strandflat or the shoreline - thus leaving a gap in the data. In these areas extrapolation of lineaments found on bathymetric and terrestrial data are important for tie-in of the seismic sections.

2.2.1   Lineament interpretation

A lineament is a linear feature that is continuous, reasonably well expressed (having discernible end points, width, and azimuth) and that is able to be related to subsurface features (Gabrielsen et al., 2014; O'leary et al., 1976). The lineaments studied in this thesis are faults, fractures and joint lineaments that are a result of tectonic activity, where these cut the lithology and are not signs of intrusions or lithological boundaries. Lineaments are a result of zones/linear features where the rock is weaker than the surrounding bedrock (fig. 2.1), leading to a preferential weathering and erosion. During the interpretation of aerial images, DEM, bathymetric and satellite images, this theory has been applied.
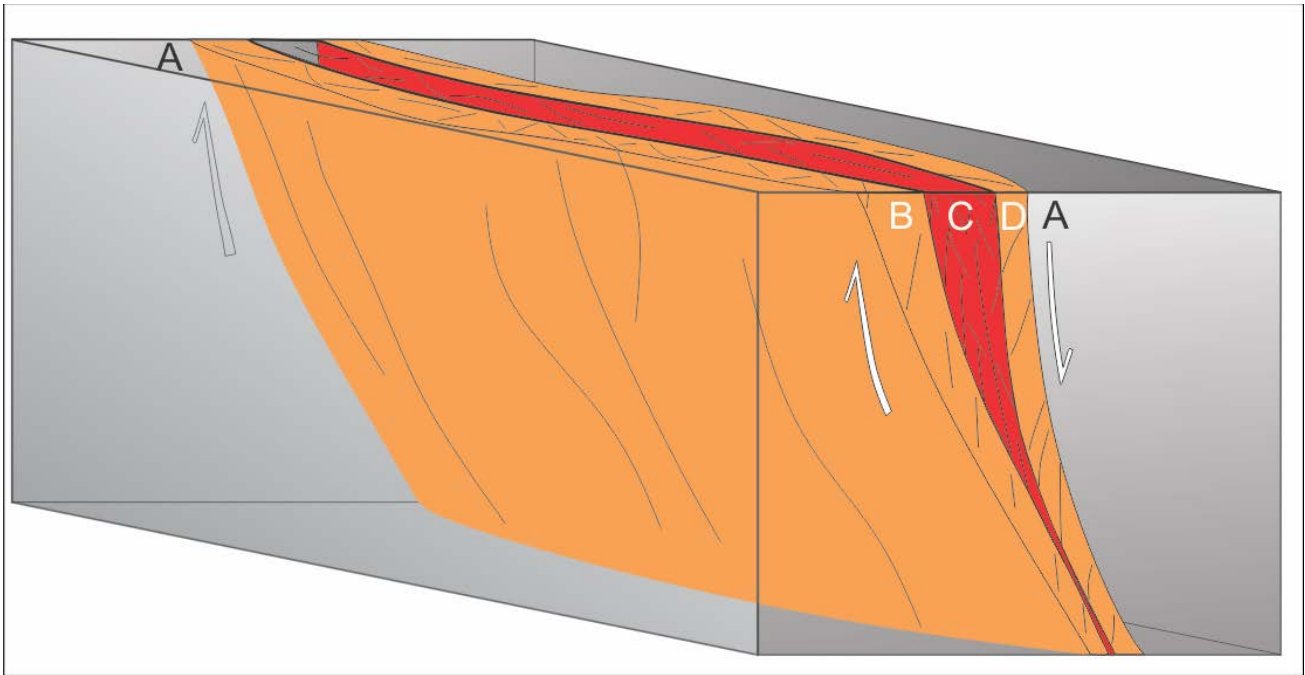
*Fig. 2.1, 3D sketch of a normal fault. **A)** Non-fractured host rock. **B)** Damage zone, consisting of fractured to heavily fractured host rock. **C)** Fault core, comprising fault rocks, e.g. fault gouge and/or cataclasite. The fault zone is a zone of weakness, and is preferentially weathered. Model based on theory from (Gabrielsen et al., 2014; O'leary et al., 1976).*

In ArcMAP 10.3, a Geographic Gnformation System (GIS), one can draw geospatial lines, allowing calculations of the azimuth (strike) of lineaments for further analysis. The following method is used to interpret lineaments in ArcMAP (fig 2.2): 1) Locate and zoom into the area studied, 2) Interpret lineaments on DEM, 3) Use aerial images to increase the accuracy by including colors and vegetation, 4) Interpret lineaments, herein shown as purple lines.

To increase the resolution of interpretation, DEM and aerial images where used as detailed maps of areas of interest especially where topography or the DEM showed signs of higher fracture rates. Most of the DEM interpretation were backed up with interpretation of aerial images, as the DEM models occasionally do not have sufficient spatial resolution to map all lineaments. The aerial images also contain geo-relevant information, as preferential weathering, biological growth, and linear depressions often appears on aerial images but not in the DEM. The reason is that DEM only records the elevation data, and not color variance.
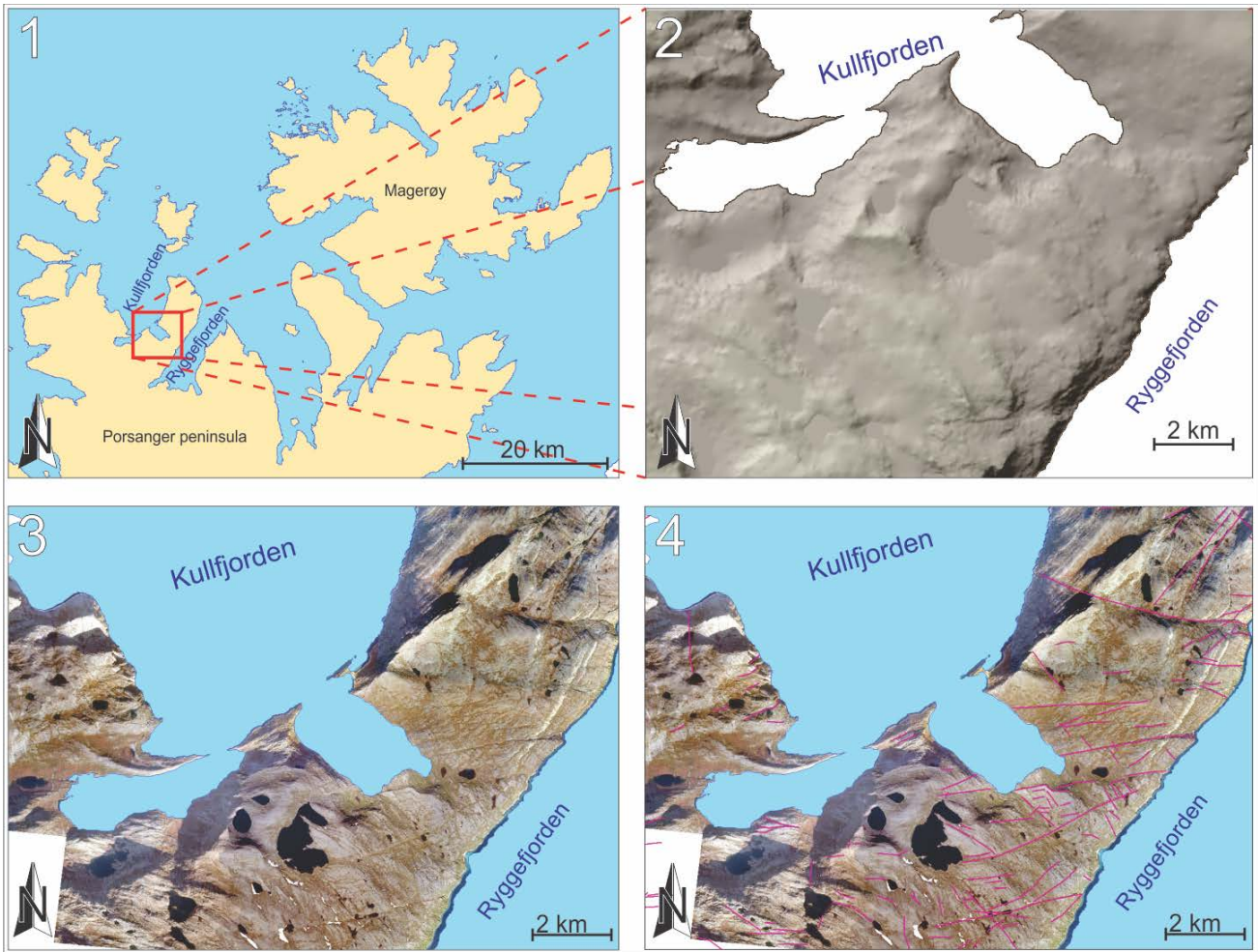
Fig. 2.2 Lineament interpretation method: 1) Large scale map of study area. 2) Zoom in of DEM with a hill-shade surface. 3) Overlay of aerial image. Note the increase in detail such as linear green features, bedrock color and scree 4) interpreted lineaments shown as purple lines.

By using "attribute calculation" in ArcMap the azimuth (trend) of interpreted lineaments can be calculated. Using the geospatial information of lines; the length and the UTM coordinates at the endpoints of the lines, the trend of the lines can be automatically calculated by ArcMap software. The coding language Python was used to implement the mathematical formula (Equation 1) for calculating the trend (App. 1).

Equation 1, Simplified mathematic formula for calculating the azimuth from ends of a line.

$$\Delta x = (North\ coordinate\ of\ start\ of\ line) - (North\ coordinate\ of\ end\ of\ line)$$
$$\Delta y = (South\ coordinate\ of\ start\ of\ line) - (South\ coordinate\ of\ end\ of\ line)$$
$$\arctan\left(\frac{|\Delta x|}{|\Delta y|}\right) = azimuth$$

2.2.2   Bathymetric Data

Since the beginning of naval transport, charts were made for navigation and to avoid hazards and shallow areas. In the early days of naval mapping crude methods where used: an end weighted rope with knots to was used to measure depth, originating the term "*fathoms*". Today the seabed is mapped by acoustic imaging (sonar). A soundwave is sent from a vessel, reflected off the seafloor, and recorded by a hydrophone. Taking into account the velocity of sound in water (varies with temperature, salinity etc.) the depth can be calculated. During high-resolution bathymetric mapping, multi-beam sonars is used, where multiple directional hydrophones are applied to gather a higher resolution of the seafloor.

The bathymetric data used in this thesis were gathered by the Mareano 2004 survey (http://www.mareano.no/), with a resolution of 25x25 m. To interpret the bathymetric data ArcMap 10.3, Petrel 2014 and Global Mapper 17 where used to process bathymetric data from the Mariano survey. The resolution for this data is 25x25 m which makes the geological features of the seafloor easy to observe and interpret. Since the focus of this thesis is on faults and fault-fracture lineaments, most geomorphological features of glacial and sedimentary origin are of little interest. To accommodate for this, select areas have been studied, as the strandflat, exposing parts of crystalline bedrock. As the seafloor has a great diversity in geomorphology and sediments, some features from the glacial activity in northern Finnmark might obscure the view.

As a basis for the analysis of bathymetric lineaments, the process involving interpretation of the bathymetry has been two-fold. Bathymetric lineaments have been interpreted in ArcGIS, where lines have been drawn and calculating the azimuth (trend), using the code in shown in Appendix 1. This has been the basis for interpretation of the azimuth (trend) distribution of interpreted fault-fracture lineaments and for further analysis and interpretation.

2.3   Seismic data

Both 2D and 3D seismic surveys were used to interpret the offshore section of the study area. The 2D seismic profiles cover the coastal area between the DEM model and the 3D seismic survey. Seismic data is an acoustic representation of the subsurface enabling the interpretation of, amongst other things, structural geological features such as strata and faults. The 2D seismic survey consists of single lines shot in an grid, giving a limited lateral resolution caused by line separation distance, where as a 3D seismic survey is shot

with multiple simultaneous lines and gives a denser grid geometry with a much better lateral resolution compared to 2D seismic data.

2D and the 3D seismic data covering the SW Barents Sea have been used to map brittle Mesozoic fractures in the study area (fig. 1.1 & 1.3). Seismic data is used in the oil and gas industry as well in academic studies to map and interpret subsurface geological features. Offshore seismic surveys, both 2D and 3D, are gathered by specialized vessels, that tow seismic arrays consisting of a sound-source and a single streamer for 2D seismic surveys, and multiple streamers for 3D seismic surveys (Veeken, 2006). Streamers consists of an array of geophones inside a flexible tube. These geophones record the signal strength, arrival time and position of reflected sound-waves sent by the sound-source (Andreassen, 2009). Due to the nature of sound traveling through different mediums, part of the energy of a sound-wave is reflected when the soundwave passes through a boundary where the sound velocity and/or material density changes. This boundary is often referred to as an interface, and often represents one of the following four situations (Veeken, 2006):

- Sedimentary reflections, represents bedding planes
- Unconformities; discontinuities in the geological record (e.g. erosional surfaces)
- Artefacts; e.g. multiples, diffractions etc.
- Non sedimentary reflections; fault surfaces, fluid contacts, salt diapir etc.

Based on the different arrival times of sound waves reflected from the subsurface reflectors, the acoustic impedance of the subsurface can be determined. The determined impedance can be used to deduce the medium i.e. rock or sediment types the soundwave has traveled through. The signal created as the wave travels through different types of material can also be influenced by the pore fluid, e.g. water, gas, oil etc. (Andreassen, 2009; Veeken, 2006). Artefacts are a phenomena visible in seismic profiles that are a result of data acquisition or processing methods that do not reflect changes the geology of the system, and can complicate the interpretation of seismic sections and the establishment of direct linkages between the seismic section and the geological profile. The origin for these artefacts can be from multiple sources, manmade, biological and geological reflections, where the sound wave can be bounced/reflected between multiple reflectors, before it arrives at the geophone. This makes it somewhat difficult to make a direct link between the seismic section and a true geological profile (Badley, 1985). However, this is not an accurate representation of a true cross-section of the subsurface earth, as there are some limitation to the vertical and horizontal resolution of seismic study.

The data collected is mathematically processed to remove artefacts for further interpretation. The process/method for processing seismic data is under constant development and the processing techniques are constantly improving, enabling better representations of the subsurface. Newer processing techniques can also be used to reprocess old seismic data, in order to improve the quality and recover details that may previously have been obscured (Andreassen, 2009).

The seismic data interpreted in this thesis originates from the Petrel-ready database from NTNU and Schlumberger. Both 2D and 3D data is migrated and zero-crossing seismic data. The interpretation of the seismic data is performed using the software Petrel 2013 developed by Schulmberger. The surveys in the database cover large areas of the SW Barents Sea, as well as most of the offshore area in the study area. The coverage grid of the 2D seismic lines consists of multiple surveys. Three different surveys have been interpreted and mapped in the area. The coverage grid of the 2D seismic lines consists of multiple surveys, spaced 10 km apart.

Since the study area contains the transition from continental margin to deeper sea, the undifferentiated and crystalline basement is prevalent in the seismic sections. However, due to the large acoustic impedance the basement reflector is often distorted and difficult to pick in the shallow areas. Often, there are multiples below, making the basement difficult to interpret.

2.4   Magnetic anomaly data

Most of Norway, both onshore and offshore, is covered by magnetometric surveys. In this thesis, magnetometric data is used to support and correlate the onshore-to-offshore transition of the interpreted fault-fracture lineaments. Magnetic anomalies are caused by the magnetic susceptibility of the rock or material and the variations in the local magnetic field from the total magnetic field of the earth. These anomalies are results of magnetic minerals found in the bedrock, sediments and intrusive rocks, that affects the total magnetic field and shows up as anomalies (Reynolds, 2011). The data used is the regional magnetic anomaly map produced by the Norwegian Geological Survey (NGU updated 2014, www.ngu.no), where fractures, faults or magmatic dykes that contain magnetic minerals (e.g., Titanite, Magnetite and Phyrrhotite (Robb, 2013)) show up as linear magnetic anomalies, and are of interest as these can indicate fractures and faults (Olesen, O et al., 2007; Reynolds, 2011).

2.5   Definitions and Abbreviations

To accommodate for varying terminology used in scientific literature, this section introduces the terms and abbreviations used in this thesis, as it is important to avoid ambiguity and misconceptions surrounding some terms used differently by different authors.

Table 1: Terms used in this thesis

Term:	Definition:
Accommodation Zone	A zone where local faulting and/or folding develops to accommodate space problems during the development of a larger structure. (Neuendorf, 2005)
Anastomosing	Branching pattern/geometry, where several features terminates in feature. E.g. Branches of a tree.
Antithetic fault	Secondary fault to a larger fault, dipping in opposite direction of the main fault.
Cataclasite	Fine grained, cohesive cataclastic rock, formed during fault movement.
Cataclastic rock	Chotic fault rock that developed with cohesion, mainly generated by frictional flow (Braathen et al., 2004)
Dip-slip fault	A normal fault on which the movement is parallell to the dip
En echelon	Geological features that are in an overlapping or staggering arrangement, where they collectively form a linear zone, where the individual features are oblique to this zone (Neuendorf, 2005)
Fault gouge	Soft, unscemented pulverized clayey or claylike mineral, commonly a mixture of fine-grained minerals in finely divided form, found along some faults or fault zones. (Neuendorf, 2005)
Fault rock(s)	One of several rock types physically associated with fault surfaces and genetically linked to fault movement (Neuendorf, 2005)
Geospatial data	Data or features with specific information about the orientation of the object in the real world. E.g. lines with UTM coordinates and/or orientation data
Lineaments	In this thesis context, describes linear feature interpreted from remote sensing, assumed to be related to fault/fractures
Listric fault	A curved downward-flattening faults that are downwards flattening (Neuendorf, 2005)
Oblique slip- fault	A fault on which the movement is intermediate in orientation between dip slip and strike-slip
Remote sensing	Information gathered by a recording devise not in physical contact with the medium studied, e.g. Aerial photos, satellite images. (Neuendorf, 2005)
Salt weathering	The granular disintegration or fragmentation of rock material effected by saline solutions or by salt-crystal growth (Wellman & Wilson, 1965)
Strandflat	A rim of gently sloping bedrock plain in front of higher

Methods

Table 2, Abbreviations used in this thesis:

DEM	Digital elevation model
GL	Gjesvær Low
GPS	Global positioning system
GIS	Geographic Information System
MFC	Måsøy Fault complex
TFFC	Troms Finnmark Fault complex
TKFZ	Trollfjord Komagelv Fault Zone
KNC	Kalak Nappe Complex
HB	Hammerfest Basin
NB	Nordkapp Basin

3   Description of onshore lineaments, brittle fractures and faults

3.1   Introduction

The study onshore areas of northwest Porsanger Peninsula, Magerøy and the islands towards the Finnmark platform (fig. 3.1) all comprise brittle faults and fractures with varying azimuth (trend) and crosscutting relationship (fig. 3.1). The pattern observed is a part of a major NE-SW and E-W striking fault-fracture and topographic lineament pattern distributed throughout the study area. Brittle fractures, faults, and lineaments are widespread and easily recorded on both on aerial images, and in outcrops. However, some areas inland on Porsanger Peninsula and Magerøy are covered by talus, scree, and vegetation obscuring the brittle faults, joints, and lineaments. In aerial images, the lineaments either are outlined as erosional or landscape features, or as narrow lineaments in the bedrock, leaving a depression/escarpment in the area that crosscut the natural features (fig. 2.1).

Aerial imagery was used to obtain a two-dimensional view of the study area in large scale while the small scale structures were observed in road-cuts. DEM interpretation were used in combination with aerial imagery as the high resolution, 5x5 m, of the DEM model. This gives an excellent possibility for study of larger lineaments, combining these features with an overlay of the aerial images the lineaments can be differentiated from Quaternary and biological features that could be mistaken as lineaments in the bedrock.

This chapter starts with the description of regional lineaments, followed by description of small-scale fault-fractures from six selected key areas (fig. 3.1), including their geometry, kinematics and preliminary interpretations. The results presented in this chapter along with the results from chapter 3 will form the basis for the analysis and discussion presented in chapter 6.

3.2   Large scale lineaments

DEM data and aerial/satellite data of the study area were studied prior to field work in order to identify lineaments and areas suitable for further investigation (fig. 3.1). Suitable areas were studied in more detail, both on the DEM and in the aerial images and followed up with structural fieldwork. This preliminary screening identified five areas (fig 3.1) where the intersection of multiple different oriented lineaments and well-exposed road-cuts were chosen for further studies.
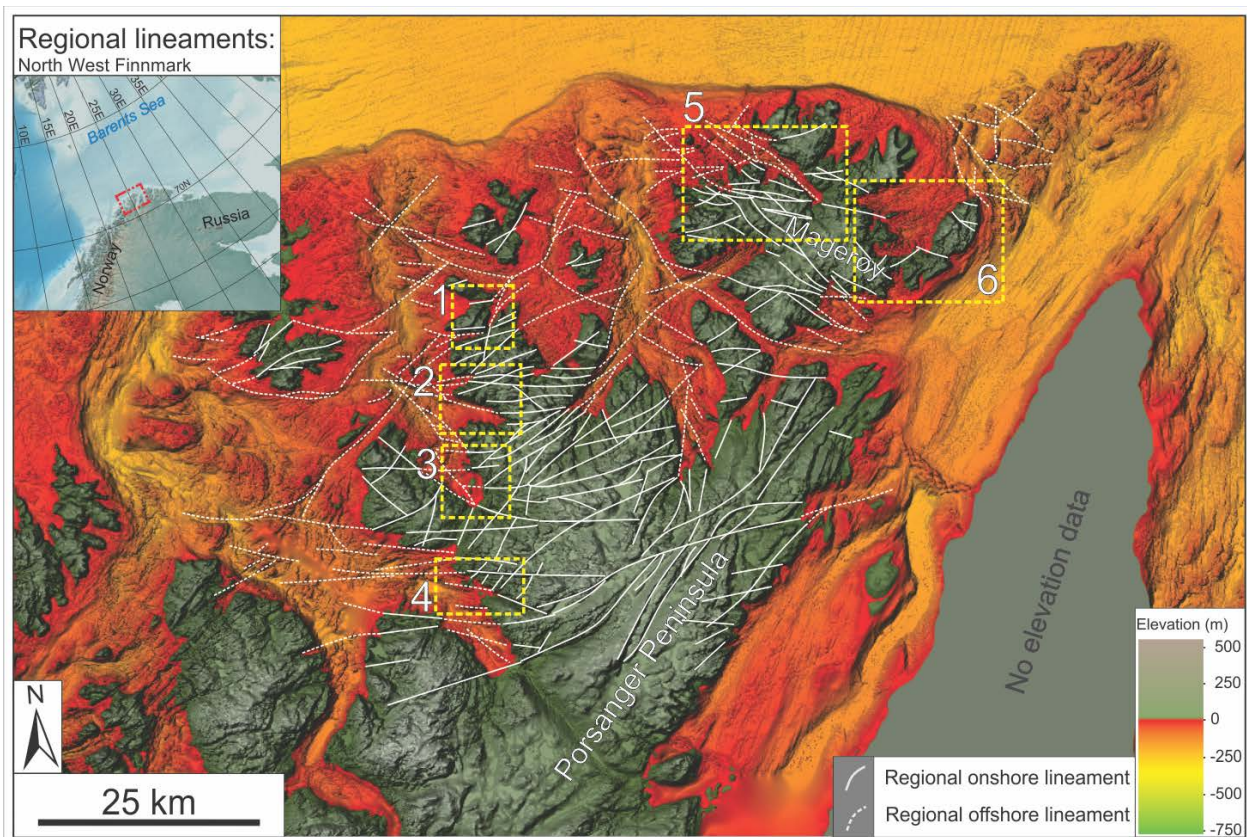
Fig. 3.1, Regional DEM and bathymetric map; lineaments onshore shown as solid white lines, lineaments offshore shown as dotted white lines. 1-6, represents fieldwork areas. Elevation color scale shown in lower right corner. Modified from MAREANO and Statens Kartverk

Previous regional studies in northwest Finnmark (Gabrielsen et al., 2002; Roberts, D. et al., 2005) have identified several large-scale lineaments striking NE-SW and NW-SE. The NW-SE trend is presumed to be the onshore representation of TKFZ (Gabrielsen et al., 1989), and the NE-SW and E-W trend is thought to be parallel with the main offshore fault trends, i.e. the TFFC and the Hammerfest and Nordkapp Basin trends (Faleide et al., 2008; Johansen et al., 1994).

3.3 Lineament distribution on northwest Porsanger Peninsula and Magerøy

Fig. 3.1 shows the overall distribution of small-scale lineaments on Magerøy and Porsanger Peninsula onshore, mapped and interpreted from aerial photos and bathymetric data. The bathymetric data are described in chapter 4.2. The landscape of the study area is dominated by rounded mountains and with narrow linear escarpments, valleys, ridges and gullies/depressions. When comparing the landscape and topography of the study area with the bed rock architecture and existing lineament maps of northern Norway (e.g. Gabrielsen et al. 2002; Indrevær et al. 2013) the study area contains multiple similar large-scale lineaments (fig 2.1) that can indicate the presence of major brittle fault-fracture trends.
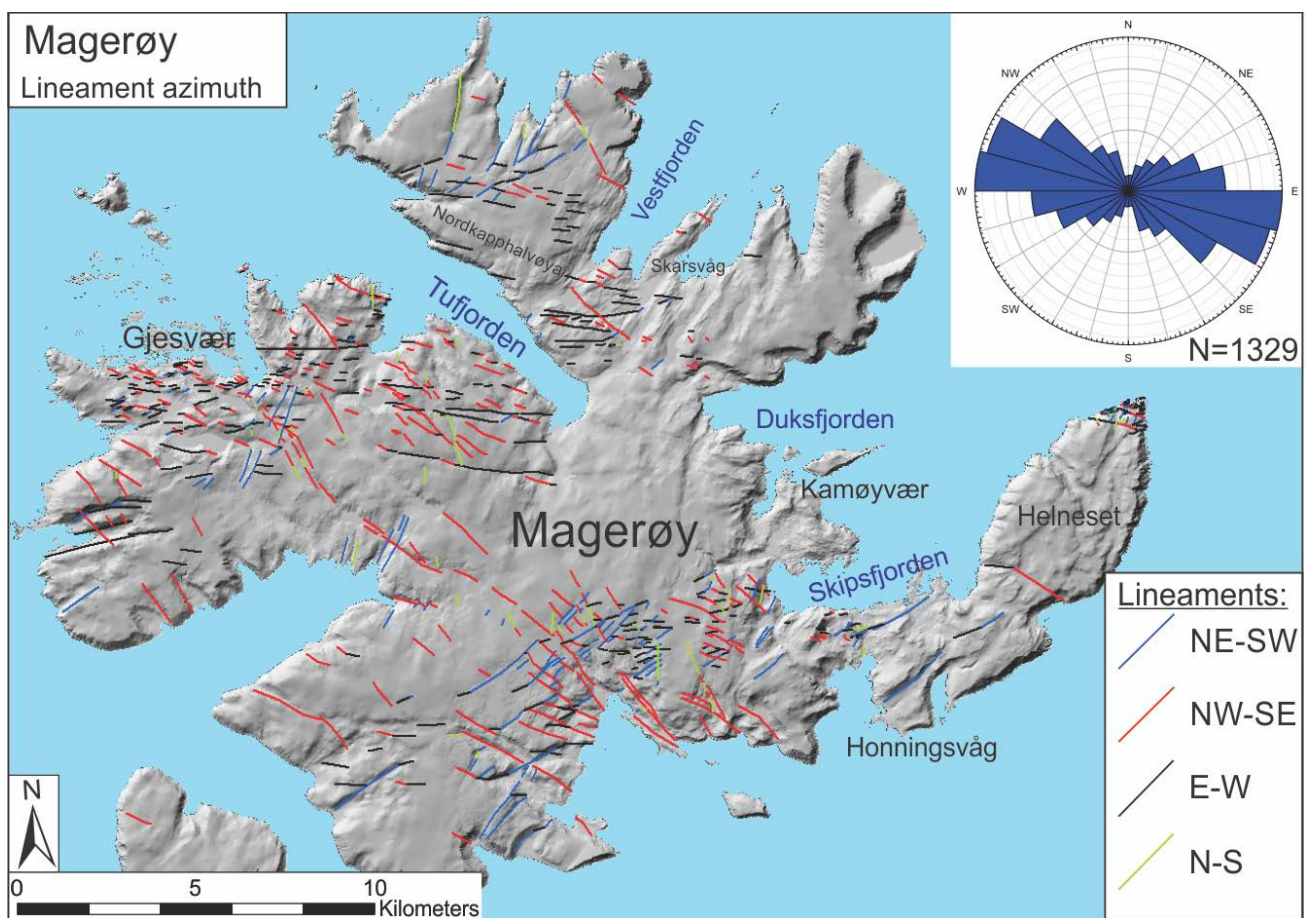
Fig. 3.2, Relief map over Magerøy, displaying onshore lineaments on Magerøya. Lineaments are colored based on their azimuth. Rose plot with orientation data for all faults-fracture lineaments. N= number of measurements.

The lineaments on Magerøy have a dominantly NW-SE to NWW-SEE trend, whereas Porsanger Peninsula trends from W-E to NNE-SSW. The areas record a high density of parallel lineaments, e.q. area 2 and 5, identified from large a scale DEM, but also irregular patterns exist, such as anastomosing, en echelon/step-

wise and curved geometries (fig. 3.1). In some areas on the NW coast of Porsanger, for example in fjords and valleys, a high density of lineaments occur, and the lineaments terminate in and around the mouth of the fjords. Some of the lineaments follow the lower boundary of the KNC and internal thrust faults, in the central Porsanger Peninsula (fig. 1.2)

The regional lineaments in the study area comprise fault-fracture lineaments that offset some of the lithological boundaries in addition to geomorphological effects (fig 3.19 & 3.22). The major trends are E-W to NE-SW and NW-SE on NW Porsanger peninsula, and NW-SE to E-W and NE-SW on Magerøy (fig. 3.1). The lineaments vary from unlinked to partially linked, connecting E-W and NE-SW trending lineaments through the Porsanger Peninsula. Magerøya comprises large-scale lineaments with a dominant trend NW-SE (fig. 3.2), that cut the foliation and bedding of Magerøya and KNC. In some areas, e.g. Gjesvær and to the south of the island, the landscape (e.g. the fjords, escarpments, gullies etc.), follows the same large scale trend (fig. 3.1).The NW-SE and E-W oriented lineaments on Magerøy, compose a rhombic pattern, seen near Gjesvær and Southeast of Honningsvåg (fig. 3.2). The areas southeast of Honningsvåg the NE-SW and E-W striking lineaments appears as rhombic patterns, cut by the NW-SE striking lineaments. Near Gjesvær the NE-SW and E-W striking lineaments make up rhombic patterns, and are cut and offset by longer continuous NW-SE, E-W and NE-SW striking lineaments.

The northwest part of the Porsanger Peninsula comprises large-scale lineaments striking mainly E-W to NE-SW, with a minor constituent striking NW-SE and N-S (fig. 3.1 & 3.3). Similarly to Magerøya, the landscape seems to be influenced by the lineaments, where fjords, gullies and escarpments follow the main trends. However, some of the fjords (Snefjord, Lillefjord and Bakfjorden) appears to follows a NW-SE trend, opposite to the main lineament trends (NE-SW and E-W). In addition, northwest Porsanger Peninsula also contains Caledonian thrust faults, located at the middle of the peninsula, that follows the NE-SW lineament trend (fig. 1.2). The lineament also show a geometry where NE-SW to E-W striking lineaments create anastomosing patterns near fjords, e.g. near Bakfjorden and Ryggefjorden, where NE-SW to E-W trending lineaments flow into the fjord-mouth. Other areas show acute rhombic to sub-rhombic geometries (e.g. Snefjord). Overall, the lineaments on the northwestern parts of Porsanger Peninsula create rhombic to sub-rhombic rectangular geometries, where the NE-SW appear to cut the E-W striking lineaments, as can be seen from Revsbotn to Snefjord and Ryggefjorden. The distribution in the rose plots (fig. 3.2 & 3.3) shows that the

Description of onshore lineaments, brittle fractures and faults

lineaments differ in orientation between Magerøy, NW-SE to E-W strike, and northwest Porsanger Peninsula, E-W to NE-SW trend.
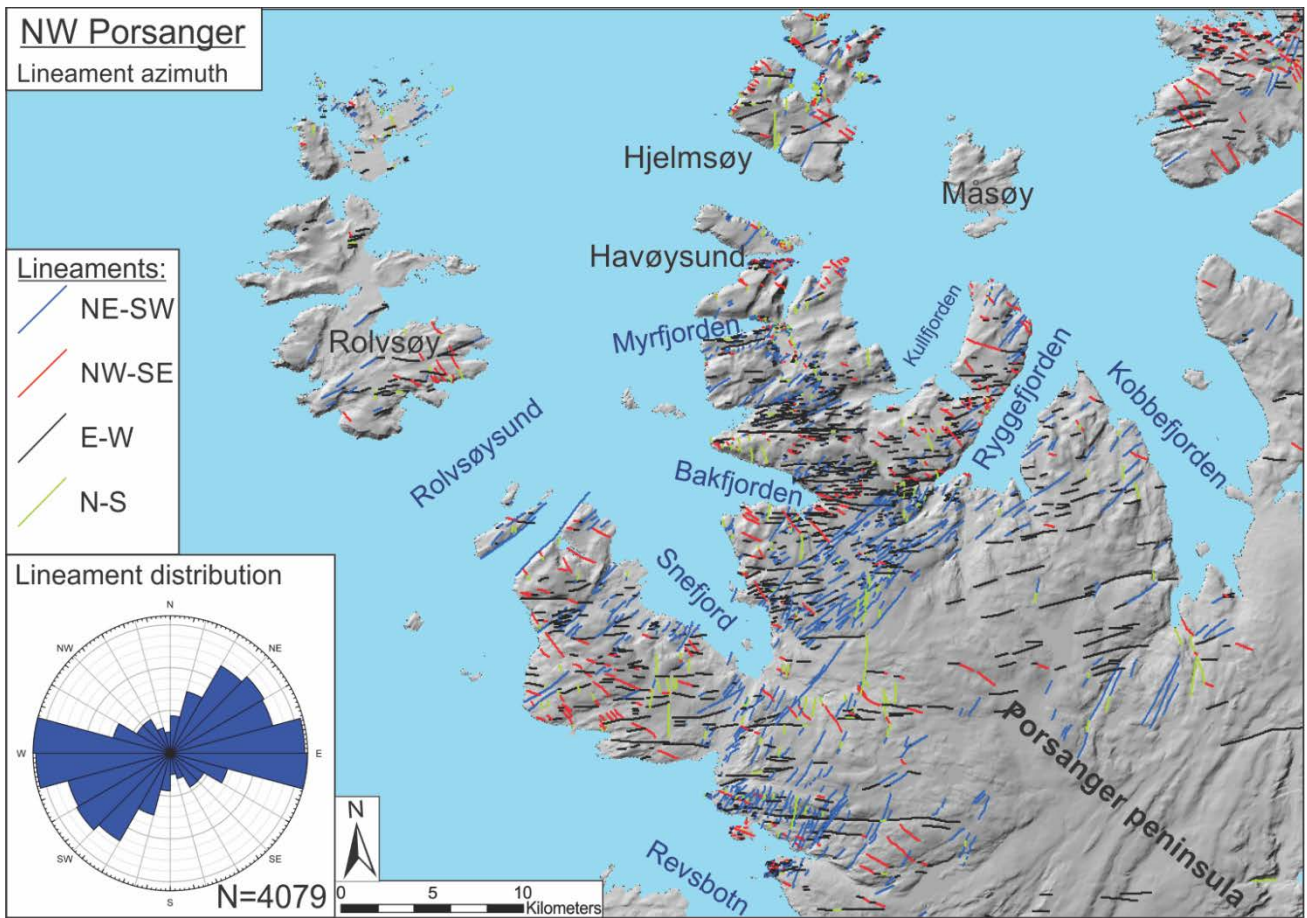
Fig. 3.3, Relief map of northwest Porsanger Peninsula, displaying onshore lineaments on Magerøya. Lineaments are colored based on their trend. Rose plot with orientation data for all faults-fracture lineaments. N= number of measurements.

3.4 Description of onshore brittle fractures and faults

The bedrock in the study area shows many brittle fractures and faults, sometimes with cataclastic fault core rocks and slickensides. This chapter will describe these brittle fractures and faults, as well as smaller scale lineaments in selected key areas (fig. 3.1), including their field relations, geometry and kinematic indicators, followed by a summary.

As presented in chapter 1.3, the Caledonian rocks on Magerøya and the Porsanger Peninsula are made up of meta-sedimentary rocks and intrusives (Gayer et al., 1987; Roberts, D. et al., 1991). The general foliation on the Porsanger Peninsula is horizontal to sub-horizontal in some areas, whereas other areas record steeply dipping foliation, all with varying dip directions. Fieldwork has made it possible to characterize several orientations of brittle fractures and faults, enabling the correlation of onshore lineaments with the lineaments interpreted from bathymetric data and faults interpreted from seismic data in chapters 4 and 5. All structural data has been plotted in Schmidt equal-area lower hemisphere stereoplots (Vollmer, 2015). The kinematic data is plotted showing slip lineation as tangent arrows (red), indicating the displacement sense of the hanging wall, and the strike and dip are represented by a great circle (black) (Vollmer, 2015).

The six selected areas have been studied in detail due to their high frequency of brittle faults, fractures, fault rocks and slickensides, as well as their connection to larger scale lineaments identified on bathymetry or in the DEM. These areas are marked in fig. 3.1, and are given the following names:

1. Havøysund & Myrfjord
2. Bakfjorden
3. Snefjord
4. Lillefjord
5. Honningsvåg
6. Gjesvær

3.4.1   Area 1 - Havøysund & Myrfjord

Field relations and rock description:

The Havøysund and Myrfjorden areas are located in the northwestern most part of Porsanger Peninsula (fig. 3.1) The bedrock in the area belongs to the KNC, and includes various meta-sandstones shales/slates, mica-schists, dioritic to granitic gneisses as well as some intercalated gabbroic and amphibolitic gneisses on some of the mountains tops (Kirkland et al., 2008). Bedrock in the area is well exposed and records many well-preserved fractures in road-cuts and outcrops. These comprise brittle fractures striking in many directions, and dipping both ways relative to the strike (fig. 3.4). Some of the fracture and fault surfaces have preserved slickensides, while other show signs of eroded slickensides. The bedrocks in the area is well foliated, and generally has a competent consistency and is horizontal to sub-horizontal dipping to the south. The topography in the area is heavily influenced by the large-scale lineaments where escarpments, fjords and sounds have the same orientation as the main lineaments, trending NE-SW and E-W (fig. 3.1).
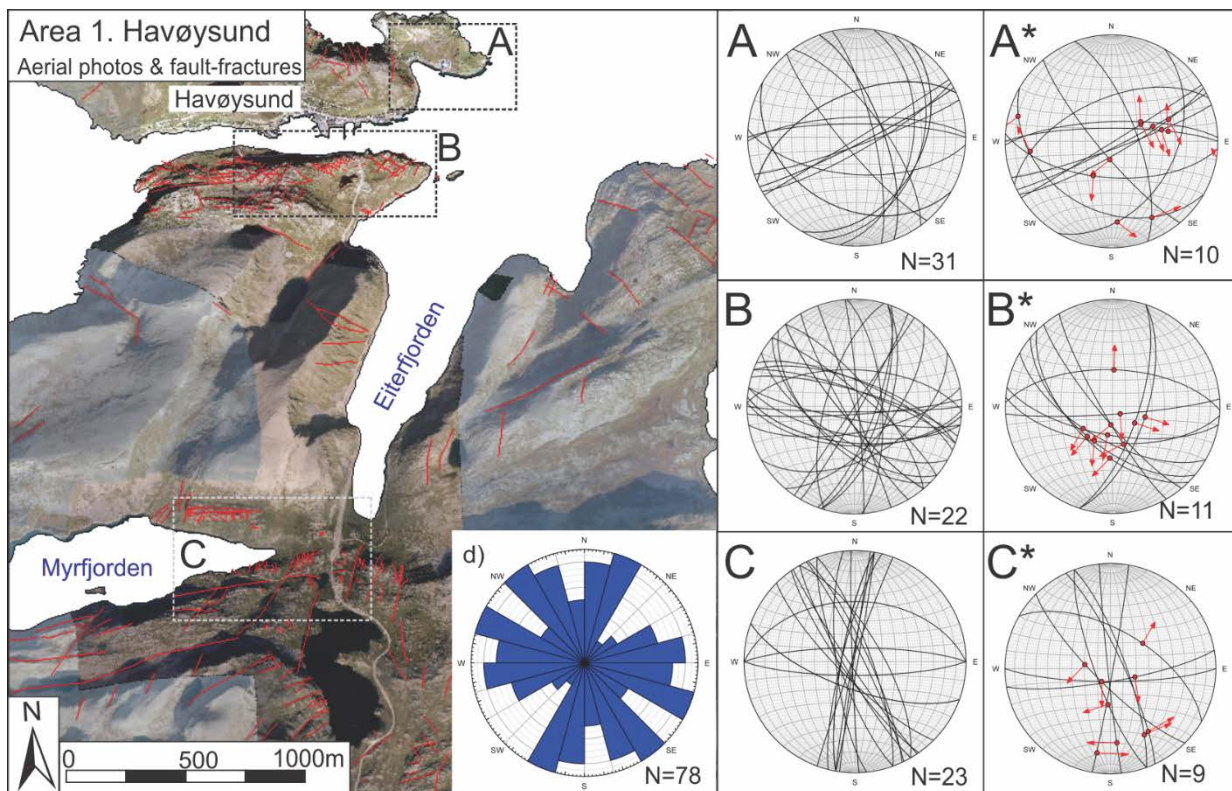
*Fig. 3.4, Aerial photograph showing onshore data of area 1, Havøysund. **A-C**; Lower-hemisphere Schmidt stereonet displays fracture orientation data from field localities. **A*-C***; Kinematic data plotted in lower-hemisphere Schmidt stereonet showing slip lineation as tangent arrows (red) at intersection of M-plane and fault/fracture surface, indicating the displacement sense of the hanging wall, the strike and dip is represented by a great circle (black) (Vollmer, 2015). **d)** Rose plot showing the strike-distribution of all fracture and fault surfaces measured.*

Description of onshore lineaments, brittle fractures and faults

Lineament data:

As shown in chapter 2.1, the north Porsanger Peninsula area has regional-scale lineaments striking NE-SW to E-W (fig. 3.1). In higher-resolution aerial photographs, the interpreted lineaments can be seen to compose a somewhat different and more mixed trend (fig. 3.4 & 3.5). The rose plot distribution of smaller lineaments in the area shows two dominant and distinctive trends: 1) NE-SW strike, including N-S trending lineaments that change direction and terminate in the more common NE-SW trending lineaments and 2) NNW-SSE to WNW-ESE strike, in addition to subsidiary trending lineaments faults (fig. 3.5). E-W striking lineaments are seen as a more individual trend, crosscutting the dominant trends.
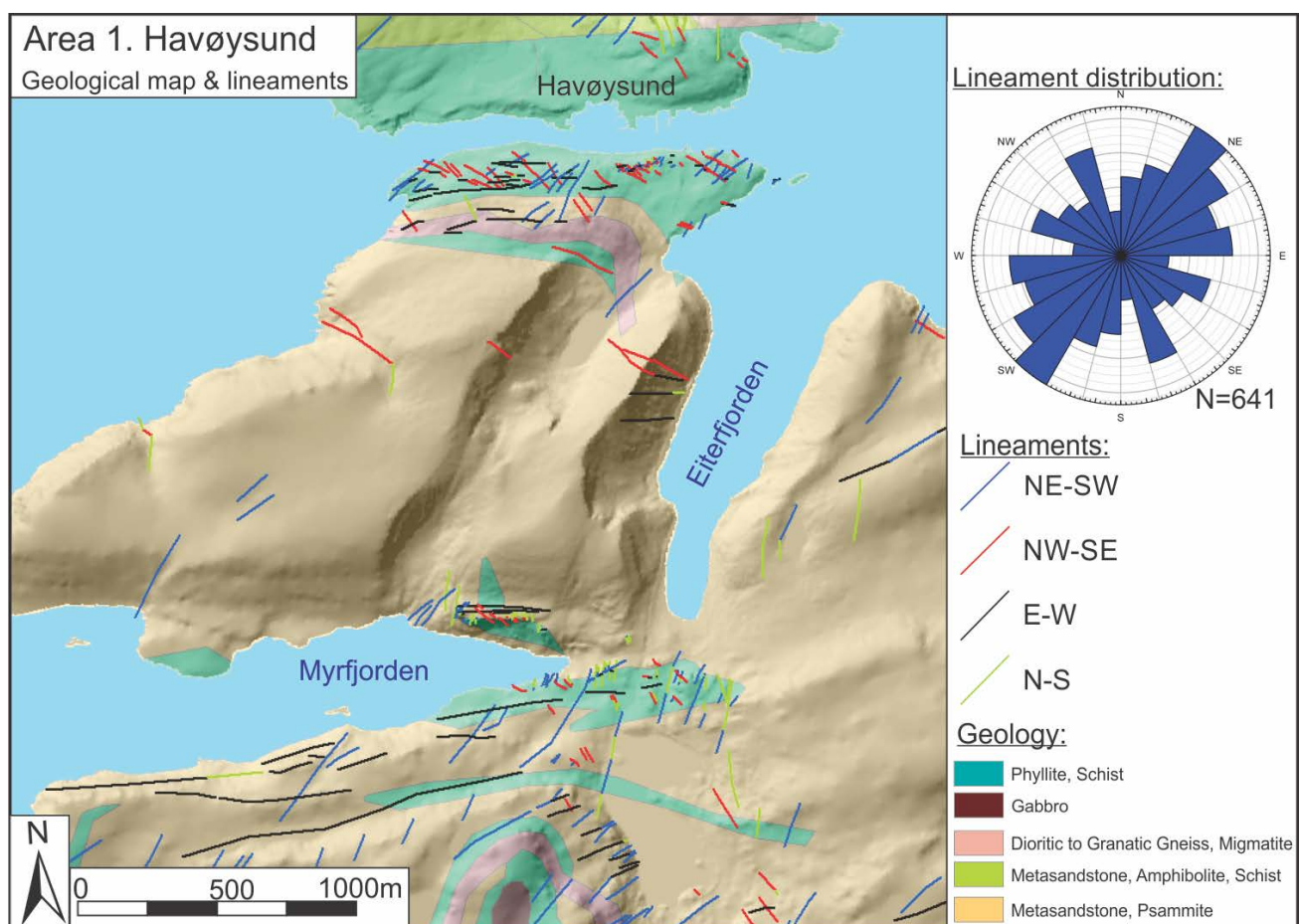
Fig. 3.5 Geologic relief of Area 1, showing lineaments interpreted from aerial images, lineaments marked as colored lines, where the color indicate the azimuth, see legend. Rose plot displays the distribution of lineament azimuth. N indicates sample size in all rose plots Geologic map modified from NGU, Roberts, D. (1981)

Brittle faults and fractures:

The brittle fractures observed in Havøysund display variable strike and dip, with a preference of NE-SW to E-W and NW-SE striking fractures, dipping both directions relative to the strike (fig. 3.4). In addition, there are also steep N-S striking fractures that cut and offset the foliation (fig. 3.6). Most fractures are steeply dipping planar surfaces, but there are several examples of steeply dipping stair-stepping fractures as well. Loc. 1A records NE-SW to ENE-WSW, NW-SE to NNW-SSE and NNE-SSW to N-S steep brittle faults, where the main fault shows an undulating surface, stair stepping with the foliation showing secondary fault-fractures splaying out and terminating along the foliation. The dip range from near vertical to 40°. Additionally, the foliation on the hanging wall appears to be folded downwards along the main fault surface (fig. 3.6).
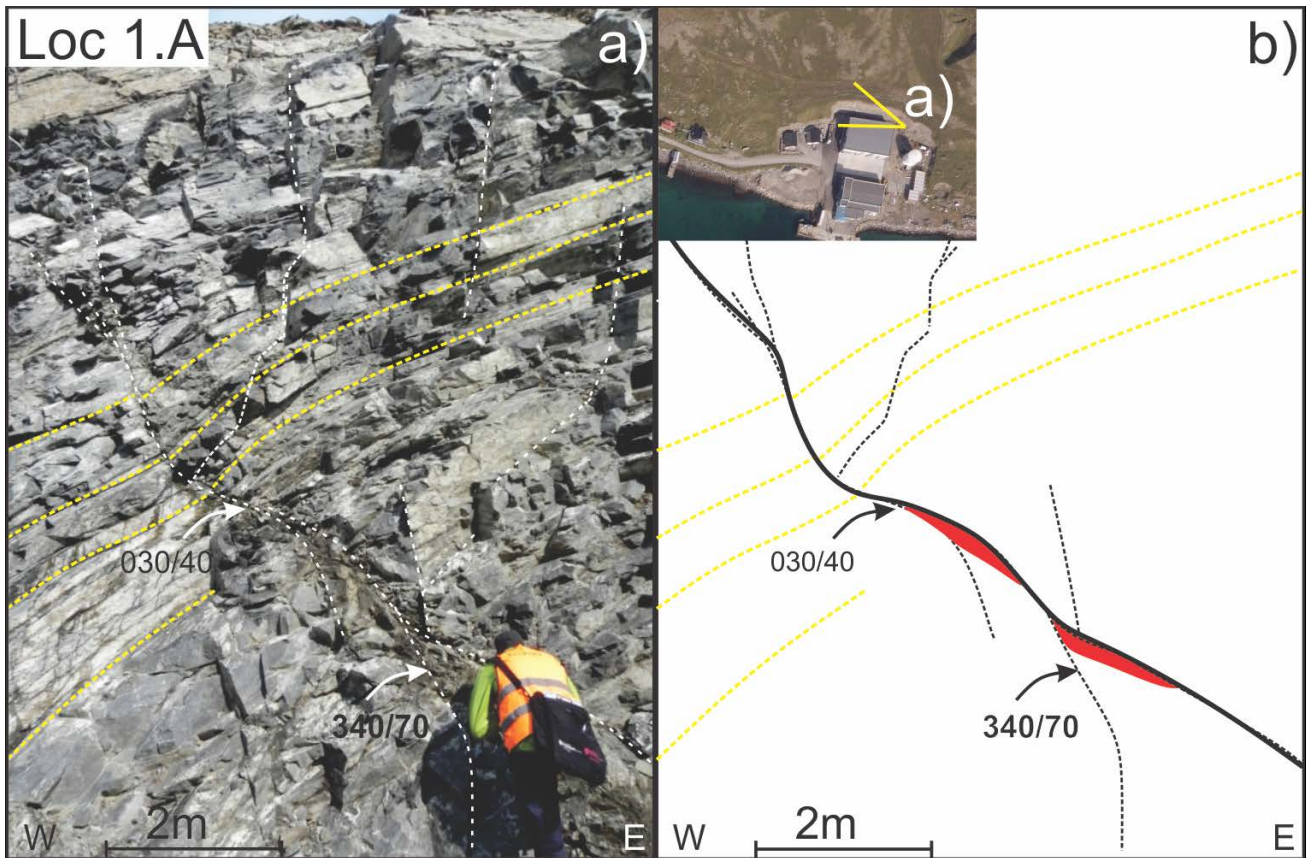
*Fig. 3.6, Outcrop photo and sketch interpretation of loc. 1A, east of Havøysund. **a)** Brittle fault at loc 1A, **b)** Sketch interpretation of a)l, note the highly fractured zones in red, and the bending of the foliation in the hanging-wall*

At location 1.C (fig 3.4), a plateau near the intersection between Myrfjord and Eiterfjorden, the rock consists of migmatized granite. This location differs from the other localities in the area, as the rock is mostly uniform in texture with indistinguishable foliation. The fractures measured at this locality show a set of parallel

surfaces striking ca. E-W and with variable dip (50° and 80°) to the south, (fig. 3.7). Crosscutting relations can be seen between fractures striking E-W and NW-SE, as evident to the right of the photo on the broken surface. Fault sets with similar strike, E-W, but different dip are observed in the road cut (fig. 3.7), indicating possible conjugate fault sets.
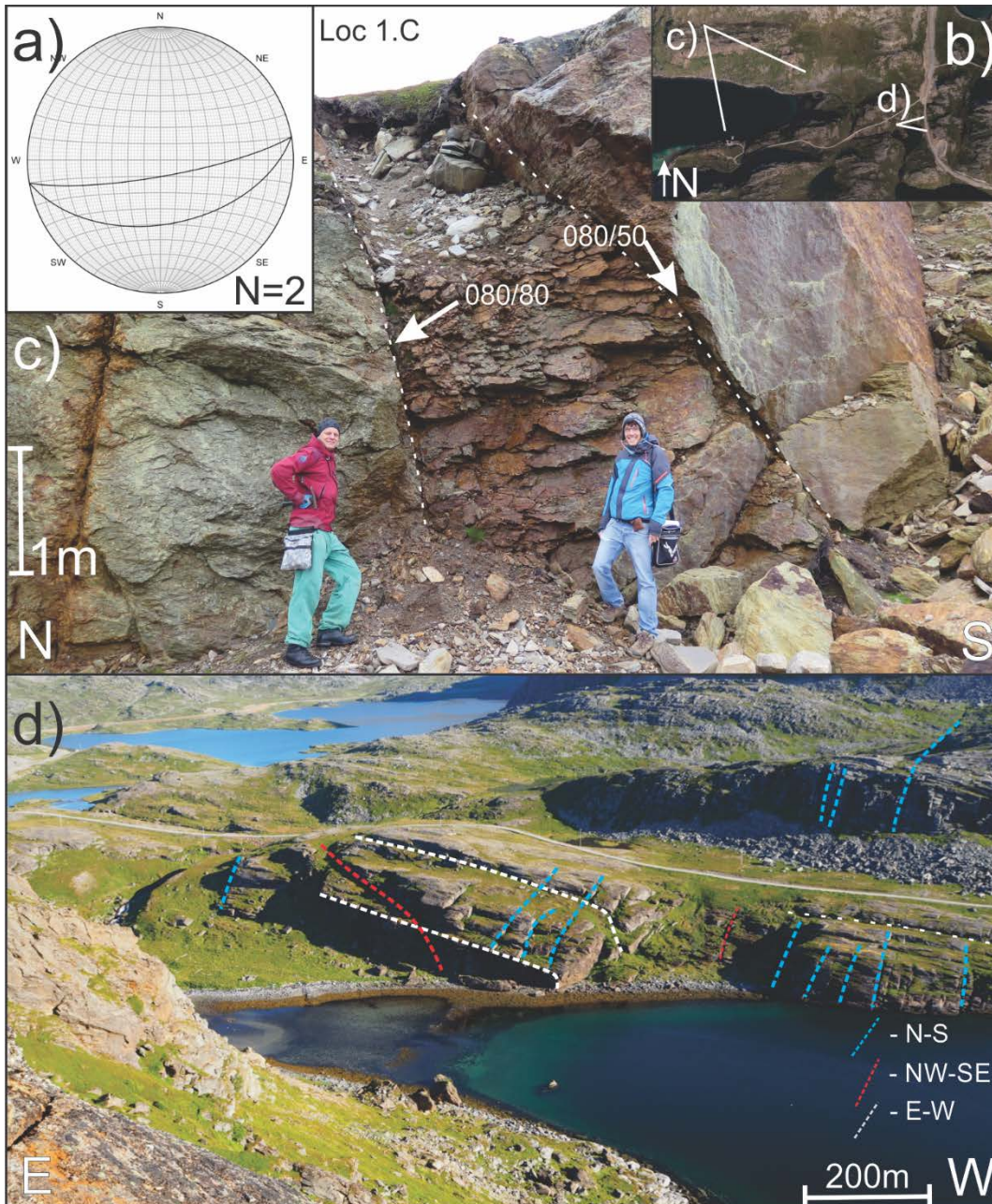
*Fig. 3.7, Outcrop photos of fractures in loc 1c: **a)** Stereonet of E-W striking faults in b), **b)** Aerial photo showing location of photos c) and d). **c)** outcrop photo showing possible conjugate faults (dashed white lines) striking E-W, showing a crushed zone in the intermediate zone. **c)** Overview photo of outcrops, showing a cross section of fault fracture lineaments. Note the parallel E-W striking fractures as they the direct continuation of faults shown in c).*

Kinematic data:

Some of the observed fault/fractures display surfaces with well-developed chlorite slickensides, recording chlorite lineation. The orientation data from the slickensides (fig. 3.4) show that the NE-SW striking faults record normal oblique-slip and normal dip-slip with components of sinistral and dextral sense of shear (fig 3.4 A* & B*). NW-SE to N-S striking faults show dominantly normal oblique-slip and dip-slip with components of dextral sense of shear (fig. 3.4 A*, B* & C*). The E-W striking faults record normal dip-slip sense of shear (fig. 3.4 A*, B* & C*).

3.4.2   Area 2 - Bakfjorden

Field relations and rock description:

Bakfjorden is located on the northwestern part of the Porsanger Peninsula; south of Area 1 and covering an area from Selvika in the north to Bakfjorden in the south (fig. 3.1 & 3.9). Bakfjorden comprises similar to rocks as area 1, the rocks belongs to the KNC. Recording various meta-sandstones shales/slates, mica-schists, dioritic to granitic gneisses, and some intercalated gabbroic and amphibolitic gneisses on some of the mountains tops (Kirkland et al., 2008), and records meta-sandstone, shale, garnet-rich mica-schist, dioritic to granitic gneisses, and gabbro/amphibolites at some of the mountains tops (fig. 3.9). The main Caledonian foliation in the area is horizontal to sub-horizontal dipping slightly to the south. The topography in the area is dominated by mountains and encompasses valleys, gullies and cliff-like beach areas. The mountainous areas show many escarpments and cliffs, as well as rocky outcrops (fig. 3.8 & 3.9).
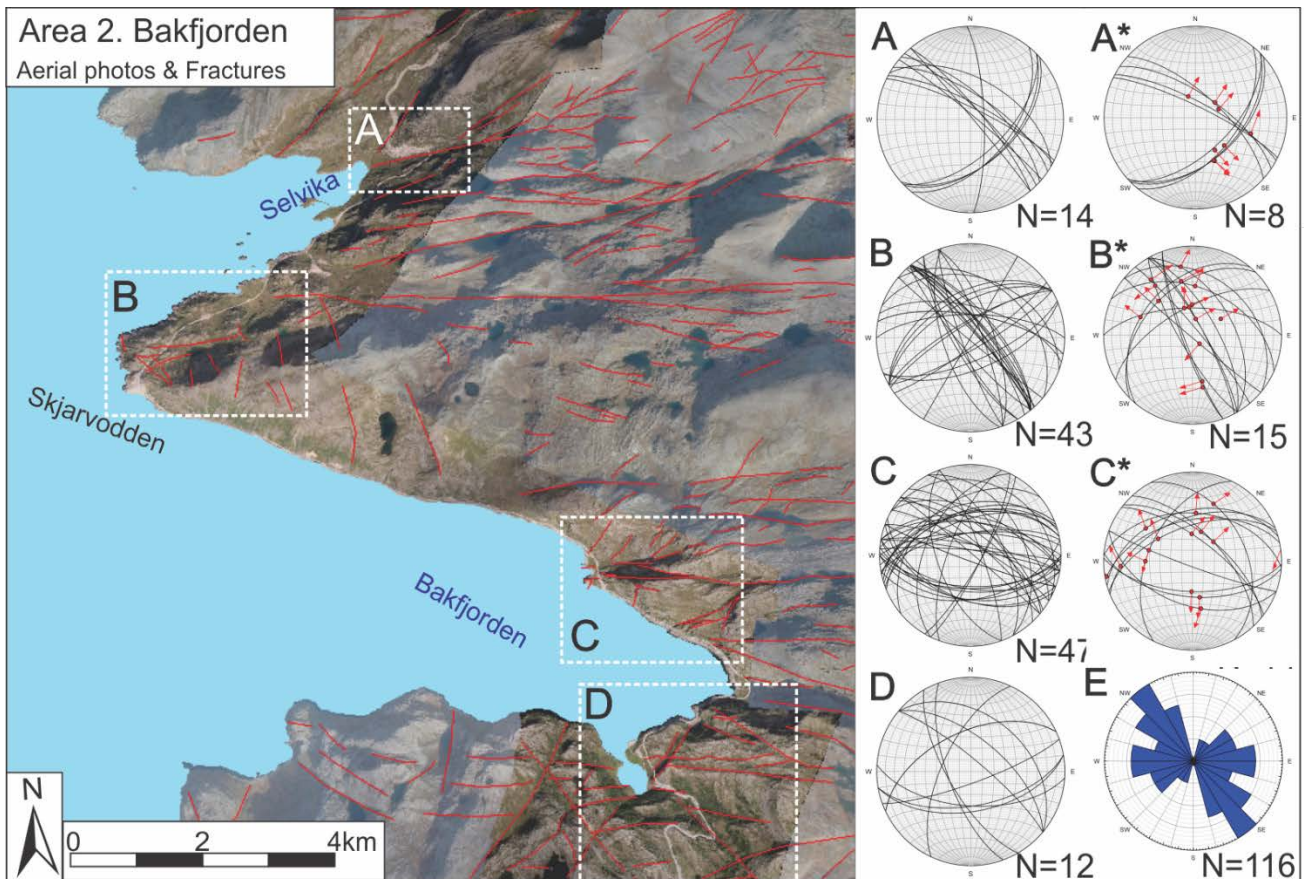
*Fig. 3.8, Aerial photo showing onshore data of Area 1, **A-D**; Lower-hemisphere Schmidt stereonet displays fracture orientation data from field localities. **A*-C***; Kinematic data plotted in lower-hemisphere Schmidt stereonet showing slip lineation as tangent arrows (red) at intersection of M-plane and fault/fracture surface, indicating the displacement sense of the hanging wall, the strike and dip is represented by a great circle (black) (Vollmer, 2015). **E)** Rose plot of the strike-distribution of all fracture and fault surfaces measured.*

Lineaments:

Bakfjorden and Selvika comprise large-scale lineaments striking NE-SW and E-W, as described in chapter 2.1 (fig. 3.1), defining an acute truncating or wedge geometry of fracture sets (fig. 3.9 and 3.10 a, b). On smaller scale aerial photographs, the interpreted lineaments at Bakfjorden and Selvika differ somewhat in orientation relative to the regional fracture pattern, and compared with that of the Havøysund-Myrfjord area (fig. 3.5 & 3.8). The smaller scale lineaments show the dominant E-W striking trend and the less dominating NE-SW trends forming acute truncating and wedge geometries. Whereas some NW-SE striking lineaments, e.g. south of Bakfjorden and on Skjarvodden, cut the wedge geometry, other lineaments take part in the wedge geometry (fig. 3.9). As seen on rose diagrams the dominant fracture trend is E-W, while the NW-SE and NE-SW trending fracture sets do not define distinct peaks, but rather, create overlapping zones (fig. 3.9). Comparing the lineaments seen on the map and in the rose diagram, the E-W trends seem to gradually merge into the NE-SW and NW-SE trends, the few N-S lineaments follow the same pattern, as they

gradually change direction and terminates in either NE-SW or NW-SE trending lineaments. In contrast, the NW-SE and NE-SW trending sets at Bakfjorden clearly cross-cut each other (fig. 3.9).
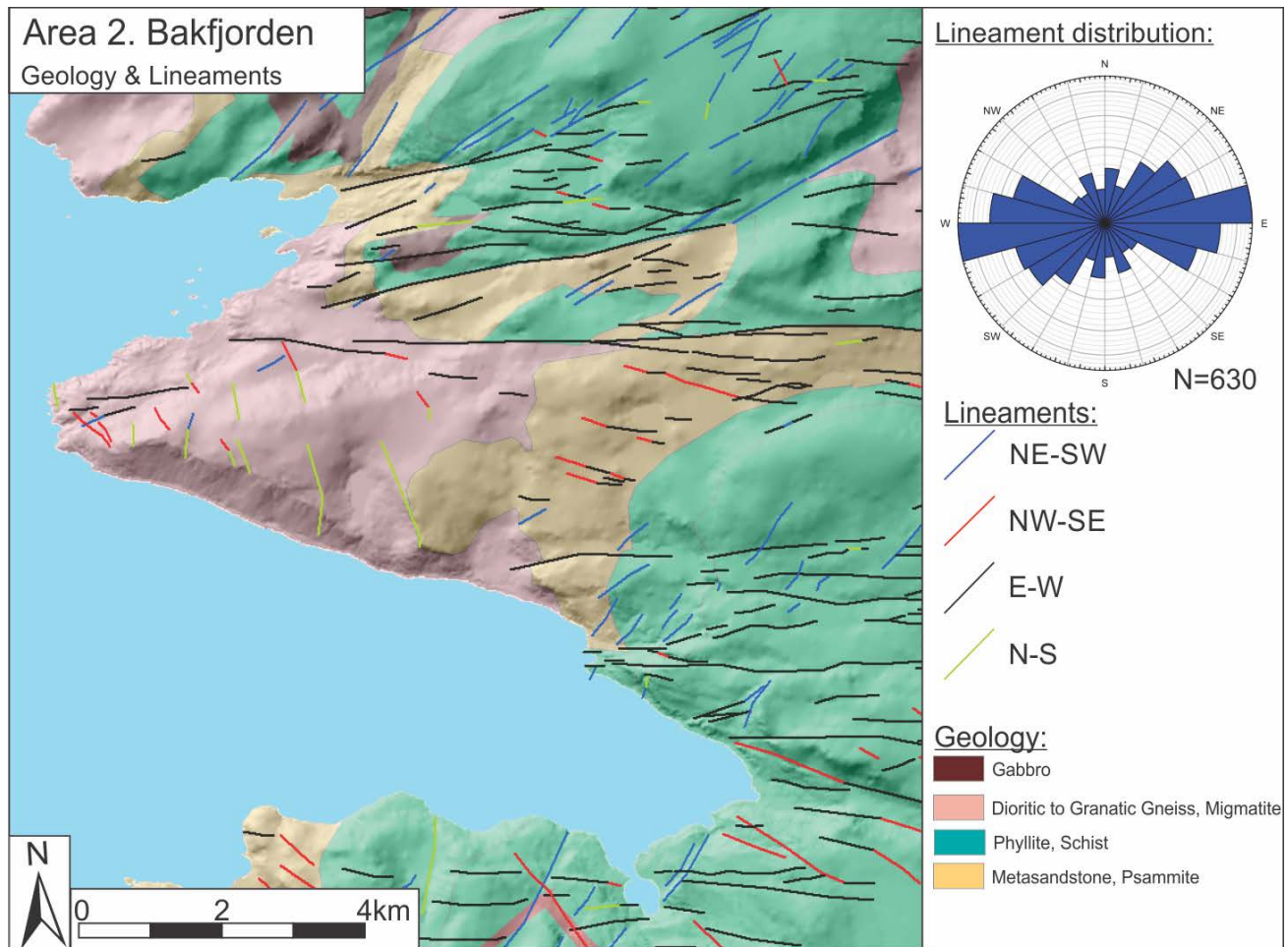
Fig. 3.9, Geologic and DEM relief map. Displaying fault-fracture lineaments interpreted from aerial images. The colors mark the trend of the lineaments. Circular rose diagram shows trend distribution. Geologic map modified from Roberts, D. (1981)

Brittle fault and fractures:

The dominant E-W trending brittle fractures and faults mapped in Bakfjorden vary in dip and dip direction (fig. 3.8 A-C). Moreover, these fractures are generally steeply dipping and cut the foliation of the bedrock. Most of the fractures measured have planar surfaces, but there are several examples of en echelon stepping fractures with irregular curved and anastomosing surfaces, as well as some listric geometries with approximately 20° dip. At location 2.A, near Selvika the measured NE-SW and NW-SE fractures follow the same trends as in Bakfjorden (fig. 3.8).

Description of onshore lineaments, brittle fractures and faults

The brittle fractures at location 2.A (fig. 3.8) show a varied geometry and a high degree of crosscutting and fault interaction. Several faults show both kinematic indicators and fault gauge along the surfaces (fault cores) of NW-SE striking faults. The faults in fig 3.10 c show secondary faults splaying outwards into the damage zones from the intersection to the main fault surface, whereas the footwall along the main fault shows a crushed zone. Figure 3.10 d shows a near-vertical NE-SW striking fault, off-setting a NW-SE striking fault vertically, as one can see from the 1-2 m offset of the damaged zone of NW-SE striking fault. Both, the NE-SW striking faults show cm-scale stair stepping along the fault-surface, where chlorite slickensides are found on the shallow angles (fig. 3.10 c & d).

The area at Skjarvodden, loc. 2.B, comprises NE-SW, NW-SE and E-W striking faults. The E-W and NE-SW striking faults comprises fault gouge and slickenside surfaces, while the NE-SW striking faults show some slickensides, but lack fault gauge. NNW-SSE striking faults cut the NE-SW and E-W striking faults (fig. 3.11). NE-SW and E-W faults are characterized by undulating fault surfaces and meter- scale damaged zones, as well as SE to S dipping secondary faults (fig. 3.11b & d). In addition, NE-SW striking faults are characterized by planar fault surfaces, where larger fault surfaces have oppositely dipping secondary fractures terminating at the major fault surfaces, similar to loc. 2.A (fig. 3.10 c &. 3.11 d).

Loc 2.A

Selvika

a)

b)

N=5

c)

040/75

050/40

040/50

3m

W

E

E

c')

040/75

050/40

040/50

3m

W

d)

- 300/55

050/88

4m

W

E

d')

- 300/55

050/88

4m

W

E
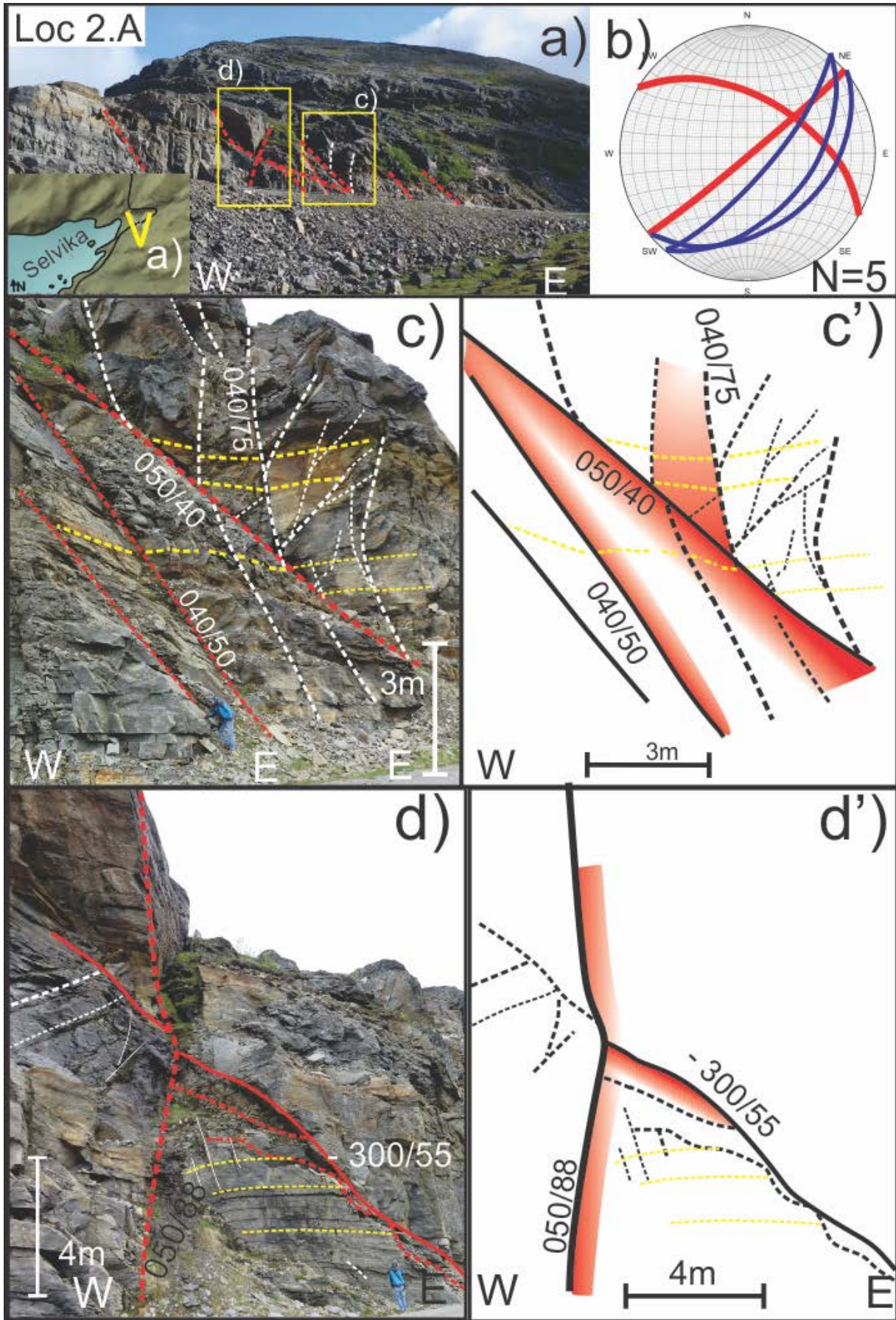
Description of onshore lineaments, brittle fractures and faults

*Fig. 3.10 (preceding page), aerial photo and outcrop examples of brittle fractures at Loc 2.A, Selvika (fig. 3.8). **a**). overview photo of outcrop b) Stereonet of faults displayed in figure, (**c**) - **blue**, **d**) - **red**). C-C') outcrop photo & sketch of brittle faults striking NE-SW, dipping SE. The main and secondary NE-SW faults interacts; secondary faults splay out from main fault (dashed red & solid black lines), offsetting the foliation normally (dashed yellow lines). The listric faults create rotated fault blocks. Grey fault gouge recorded in NE-SW striking faults (red shaded areas). The listric secondary fault terminate in the main NE-SW fault plane, recording gray fault gouge. **d-d')** Outcrop & sketch of fault-fractures. The main fault surfaces (black lines) show a crushed/heavy fractured zone (red areas) in the rocks near the footwall.*
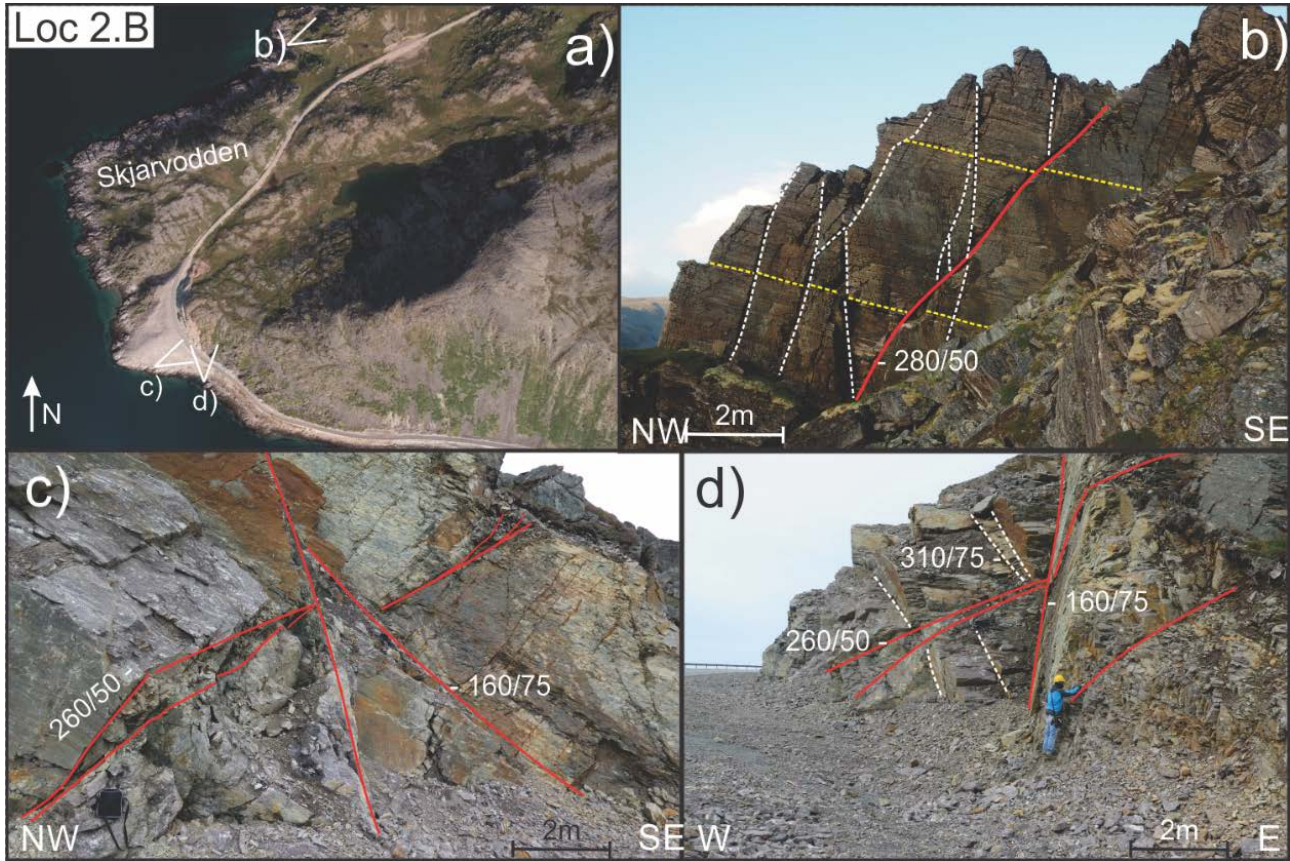
*Fig. 3.11 (this page), Aerial photograph and outcrop examples of brittle fractures at Loc 2.B, Skjarvodden. **a)** Overview aerial photographs of outcrops in b), c) and d). **b)** Main E-W striking fault dipping N, secondary faults dipping S, terminating in main fault, showing undulating surfaces. **c)** Outcrop photographs of brittle faults striking 1) NNW-SSE and 2) E-W, dipping NE to E and N respectably, the NNE-SWW fault offsets the E-W striking faults. E-W striking faults show damaged zone in the footwall, NE-SW show planar surface. The E-W striking faults record gray fault gouge. **d)** Photographs of same outcrop as c) but view to north, secondary antithetic fractures (dashed white lines) terminate in NW-SE striking fault.*

Kinematic data:

The kinematic data from Area 2 - Bakfjorden indicate an overall normal dip-slip to oblique-slip of measured fault surfaces (fig. 3.8). Faults striking NE-SW record dominantly normal dip-slip (fig. 3.8 A*, B* & C*), but also records normal oblique-slip to strike-slip with sinistral sense of shear (fig 3.8 B* & C*). NW-SE to NNW-SSE striking faults displays normal dip-slip and oblique-slip with mainly sinistral sense of shear (fig. 3.8 A*, B* & C*), however some record weak sinistral strike-slip to dextral sense of shear (fig. 3.8 B*).

3.4.3 Area 3 - Snefjord

Field relations and rock description:

Snefjord is located a few kilometers south of Bakfjorden (Area 2) on the Porsanger Peninsula (fig. 3.1).
Snefjord comprises similar geology as area 1 & 2, recording rocks from KNC (Kirkland et al., 2008), but also
records granitic to dioritic gneisses and migmatite. The main foliation of the rocks is either sub-horizontal or
gently dipping southeast. The area displays excellent bedrock-exposure on outcrops and road cuts. The
topography in the area displays rounded mountaintops and encompasses valleys, gullies, cliffs, rocky
outcrops and beach areas (fig. 3.12 and 3.13). The mountainous areas show linear escarpments and cliffs.
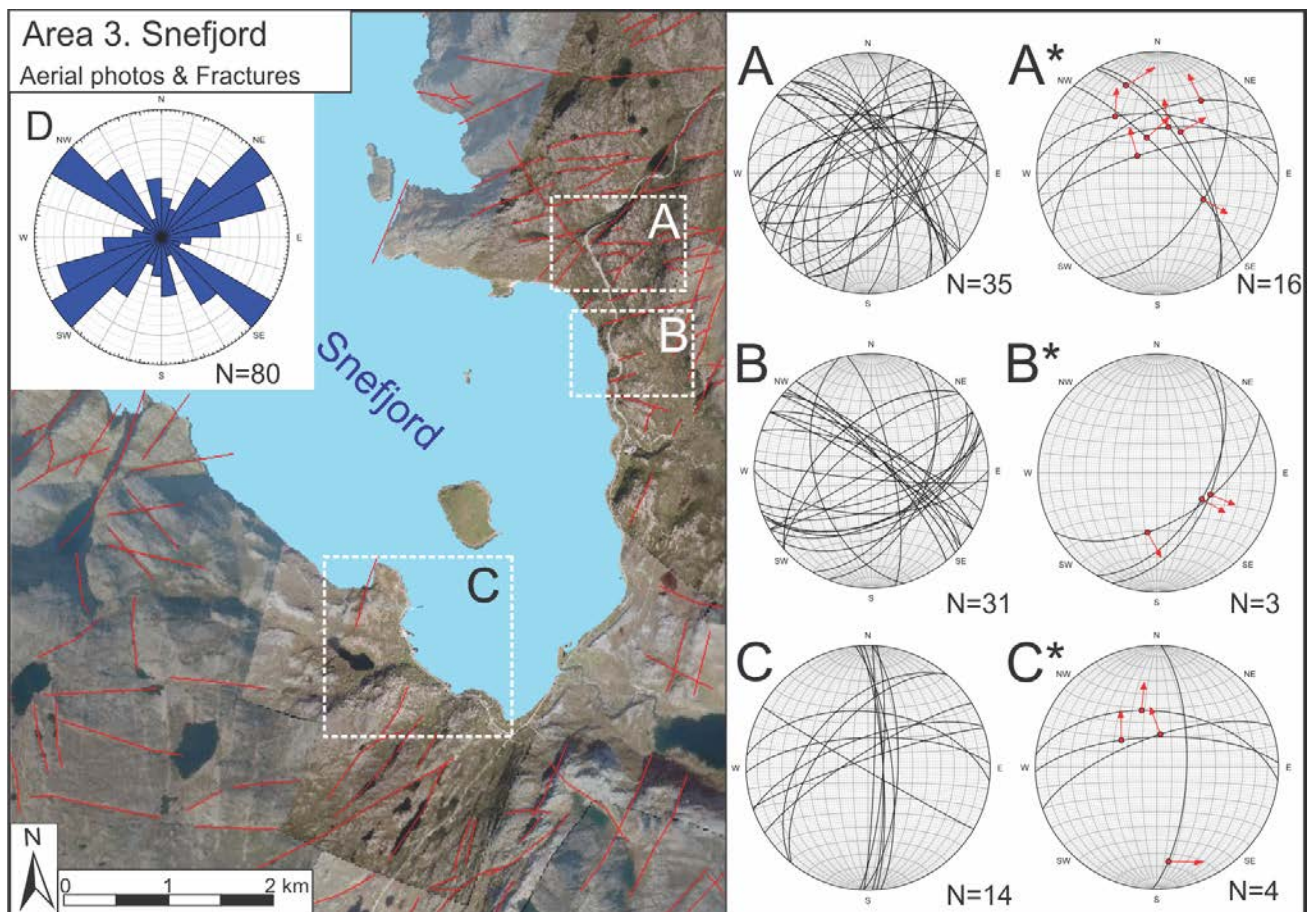
*Fig. 3.12 Aerial photo showing onshore data of area 3, Snefjord, **A-C**; Lower-hemisphere Schmidt stereonet displays fracture
orientation data from field localities. **A*-C***; Kinematic data plotted in lower-hemisphere Schmidt stereonet showing slip lineation as
tangent arrows (red) at intersection of M-plane and fault/fracture surface, indicating the displacement sense of the hanging wall, the
strike and dip is represented by a great circle (black) (Vollmer, 2015). **D**; Rose plot showing the strike-distribution of all fracture and
fault surfaces measured.*

Lineaments:

The large-scale interpreted lineaments in the Snefjord area include a dominance of E-W trending lineaments (Fig. 3.1). These lineaments have in subsidiary NE-SW and NW-SE trending lineaments. Small-scale aerial photographs shows a somewhat similar pattern dominated by ENE-WSW and NE-SW striking fracture pattern as well as some distinct NW-SE striking fracture systems (fig. 3.12 & 3.13). Comparing the rose-plot of small-scale fractures (fig. 3.13) and the map-view of lineaments (fig. 3.1), the E-W and NE-SW trending lineaments create a wedge pattern, where lineaments with intermediate trends splay into these two main lineament trends. Notably also, the NW-SE trending lineaments truncate the NE-SW and E-W striking lineaments, suggesting a time relationship (see discussion chapter 7).
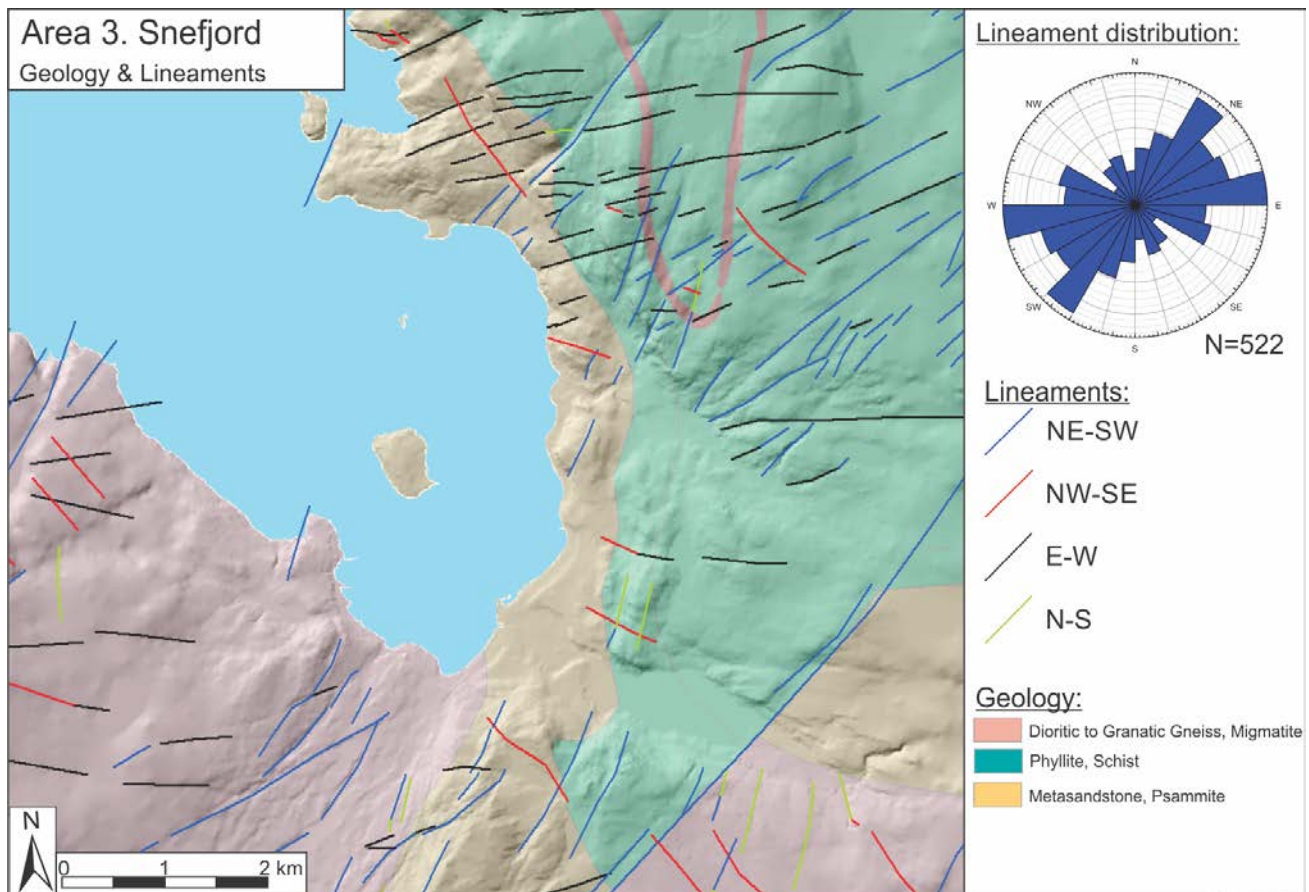
Fig. 3.13, Geologic map with lineaments interpreted from aerial images of Area 3; lineaments marked as colored lines, where the color indicate the azimuth, see legend. Rose plot displays the distribution of lineament azimuth. Geologic map modified from Roberts, D. (1981)

Brittle fractures and faults:

Area 3, Snefjord, contains many brittle faults and fractures, where NE-SW to ENE-WSW, NW-SE are the dominant strike orientations as well as a subsidiary N-S and E-W strike orientations (fig. 3.12). The faults and fractures steeply crosscut the foliation in the area. Fault rocks were observed at loc. 3.A and 3.B, recording fault gouge and cataclastic fault rocks. Loc. 3.A records unsolidified brown to red and gray colored zoned fault gauge (fig. 3.14). Loc. 3.B records fractured host rock, solidified grey colored fault gouge and dark green cataclastic rock (fig. 3.15).
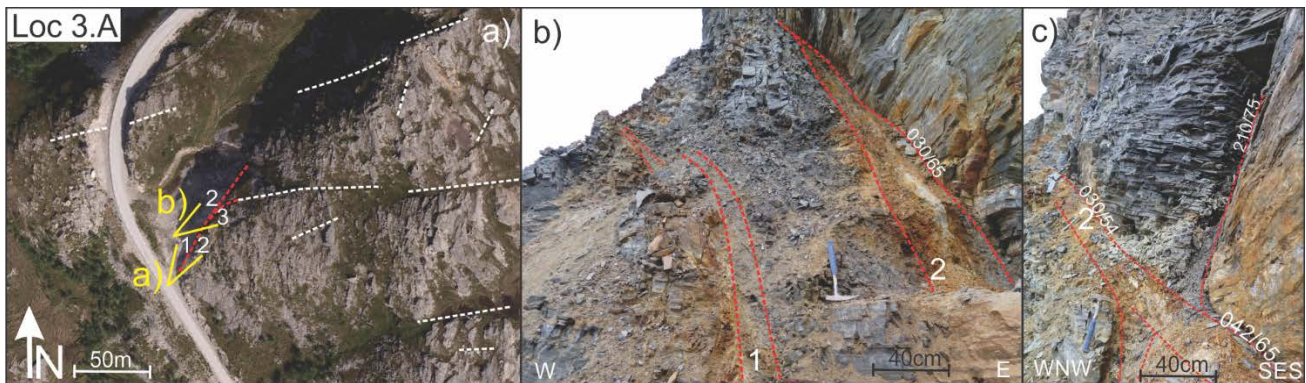
Fig. 3.14. Aerial images and outcrop photos of locality 3.A. a) Aerial photograph of location 3.A, white dotted lines indicate lineaments interpreted from the aerial photograph. Red dotted line indicate fault 1, 2 & 3 shown in b). b) Outcrop photograph of fault 1 & 2, a brittle fault with red to grey fault gauge, the section between the two fault zones are heavily fractured/crushed. Fault 2 has segmented zones where the color alters from dark red light grey, zones of crushed host rock can be found in both faults. c) Interaction of fault 2 & 3, shows that fault 2 overprints fault 3, that splays into fault 2.

At loc. 3.B, there is evidence of a lithified/solidified fault-rock with signs of crushed host-rock clasts, in addition mineralization of calcite can be found along smaller fractured and veins. The fault core zone in question has internal zonation where the narrow zones have different characters; zones labeled A-D (fig. 3.15). The host-rock, A), is well foliated and encompasses many brittle fractures, zone B) consists of fractured host rock with green (possibly chlorite) and white (calcite) mineralization in the fractures. Zone C) is a matrix of green (possibly chlorite) and white (calcite) minerals supporting smaller clasts of fractured host rock. Zone D) is a loose matrix of highly fractured host rock, where some of the larger fractures contains fine-grained fault gouge.
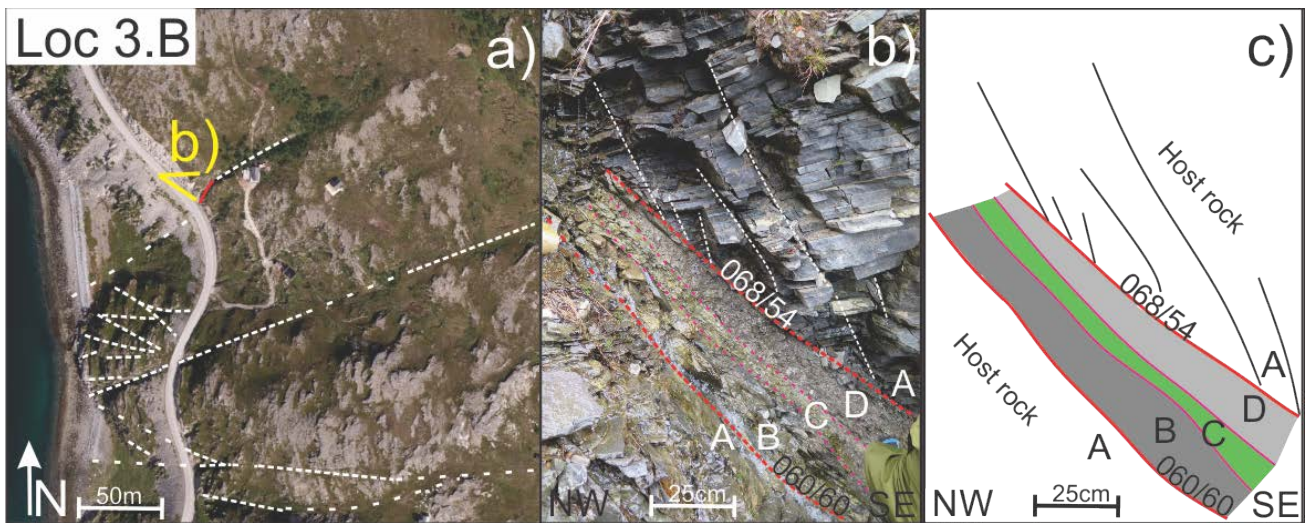
*Fig. 3.15. 1) Aerial photograph of location 3.B, white dotted lines indicate interpreted lineaments, red lines indicate fault surfaces, 2) photo of indicated in 1). Red dotted lines show fault surfaces, white/black dotted lines show fractures. Purple dotted lines separates the different zones: **A)** host rock, **B)** fractured host-rock with green and white mineralization (calcite) in small fractures and veins. **C)** Matrix of green and white minerals supporting clasts of fractured host rock. **D)** Matrix of highly fractured host rock, some of the larger fractures contain fine-grained fault-gouge.*

Kinematic data:

The kinematic data gathered in Area 3 - Snefjord, records slickensides on NE-SW and NW-SE striking faults and fractures. The NE-SW to E-W striking surfaces show mainly normal dip-slip (fig.3.12 A* & B*), as well as normal oblique-slip with dextral and sinistral sense of shear (fig. 3.12 A*). NE-SW striking surfaces display oblique-slip with sinistral sense of shear (fig. 3.12 A* & B*). E-W striking surfaces shows normal dip-slip (fig. 3.12 A* & B*). The N-S measurement displays normal oblique-slip with dextral sense of shear (fig. 3.12 C*).

3.4.4   Area 4 - Lillefjord

Field relations and rock description:

Area 4 - Lillefjord, is located in the areas near Lillefjord (fig. 3.1). Similar to Areas 1-3, the geology consists of rocks from the KNC as well as intrusive granites (fig 3.16), showing well-foliated sub-horizontal northwardly-dipping rocks. Ridges, gullies and escarpments follow the regional lineament trends and abundant rocky outcrops characterize the topography. The area comprises NW-SE to N-S, NE-SW and E-W striking faults steeply dipping in either direction relative to the strike. Krokneset only records NE-SW and WNW-ESE striking faults (fig. 3.16). Due to presumed salt weathering and sea erosion, no kinematic indicators where identified.
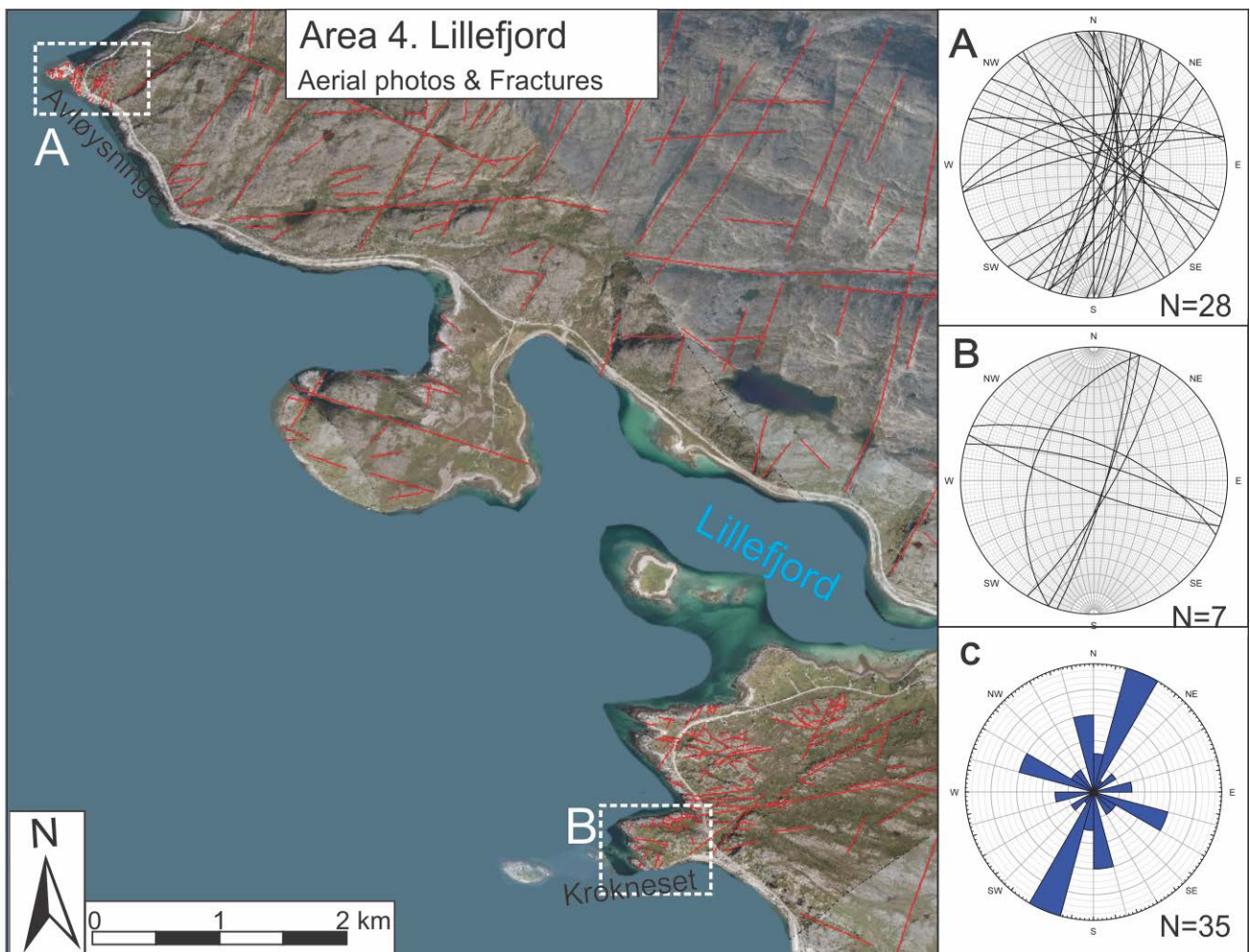
Fig. 3.16, Aerial photographs showing onshore data of Area 2 - Lillefjord. A- B: Lower-hemisphere Schimdt stereonet displays fracture orientation data from field localities. C) Rose plot showing fault-fracture strike distribution.

Lineaments:

Small-scale aerial photograph in this area (fig. 3.16 & 3.17) displays many well visible lineaments, both in aerial photos and DEM. The interpreted lineaments show a dominant E-W trend, followed by NE-SW and a small NW-SE striking trend. The lineaments show rhombic to conjugate geometries, made by NE-SW to N-S and E-W striking lineaments. E-W offsets NE-SW in some areas, whereas NW-SE offsets both E-W and NE-SW trends, in areas north of Lillefjord (fig. 3.16 & 3.17). South of the lineaments show anastomosing features, where NE-SW and NW-SE striking lineaments terminates in E-W and NE-SW striking lineaments. Both sides of Lillefjord record long (km scale) NE-SW to N-S striking lineaments cutting and offsetting (10 m scale) NW-SE and E-W striking lineaments (fig. 3.17).
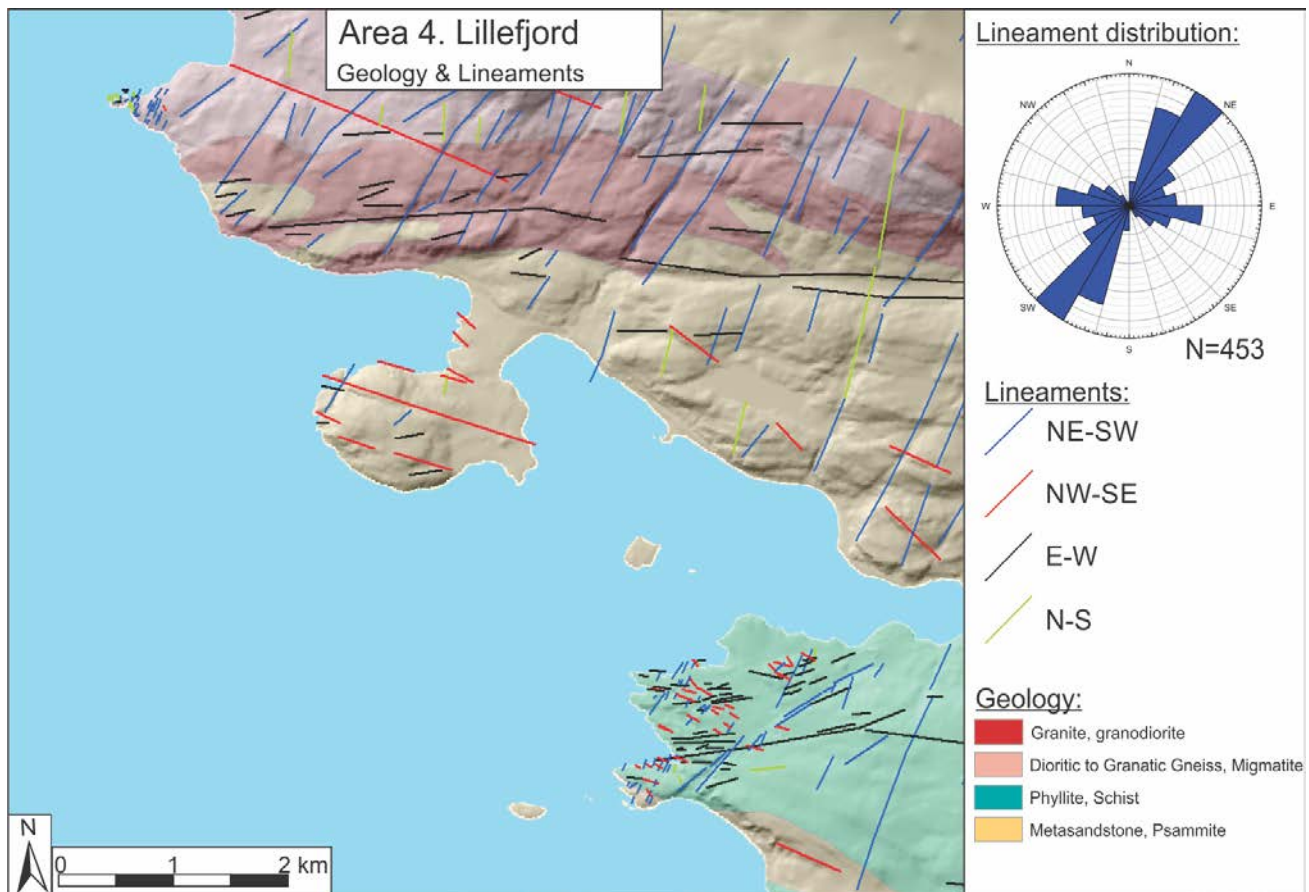
Fig. 3.17, Geologic map with lineaments interpreted from aerial images of Area 4, lineaments marked as colored lines, where the color indicate the trend, see legend. Rose plot displays the distribution of lineament trend. Geologic map modified from Roberts, D. (1981)

3.4.5   Area 5 - Honningsvåg

Field relations and rock description:

Honningsvåg is located on the northwestern parts of Magerøya, the locations visited includes the areas near Honningsvåg, Helneset, and Kamøyvær (fig. 3.1 & 3.18). The bedrock in the area consists of rocks from the Magerøy nappe (Kirkland et al., 2008), consisting mostly of meta-volcanic and meta-sedimentary (psammitic) rocks and igneous complexes (chapter 1.3) (fig. 3.19). The psammitic rocks are well foliated, with horizontal to sub-horizontal dip, while the gabbro and amphibolitic rocks are largely massive and homogenous.
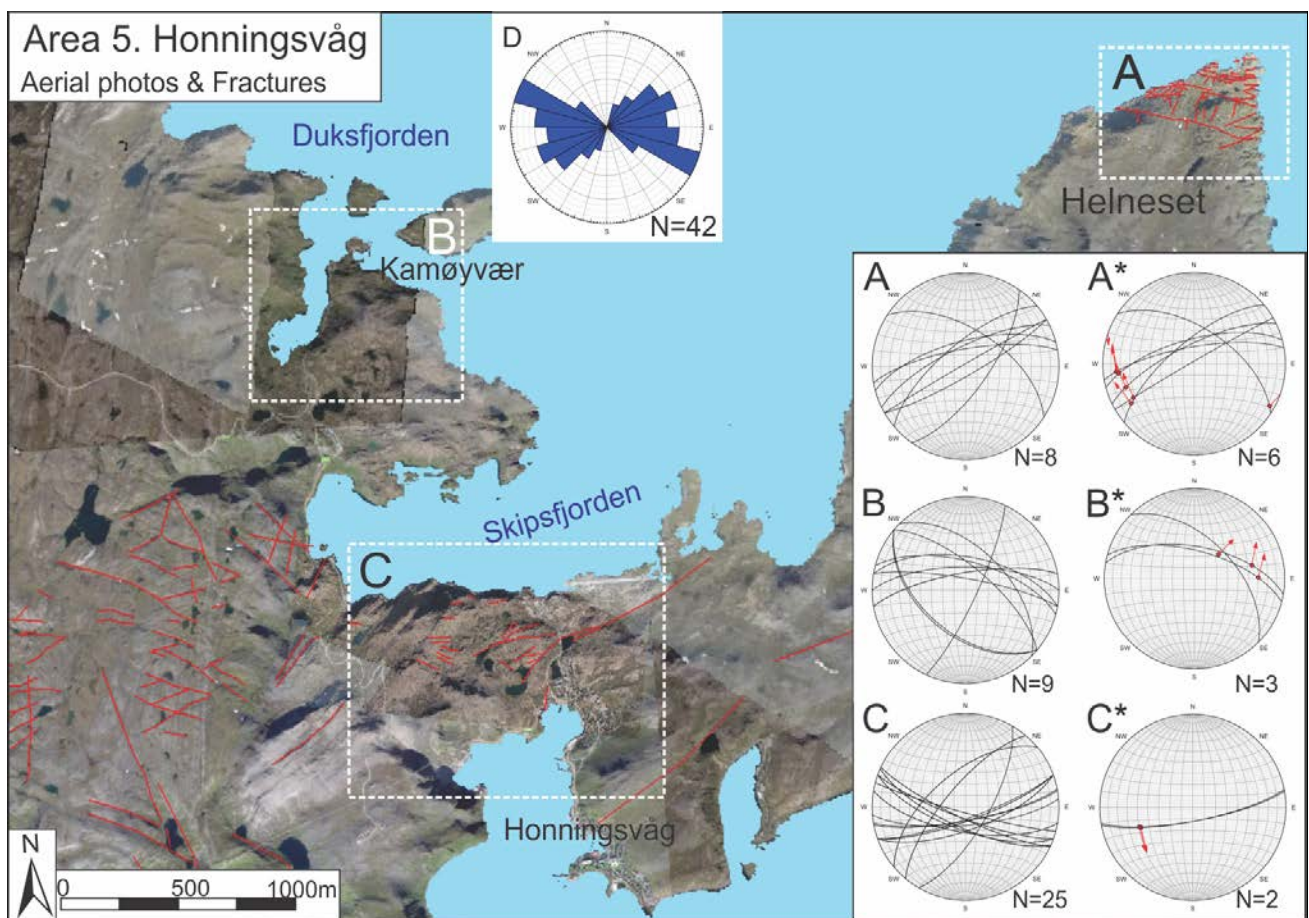
Fig. 3.18 Aerial photograph showing onshore data of area 5 - Honningsvåg. A- C; Kinematic data plotted in lower-hemisphere Schmidt stereonet showing slip lineation as tangent arrows (red) at intersection of M-plane and fault/fracture surface, indicating the displacement sense of the hanging wall. The strike and dip are represented by a great circle (black) (Vollmer, 2015). D) Rose plots of strike distribution of fault-fracture surfaces.

Lineaments:

As presented in chapter 2.1, the area contains large-scale lineaments displaying NW-SE and NE-SW trends (fig. 3.1 & 3.19). Small-scale aerial photographs shows dominantly WNW-ESE and ENE-WSW trends, as well as subsidiary N-S and E-W trends. West of Honningsvåg lineaments show NE-SW to E-W and NW-SE to N-S rhombic geometry, as well as horsetail geometry; single NW-SE lineaments splays out in several NW-SE to N-S oriented lineaments. The lineaments at Helneset show dominant E-W lineaments splaying out at the shoreline, cutting the NE-SW and N-S trends. Comparing the rose plot to the map view of the lineaments, not all areas are representative of the rose plot distribution, but rather that the orientation of lineaments change from location to location. Helneset shows a dominantly E-W to WNW-ESE trend, whereas the areas west and northwest of Honningsvåg show a more equal distribution between the two trends (fig. 3.19).
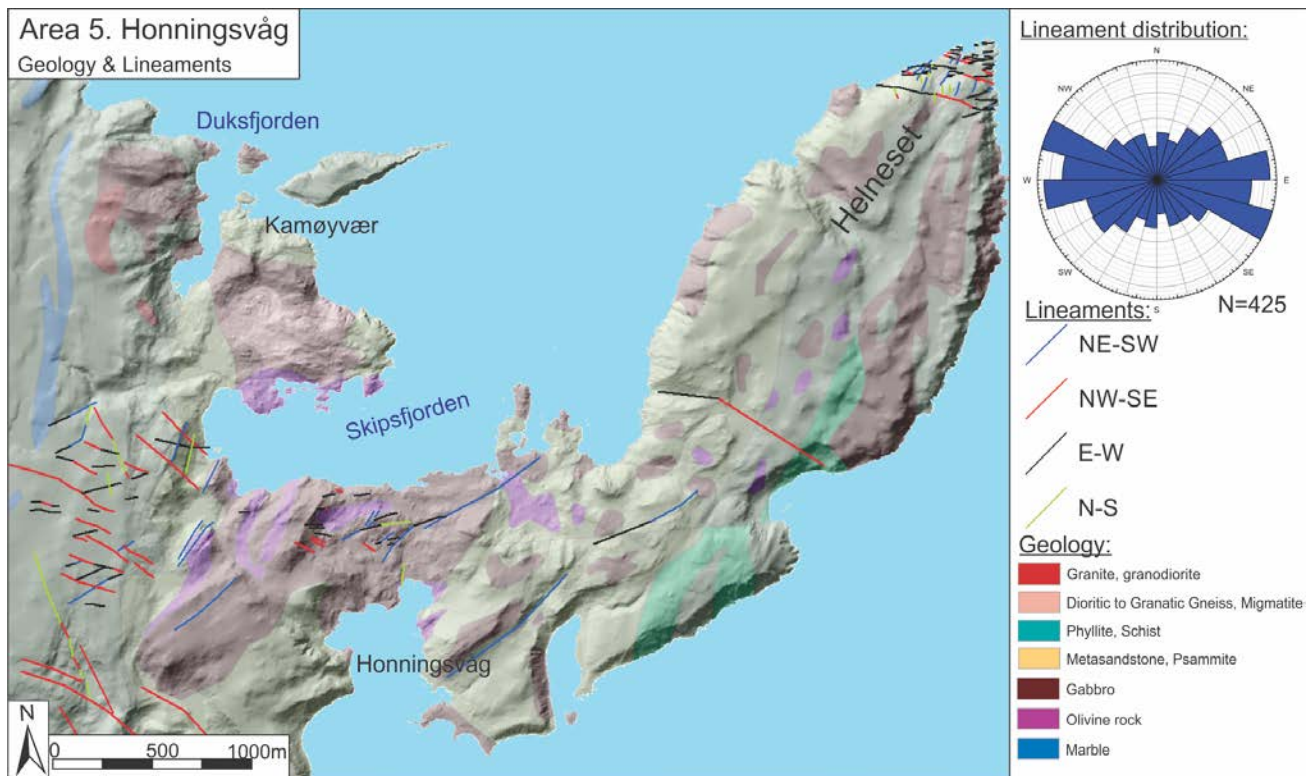
Fig. 3.19, Geologic map with lineaments interpreted from aerial images of Area 5 - Honningsvåg. Lineaments marked as colored lines, where the color indicate the trend, see legend. Rose plot displays the distribution of fault-fracture lineament trend. Geologic map modified from Roberts, D. (1981)

Description of onshore lineaments, brittle fractures and faults

Brittle fractures:

The faults and fractures observed in area 5, Honningsvåg, show two dominant and distinct strikes: 1) WNW-SES and 2) ENE-WSW, where ENE-WSW shows overlap with E-W striking fractures, minor variance in strike is seen throughout the area (fig. 3.18). Merging and crosscutting relationship are abundant at all strike-orientations, where splaying geometries are common (Fig. 3.20). The different localities show a difference in strikes; Helneset records NE-SW to ENE-SWS, Kamøyvær E-W to NW-SE, and Honningsvåg records ENE-WSW to WNW-ESE and NE-SW striking faults (fig. 3.18)
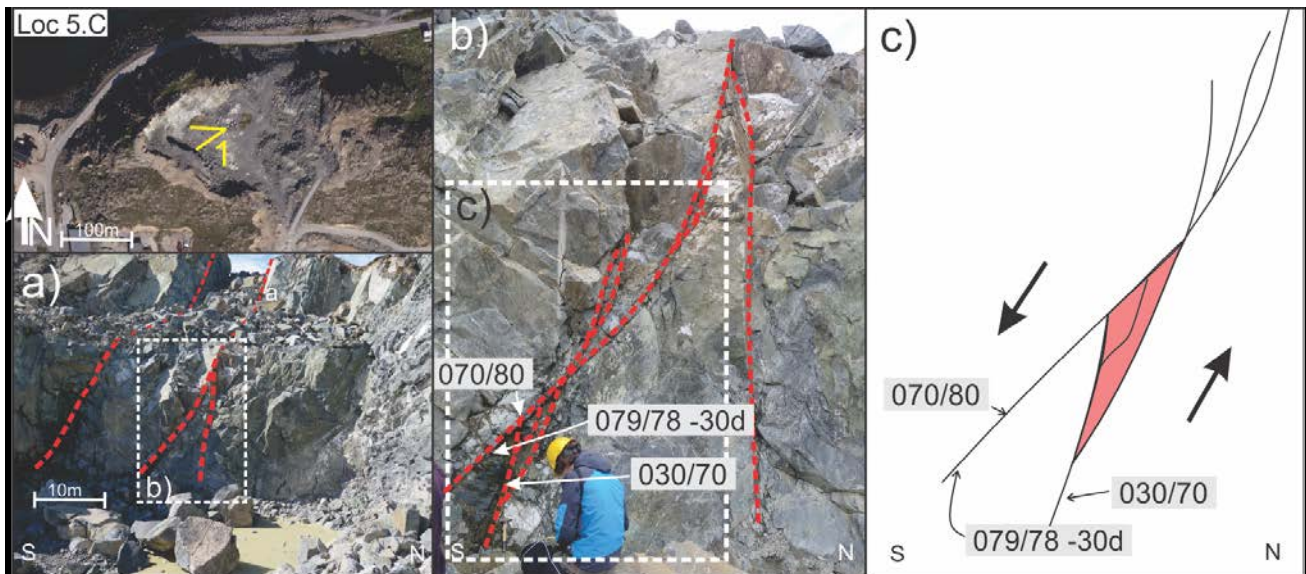

*Fig. 3.20, Loc 5.C, outcrop in rock-quarry near Honningsvåg airport. **a)** Overview photograph of outcrop containing ENE-WSW striking faults (dashed red) in quarry. **b)** Zoom in of fault interaction; note the downwards splaying of steep E-W striking fault (dashed red)), as well as interaction of fractures. **c)** Sketch of fault surface (black) interaction and movement-interpretation based on chlorite slicken fibers on footwall. Red zone marks highly fractured zone.*

Loc 5.C a rock quarry near Honningsvåg airport shows brittle faults with irregular surfaces that show various bending, interacting and overlapping geometries (fig. 3.18 and 3.21). The interaction of the two faults shows a crushed zone, with many fractures and green minerals, possibly chlorite.

Kinematic data:

Area 5 - Honningsvåg, record chlorite slickensides on several faults and fracture surfaces. These slickensides show with mineralization lineation along movement direction. The NE-SW to E-W striking faults show normal oblique-slip to strike-slip with sinistral sense of shear (fig. 3.18 A* & C*). NW-SE to WNW-ESE striking faults and fractures record normal oblique-slip and strike-slip with dextral sense of shear (fig. 3.18 A* & B*).

3.4.6   Area 6 - Gjesvær

Field relations and rock description:

This area is located on the northwest areas of Magerøya (fig. 3.1) and bedrock near Gjesvær and Nordkapp consists mainly of rocks from the Nordkapp nappe, whereas the areas near Gjesvær and the westernmost areas of Nordkapphalvøya consist of KNC (Kirkland et al., 2008), recording granite, migmatite, dioritic to granatic gneiss, phyllite, schists, psammite, metasandstone, marble, and monzonite (fig. 3.22). The bedrock comprise many brittle fractures and faults, as well as clearly visible lineaments on both DEM and aerial photographs.
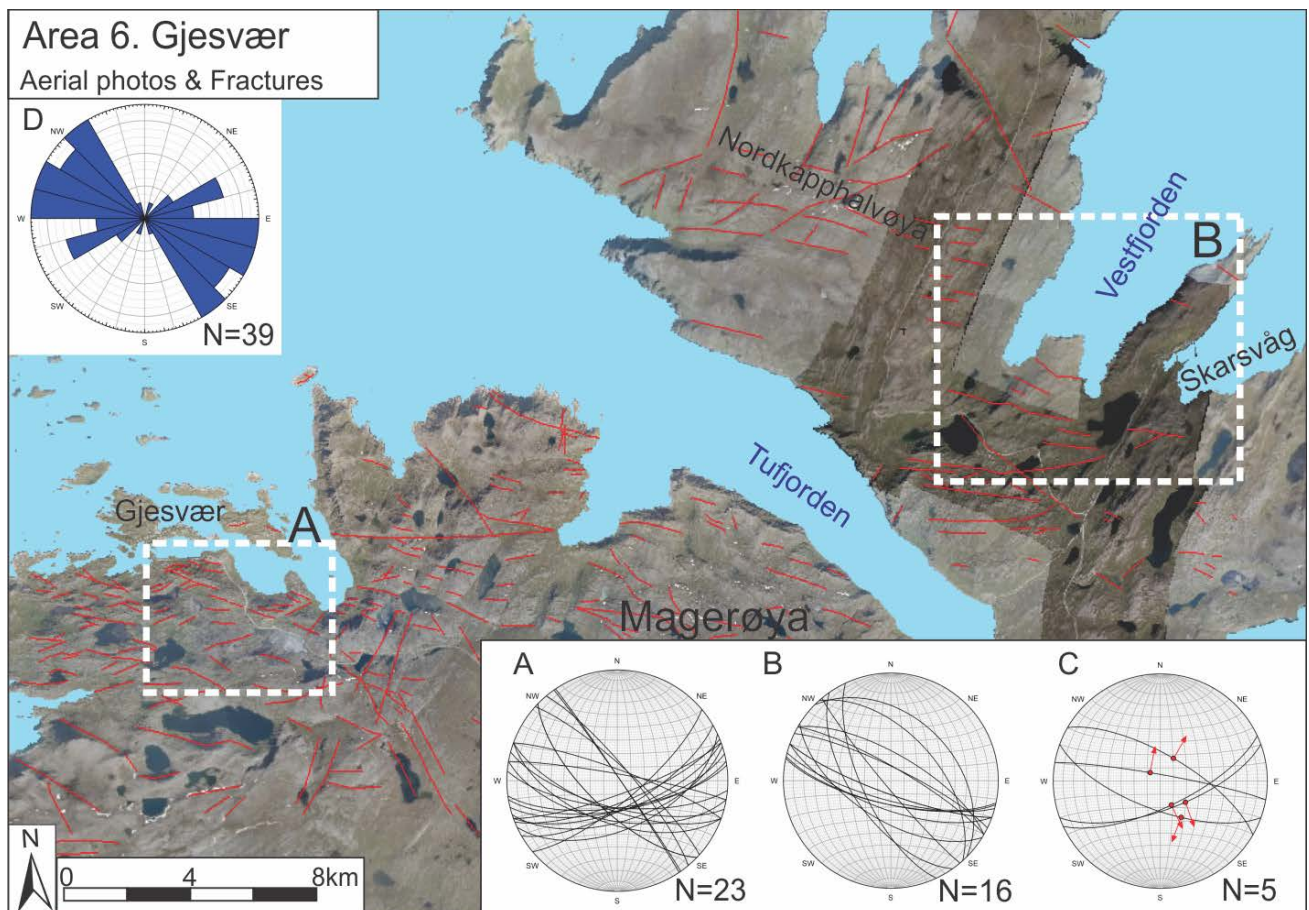
*Fig. 3.21 Aerial photographs showing onshore data of area 6, **A-B**; Lower-hemisphere Schimdt stereonet displays fracture orientation data from field localities. **C**; Kinematic data plotted in lower-hemisphere Schmidt stereonet showing slip lineation as tangent arrows (red) at intersection of M-plane and fault/fracture surface, indicating the displacement sense of the hanging wall, the strike and dip is represented by a great circle (**black**) (Vollmer, 2015). **D**; Rose plot of strike distribution of fault-fracture measurements.*

Lineaments:

The Northwestern parts of Magerøy record lineament with preferentially NE-SW to E-W trends (fig. 3.22). Longer (km scale) continuous lineaments trend mainly E-W and NW-SE (fig. 3.22). These follow escarpments and the main topography of the landscape. Long, NE-SW oriented lineament are also present. Near Gjesvær shorter (100 meter scale) NW-SE and E-W trending lineaments form a rhombic pattern, offset by the large continuous E-W, NE-SW to N-S and NW-SE trending fault-fracture lineaments (fig. 3.22). NE-SW and E-W trending lineaments on the Nordkapp Peninsula form a zigzag pattern, cut by the larger NW-SE trending lineaments (fig. 3.21 & 3.22).
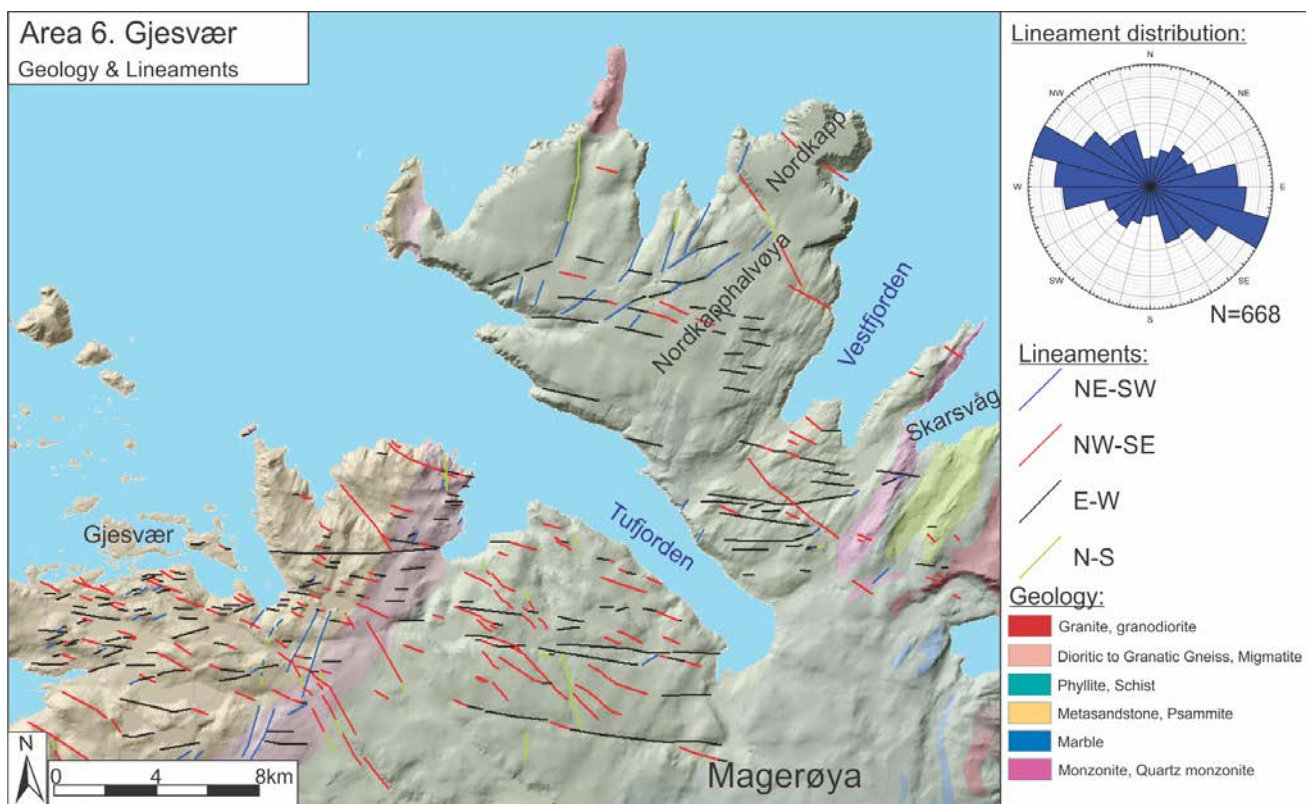

Fig. 3.22, Geologic map with fracture lineaments interpreted from aerial images of area 6, Gjesvær. Lineaments are marked as colored lines, where the color indicate the azimuth, see legend. Rose plot displays the distribution of fault-fracture lineament trend. Geologic map modified from Roberts, D. (1981)

Description of onshore lineaments, brittle fractures and faults

Brittle fractures and faults:

The brittle faults and fractures observed are preferentially NW-SE to E-W striking fault-fracture surfaces (fig. 3.21). At the Nordkapp Peninsula and near Skarsvågen, fractures strike mainly NE-SW to E-W, steeply dipping south and north respectively, while outcrops near Gjesvær record NW-SE, WNW-ESE and NE-SW striking fractures (fig. 3.21). The fractures striking NE-SW and WNW-ESE dips south, while NE-SW shows near vertical dip. Fault rocks are recorded at both localities, respectably fault gouge and cataclastic fault rock. Loc. 6.A, a road-cut in migmatized quarzitic meta-arkose records a number of faults striking ENE-WSW and dips steeply north, recording grey fault gauge (fig. 3.21 & 3.23).
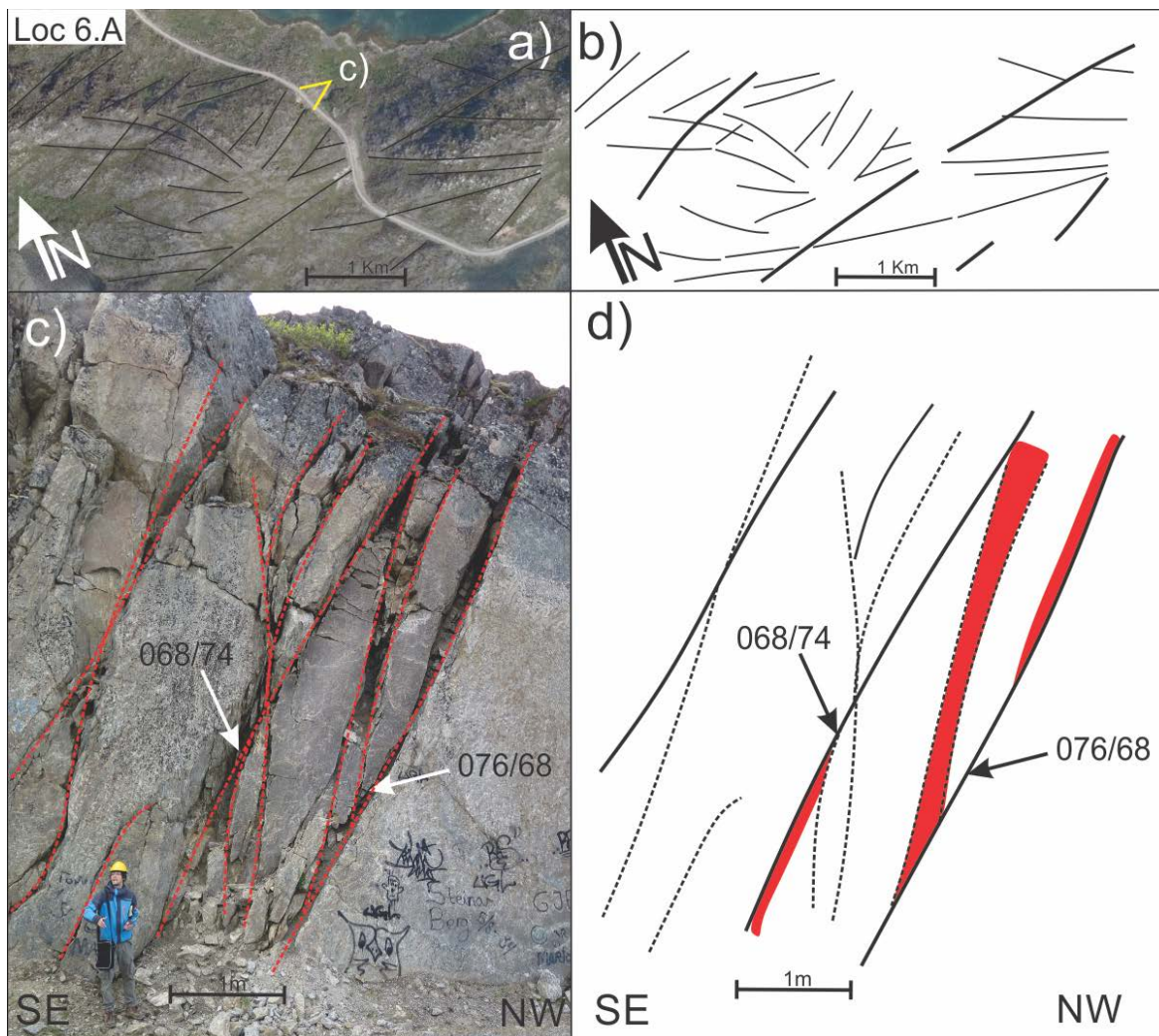
Fig. 3.23, Aerial image and outcrop photograph of brittle fractures and fault in a road-cut near Gjesvær a) Aerial photograph of area, yellow acute angle indicates outcrop locality, fault-fracture interpretation (solid black lines). b) Sketch interpretation of fault-fracture lineaments from aerial photo. c) Outcrop photograph showing interaction of NE-SW striking faults and fractures (red dashed lines). d) Sketch interpretation of b). Main ENE-WSW to E-W striking fault (solid black lines) secondary antithetic faults (dashed black lines) and faults recording fault gouge (red areas).

The WNW-ESE dipping steeply north fault at loc. 6.b is located in a gully, where WNW-ESE to E-S striking fractures and faults offset encloses the gully (fig. 3.24). One of the faults in the gully contains a dark green to gray colored cataclastic rock, with white mineralization of calcite visible in fractures surrounding the cataclasite (fig. 3.24).
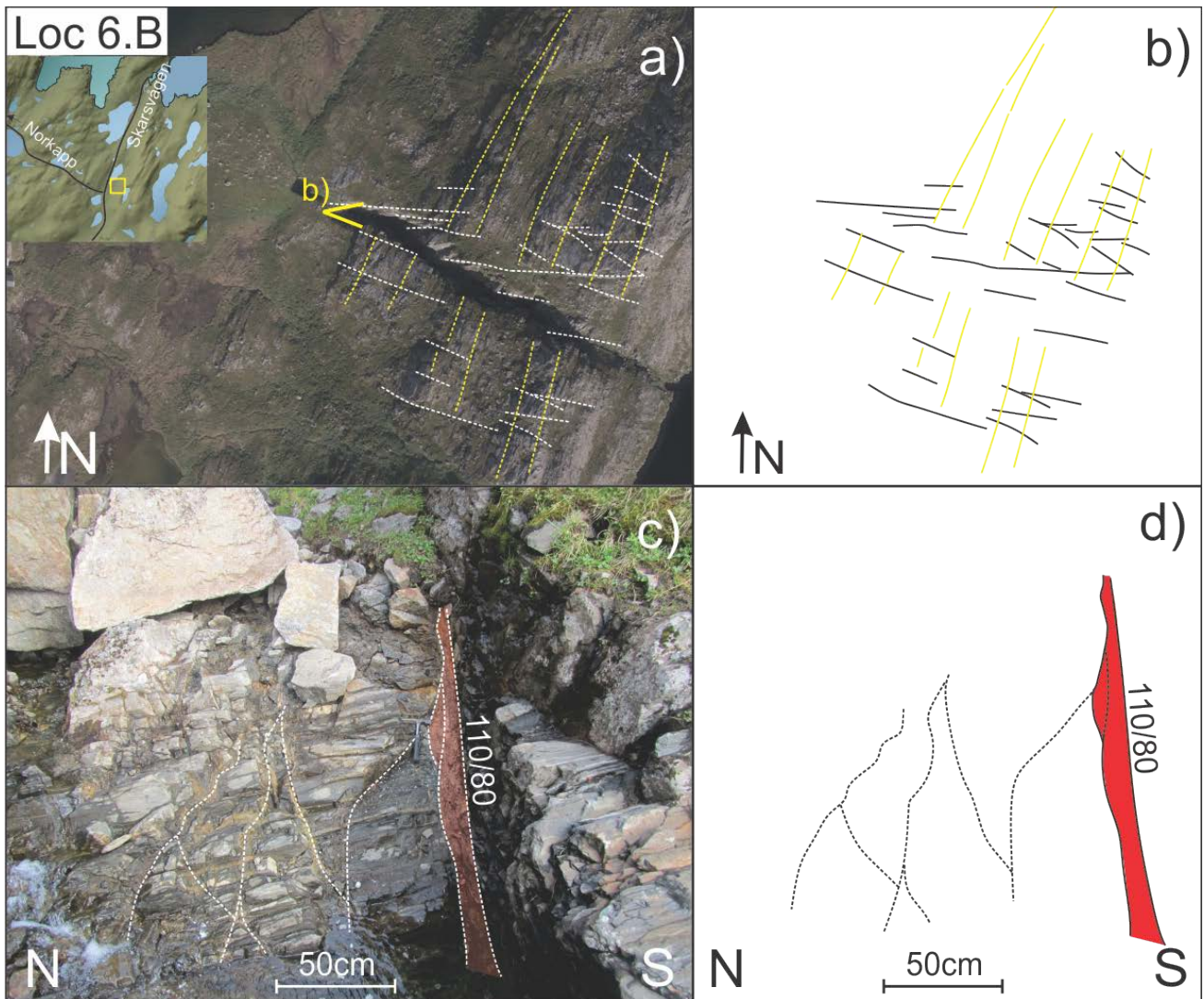
Figure 3.24. Aerial image and outcrop photograph of structures in loc. 6B, Skarsvågen a) Aerial photograph with fault-fracture lineaments (dashed white) and foliation (dashed yellow), acute angle indicates the photo locality of d) b) Sketch interpretation of a),Fault-fracture lineaments (solid black) and foliation(yellow) the right-hand stepping of lineaments along the gully and the sinistral offset of foliation. c) Outcrop photograph of dark green to gray cataclastic rock (far right) and fractures with mineralized calcite. d) Sketch interpretation of c), cataclastic rock (red) and fractures with mineralized calcite (black).

Kinematic data:

Some of the observed fault and fractures in Area 6 - Gjesvær, display surfaces with well developed chlorite slickensides, recording lineation fibers. ENE-WSW striking faults and fractures display normal dip-slip (fig. 3.21 C). WNW-ESE striking faults and fractures displays normal dip-slip to weak oblique-slip with sinistral sense of shear (fig. 3.21 C).

3.5   Summary of onshore brittle fractures and faults

Lineament data:

The fault-fracture lineaments interpreted from DEM and aerial images show random, parallel, rhombic, and anastomosing geometry throughout the study area. Where the dominant strike of the fault-fracture lineaments interpreted from regional DEM and small scale lineaments trends show 1) NE-SW, 2)NW-SE and 3) E-W trend in northwest Porsanger, and 1) WNW-ESE 2) ENE-WSW trend on Magerøy. Additionally, N-S trending lineaments can be observed throughout the study area, but appears in extension of NE-SW or NW-SE trending lineaments. The lineament data show an overlap with the fault/fracture strike-data collected at localities, where in most cases, fault and fractures can be traced in the extension from fractures observed in outcrops (e.g. fig. 3.7, 3.14, 3.23 & 3.24).

Fault and fracture data:

The faults and fractures measured at northwest Porsanger Peninsula show three dominant strike: 1) NW-SE, 2) NE-SW, and 3) E-W, in addition N-S striking faults and fractures are present, but not in abundance. The rose plot of all strike measurements on northwest Porsanger Peninsula shows an overlap from NW-SE, E-W to NW-SE strike (fig. 3.25). Kinematic data gathered from slickensides follows the same trends as the strike distribution. The kinematic data show that the three dominant strikes show distinct slip-data:

1) NE-SW striking faults and fractures show dominantly NW and SE dipping fault surfaces, with oblique-slip to dip-slip movement; in addition vertical surfaces show oblique-slip.

2) NW-SE striking faults and fractures show a more distributed dip, ranging from vertical to 45°, where sub-vertical to vertical are most dominant. The near vertical surfaces mostly oblique-slip, while the shallower

dipping surfaces exhibit dip-slip shear. The surfaces recording oblique-slip show both sinistral and dextral shear.

3) E-W striking faults and fractures record slickensides showing dip-slip, some surfaces show oblique-slip. In addition, the N-S striking surfaces records sub-vertical to vertical surfaces, showing dextral and sinistral oblique-slip, similar to NW-SE striking surfaces (fig. 3.25).
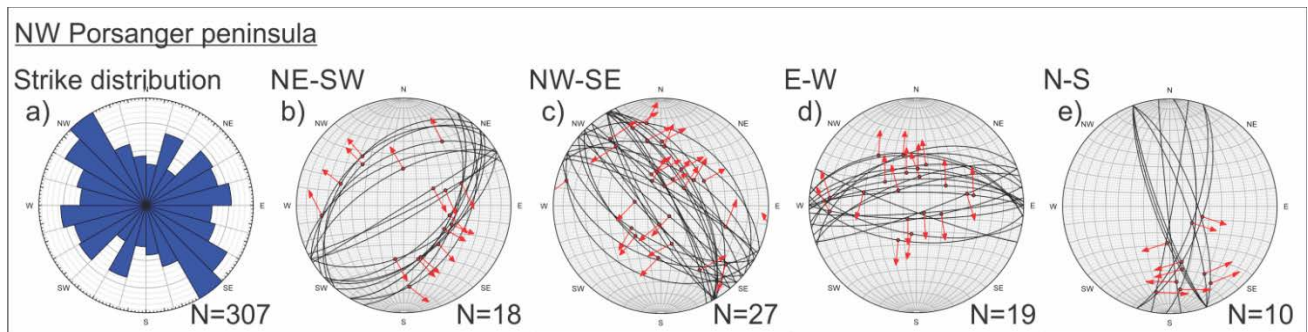
*Figure 3.25, Strike distribution and slip linear diagrams of slickensides plotted as tangent-arrows at the interaction of M-plane and strike-plane (red arrow and red dot), northwest Porsanger peninsula. **a)** Rose plot of fault/fracture strike measurements. **b)** NW-SW striking slickensides **c)** NW-SE striking slickensides. **d)** E-W striking slickensides. **e)** N-S striking slickensides.*

The rocks in Magerøy do not record as many slickensides as northwest Porsanger Peninsula. These rocks do exhibit signs of different fracture kinematics and strike distribution. The brittle fractures and faults measured show two distinct strike: 1) NW-SE to E-W and 2) ENE-SWS. The data from slickensides displays dominantly strike to oblique-slip at all strike orientations. However, there are several surfaces recording dip-slip to oblique-slip on all strike orientations.
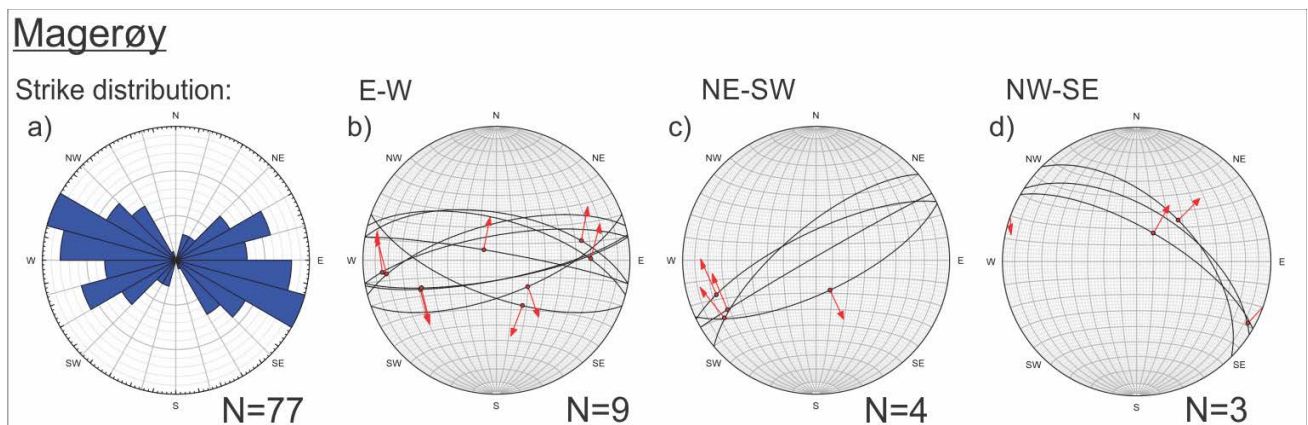
*Figure 3.26. Strike distribution and slip linear diagrams of slickensides plotted as tangent-arrows at the interaction of M-plane and strike-plane (red arrow and red dot), Magerøy. **a)** Rose plot of fault/fracture strike orientation. **b)** E-W striking slickensides **c)** NE-SW striking slickensides. **d)** NE-SW striking slickensides.*

Description of onshore lineaments, brittle fractures and faults

Summary

The study area shows a wide range of lineament, fault and fracture orientations, but there are certain strikes and trends that are more dominant, NE-SW, E-W and NE-SW. In addition, the data shows that there are several differences between Magerøy and northwest Porsanger Peninsula. However, it is possible to use the kinematic data and the dip angle to divide the fault and fractures into populations. The three most dominant strike directions are:

1) NE-SW strike with steep/moderate dip to the NW, ranging from NNE-SSW to ENE-SWS strike, primarily recording normal dip-slip movements, secondary normal-oblique slip with sinistral sense of shear (fig. 3.25). In addition, NE-SW striking faults on Magerøy records faults displaying strike-slip with sinistral sense of shear (fig. 3.26).

2) NW-SE strike with steep dip primarily to the NE and secondary to SW, ranging from NNW-SSE to WNW-ESE strike, primarily recording normal-oblique to strike-slip movement with dominantly sinistral sense of shear, and secondary dip-slip movement (fig. 3.25).

3) E-W strike and dominantly steep N dip, ranging from ENE-WSW to WNW-ESE strike, primarily recording normal dip-slip movement (fig. 3.25). In addition, normal oblique-slip to strike-slip with both sinistral and dextral components at Magerøy (fig. 3.26).

4   Description of bathymetric data

4.1   Introduction

The bathymetric data presented were gathered from parts of the MAREANO survey, which has a resolution of 25x25 m(see details in chapter 2), allowing many detailed features to be recognized on the shallow portion of the Finnmark Platform (fig. 4.1). According to Indrevær et al. (2014), the bedrock and structures present on the seafloor on the shallow strandflat off the coast of western Troms is a continuation of the rocks and structures found onshore in the same area (described in chapter 1.3.7). We attempt to test if similar conclusions can be drawn for the Finnmark Platform areas (fig. 4.1), enabling a comparison of lineaments interpreted onshore and offshore. This is important as it allows comparison and correlation of onshore-offshore data.

Large-scale bathymetric data from the shallow shelf (strandflat) to shelf edge (Finnmark platform) show deep fjords, drainage channels, moraines, rocky outcrops and marine sediments deposited in troughs and linear depressions below the seafloor (fig. 4.1). Coastal areas also show widespread glacial drainage and erosional patterns following the same trends of the fjords and offshore valleys (fig. 4.1). Bathymetric data covering the study area have been analyzed and interpreted, and forms a database for further description and analysis (fig. 4.1). The database records the bathymetric lineaments and consist of up to 4000 individual lineament lines, thus representing a base for further discussion in chapter 6.3. The study area has been divided into four smaller subareas, labeled A-D, to avoid confusion with onshore areas. The marine geomorphology of areas will be described in the following order, 1) Large scale bathymetric lineaments in the study area, including marine areas near Magerøya and northwest Porsanger Peninsula, 2) the subareas Hjelmsøy (A), Gjesvær (B), Helneset (C), Snefjord (D) followed by a summary and a preliminary interpretation.

4.2   Large-scale bathymetric lineaments

The large-scale lineaments have been identified and analyzed from the 25x25 m bathymetric data (fig. 4.1). The study area is heavily influenced by glacial activity. The glacial flow direction coincide with many of the regional lineaments seen in the study area. The fjords, sounds, channels and depression in the study area generally show linear attitudes with the same orientation as the glacial flow direction (fig. 4.1). However, the presumed fault-fracture lineaments do not show the same linear trend as the glacial flow directions. The tectonic lineaments follow a more zig-zag pattern, where the walls display clear reflections and jagged features, indicating they occur in crystalline bedrock, and not in glacial sediments. Rocky outcrops and escarpments in the study area continue the same trends found onshore, and are often seen as an extension of similar features found onshore. These escarpments follow NE-SW and E-W trends (Fig 4.1). In addition, the regional bathymetric lineaments have a dominant E-W followed by NW-SE and NE-SW trend, where the bathymetric lineaments can be seen as a continuation of onshore large-scale fault-fracture lineaments (fig. 4.1). The smaller-scale lineaments interpreted in the study area show distinct trends, that shows a variance in the areas around Magerøy and northwest Porsanger Peninsula (fig 4.1, a-b), NW-SE to E-W, NE-SW striking lineaments can be seen on both rose plots, where the most dominant trend NW-SE near Magerøy, and E-W near northwest Porsanger Peninsula. Both areas record E-W striking lineaments (fig. 4.1, a-b).

The coastal areas around northwest Porsanger and Magerøya is characterized by a shallow shelf (strandflat) with depressions, escarpments, glacial erosional and depositional features and many fractures (fig. 4.1). The sound between Måsøy and Magerøy, defining the boundary between Magerøya and Northwest Porsanger Peninsula, shows a deep fjord with steep irregular enclosing walls, striking NW-SE, NE-SW and E-W, of what seems to be fragments of crystalline bedrock. On the Northeast side of Magerøy, northeast of Helneset, the strand-flat shows numerous examples of rounded ridges tapering off from tops and points, channels and scour marks, as well as distinct fractured heights. In the areas east of northwest Porsanger Peninsula, points, peninsulas, and ridges appears to continue under sea level, as plateaus with similar outline as the onshore landforms, as seen from Skjarvodden to Havøysund.
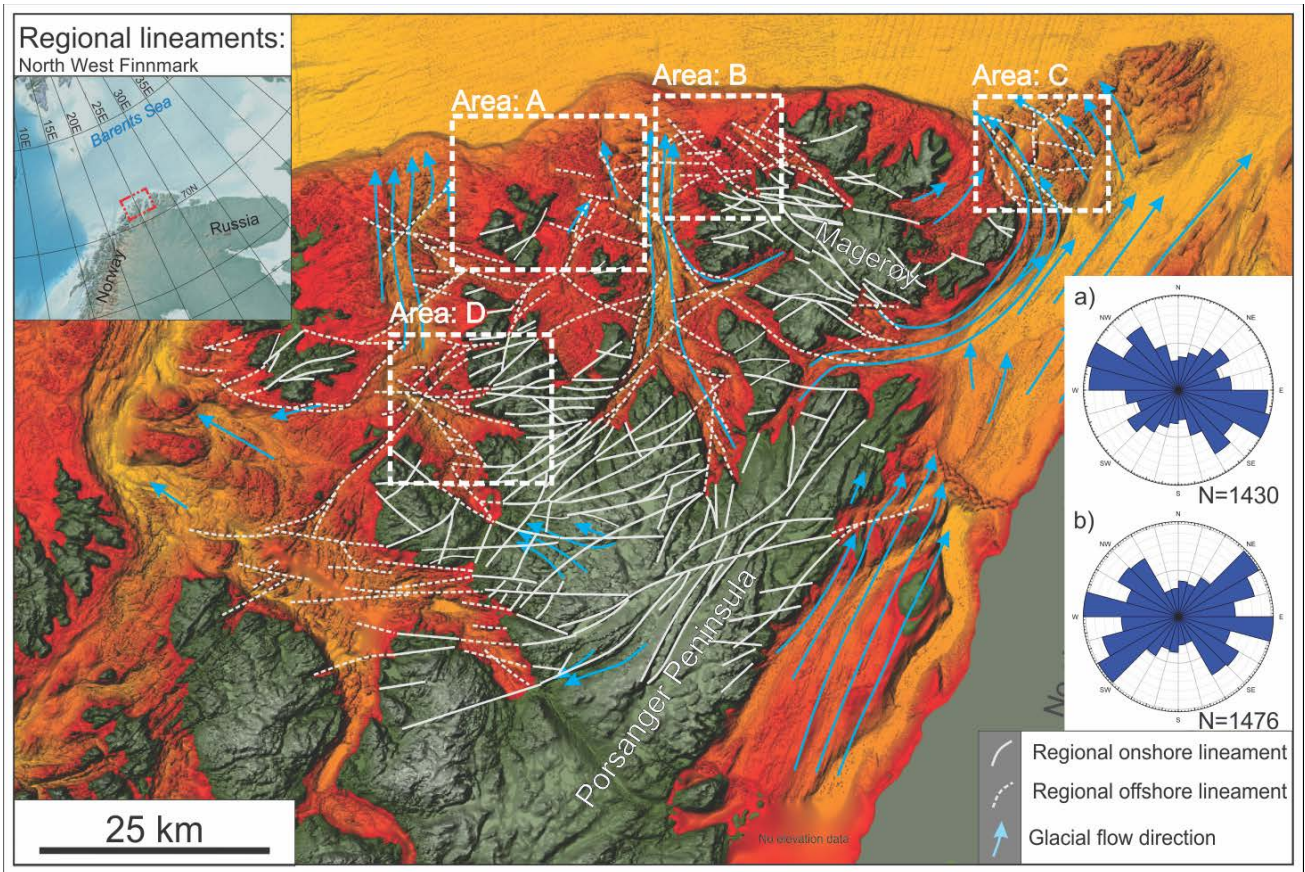
*Fig. 4.1, DEM and bathymetry of the study area, with interpreted lineaments as white lines. **a)** rose plot of lineament distribution on the coastal areas near Porsanger Peninsula. **b)** Rose plot of bathymetric lineament distribution on the coastal areas near Magerøya. **A-D)** Locations of the sub-areas presented in later in this chapter.*

4.3   Area A - Hjelmsøy

The area northeast of Hjelmsøy is characterized by parallel ridges, troughs, channels, smaller basins, and linear erosional features, and rounded featured such as troughs and heights are observed (fig. 4.3). Several features on the strandflat are observed: NE-SW trending parallel ridges and troughs, crosscut by NE-SW and E-W striking channels and northeast of Hjelmsøy (fig. 4.2 & 4.3). The NW-SE and E-W trending channels form rhombic patterns, whereas the NE-SW to N-S trending channels wedge and taper into the E-W trending ridges (fig. 4.3). Larger rhombic to square depressions are seen, bound by NW-SE, NE-SW and E-W trending escarpments, where the escarpments of the depressions show similar trend.

The rose plot shows a predominantly WNW-ESE distribution, in a continuous area from NW-SE to E-W, also a small contingency of NE-SW trending lineaments are present (fig. 4.4). Comparing the rose plot and the geometry seen in the map-view, the lineaments main NW-SE and E-W trend makes up small rhombic patterns cut by NE-SW to N-S trending lineaments.
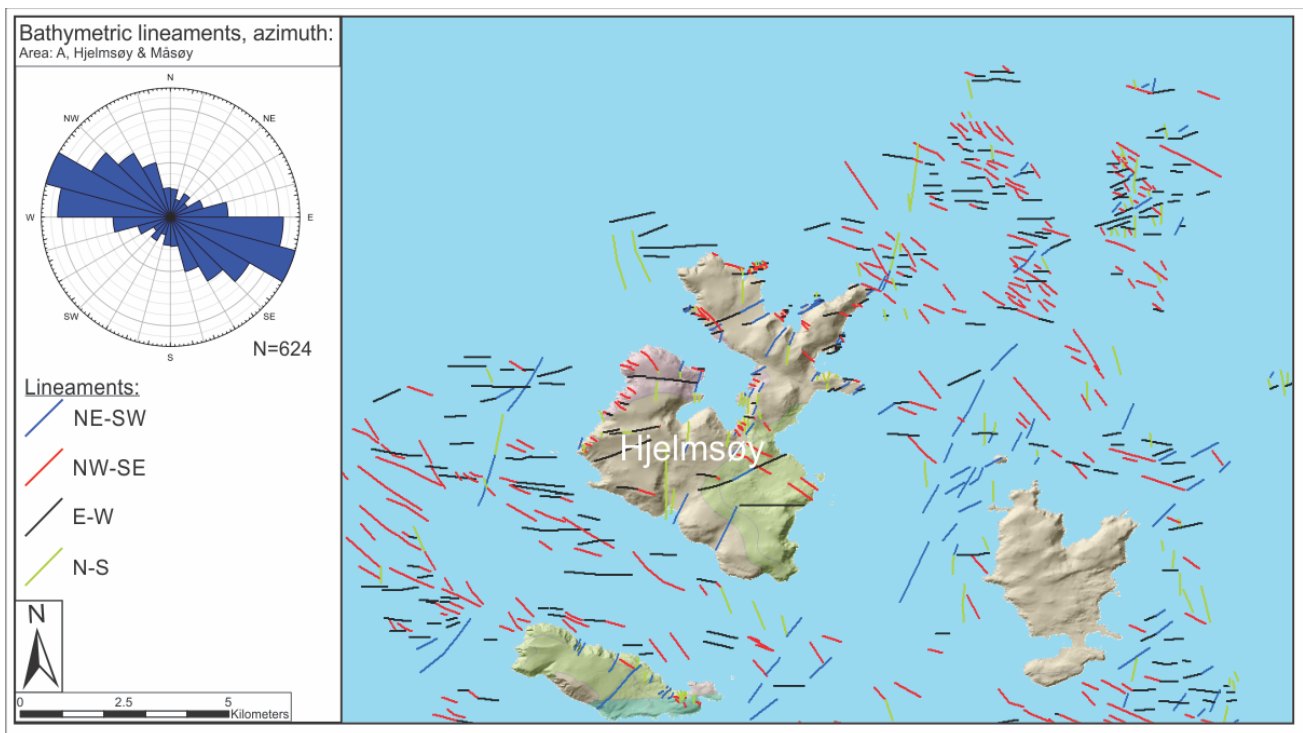
Fig. 4.2, Interpreted bathymetric data of Hjelmsøy area. Azimuth of lineaments indicated by different colored lines. Rose plot shows the distribution of Lineament azimuth.
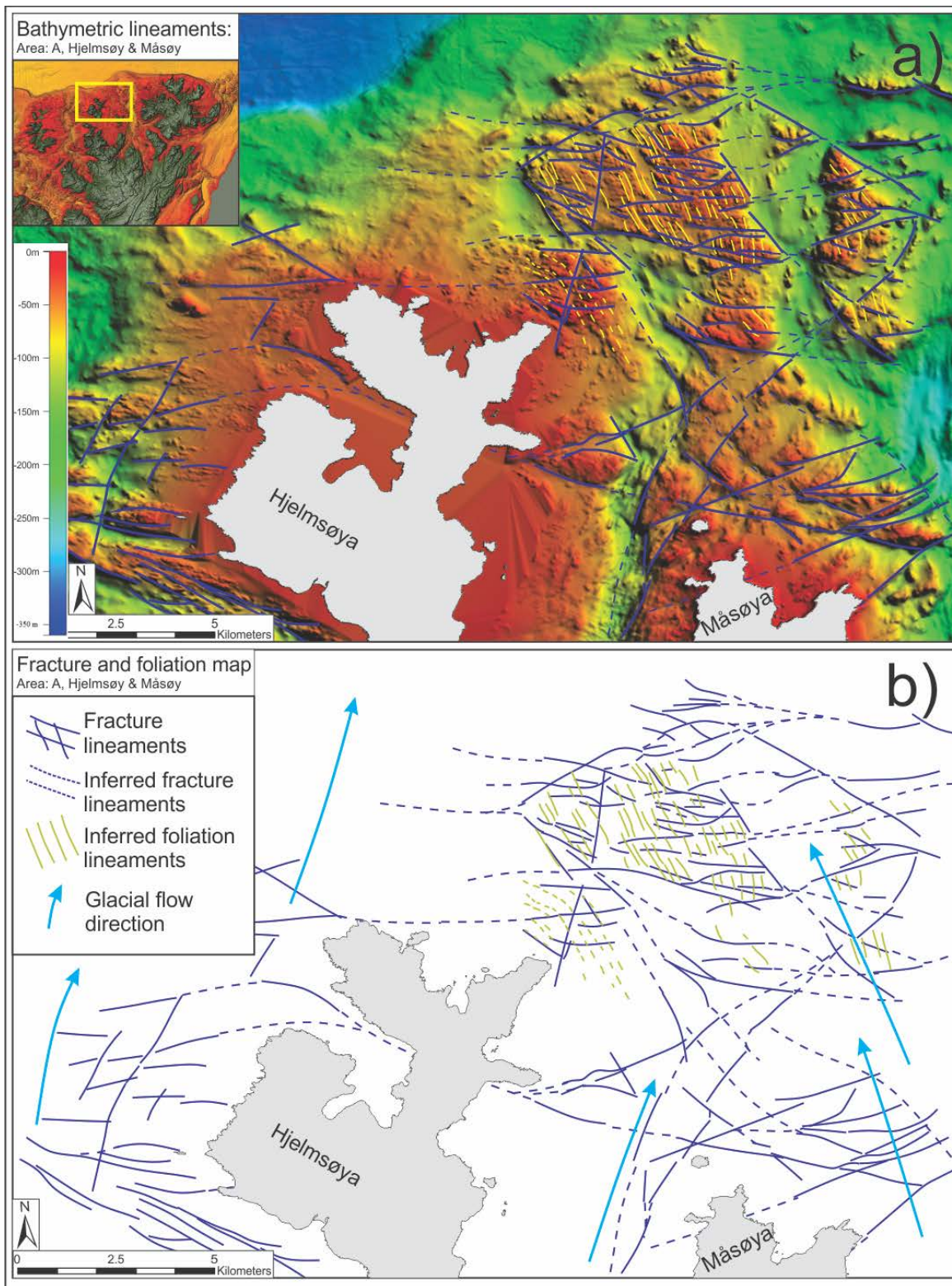
Fig. 4.3 Bathymetric map and sketch interpretation of lineaments in Area B, near Hjelmsøy. **a)** Bathymetric surface, blue lines indicate lineaments, parallel ridges and troughs indicated by yellow lines. **b)** Interpretation of lineaments. Fault-fracture lineaments interpreted as solid blue lines, dashed lines indicate inferred fault-fracture lineaments. The parallel ridges and troughs are interpreted as foliation in the crystalline bedrock.

4.4   Area B - Gjesvær

The area near Gjesvær comprises the similar features as Hjelmsøy (Area A), where NW-SE, NE-SW and E-W trending ridges, troughs, and peaks characterize the strandflat, NE-SW to N-S trending parallel ridges and troughs are seen in the areas northeast of Gjesvær and east of Knivsjelodden. The area north of Gjesvær consist predominantly of E-W and NW-SE trending escarpments. Tufjorden is characterized by NW-SE to E-W trending escarpments, bounding rhombic and parallel depressions, trending along the glacial flow direction (fig. 4.4).

The lineaments distribution (fig. 4.4), displays three dominant trends, where the NE-SW, NW-SE and E-W. In addition, N-S trending lineaments are present, mainly in the outlet of Tufjorden. The geometry of the fractures are predominantly rhombic, contained by NE-SW to E-W and NW-SE trending lineaments, similar to the geometry found onshore near Gjesvær.
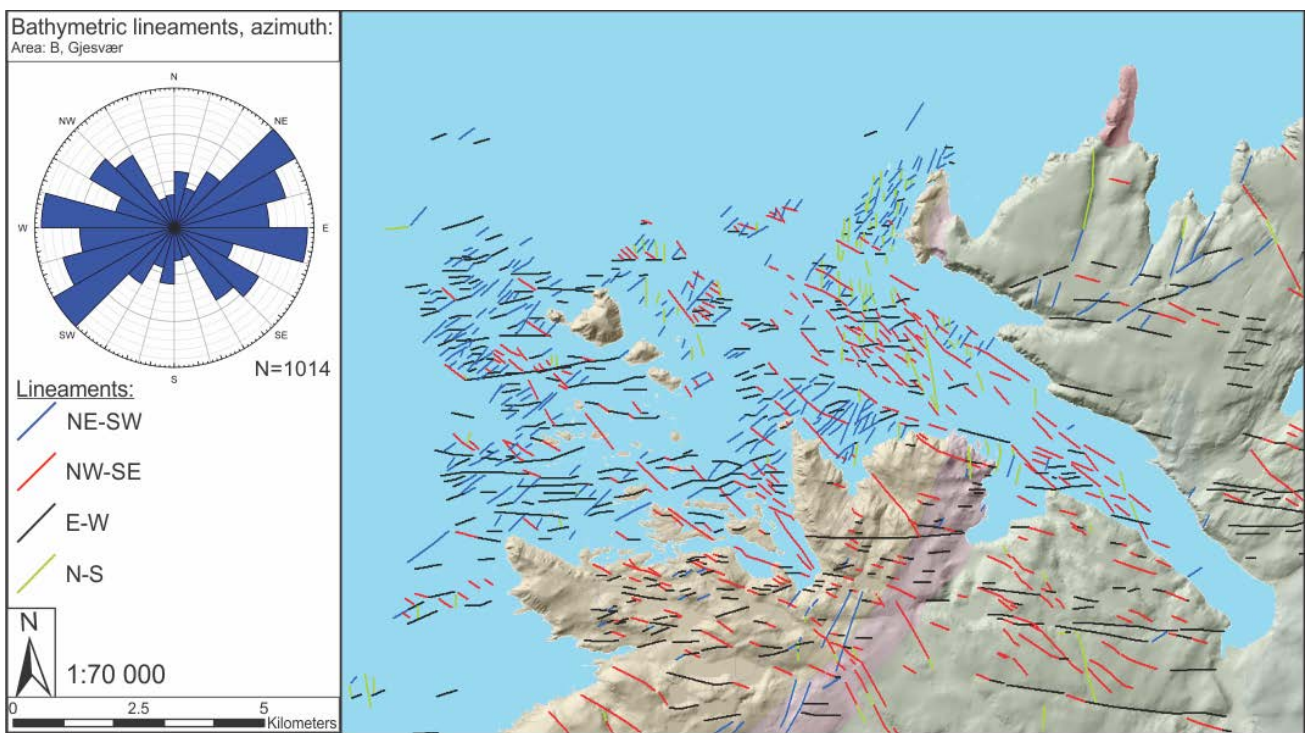
Fig. 4.4, Bathymetric data of Gjesvær area. Azimuth of lineaments indicated by different colored lines. Rose plot shows the distribution of bathymetric lineaments
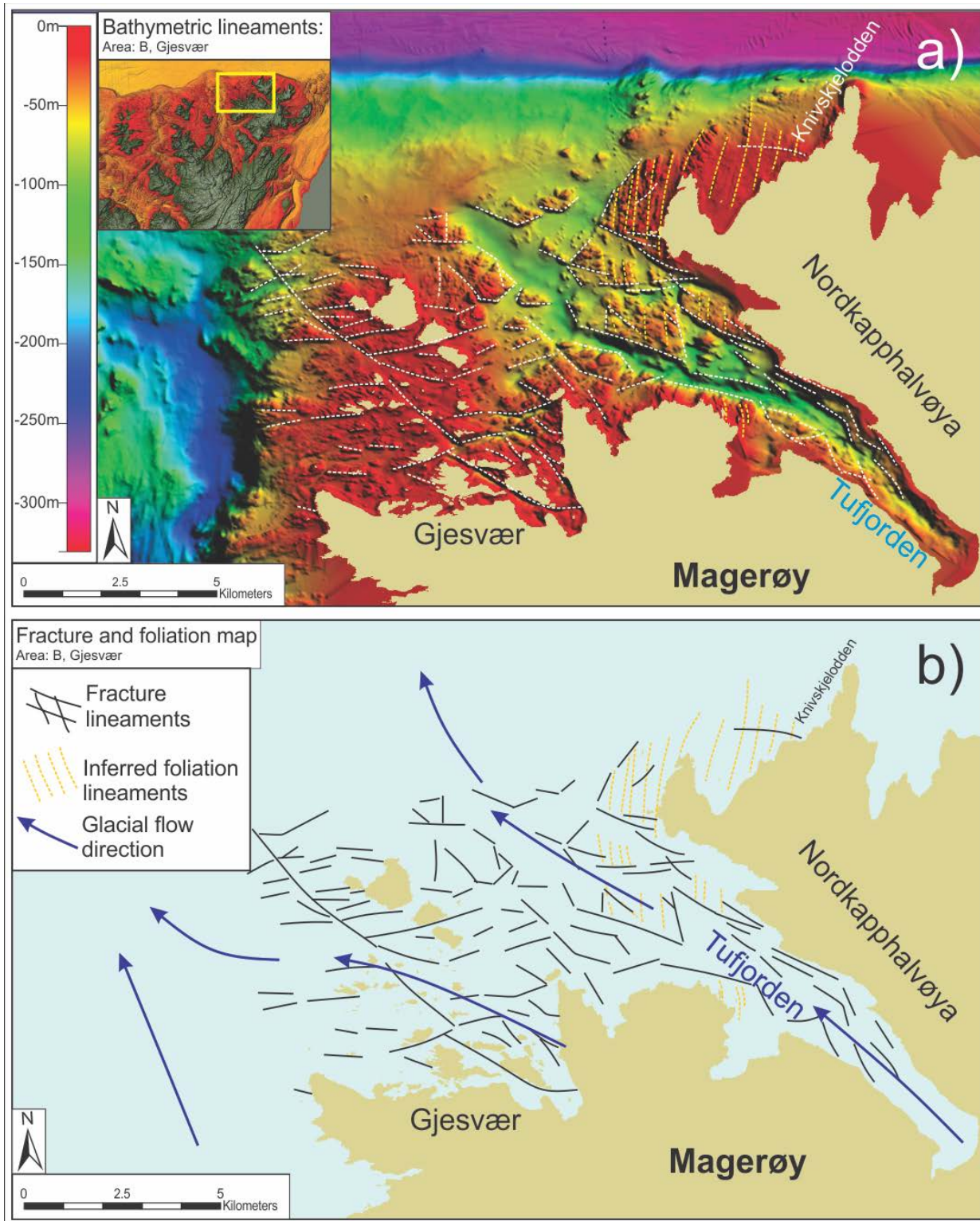
Fig. 4.5, Bathymetric map and interpretation of lineaments in Area B, near Gjesvær, a) bathymetric surface, white dashed lines indicate lineaments, parallel ridges and troughs indicated by yellow lines b) Interpretation of lineaments. Fault-fracture lineaments interpreted as solid black lines, dashed yellow liens indicate parallel ridges and troughs, and is interpreted as foliation in the crystalline bedrock.

4.5   Area C - Helneset

The marine areas northeast of Helneset encompasses ridges, troughs, channels, escarpments, and depressions. Compared to the other areas, this strandflat displays more rounded peaks, ridges, and channels running parallel to the glacial flow direction (fig 4.7); NW-to E-W and NE-SW trending escarpments characterizes the rounded topography.

The interpreted bathymetric lineaments northeast of Helneset show a predominantly NW-SE to E-W distribution (fig. 4.6), as well as a distinct NE-SW striking trend. The geometry of the lineaments shows a variance throughout the area, the fjord NW of Helneset show rhombic to linear ridges and lineaments, whereas the areas northeast of Helneset displays a rhombic shapes oriented NW-SE near Helneset, and parallel to sub-parallel lineaments further to the northeast.
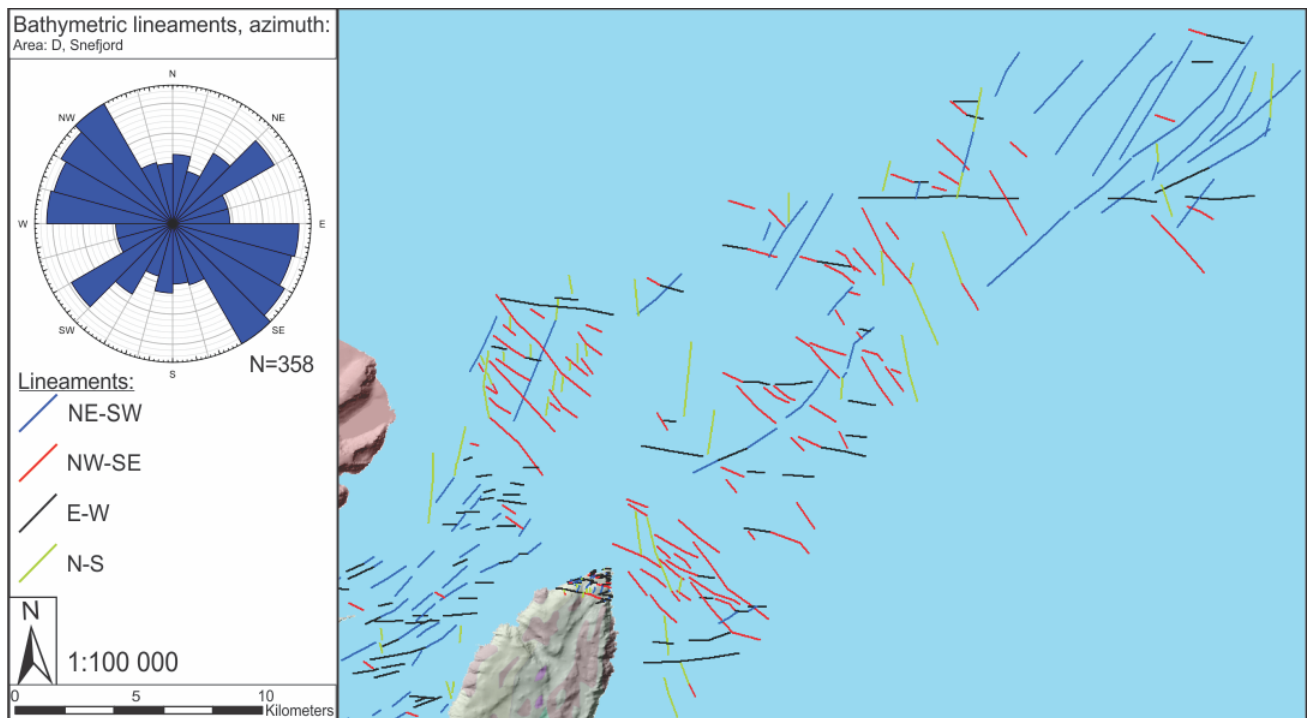
Fig. 4.6 Bathymetric data of Helneset area. Azimuth of lineaments indicated by different colored lines. Rose plot shows the distribution of Lineament azimuth
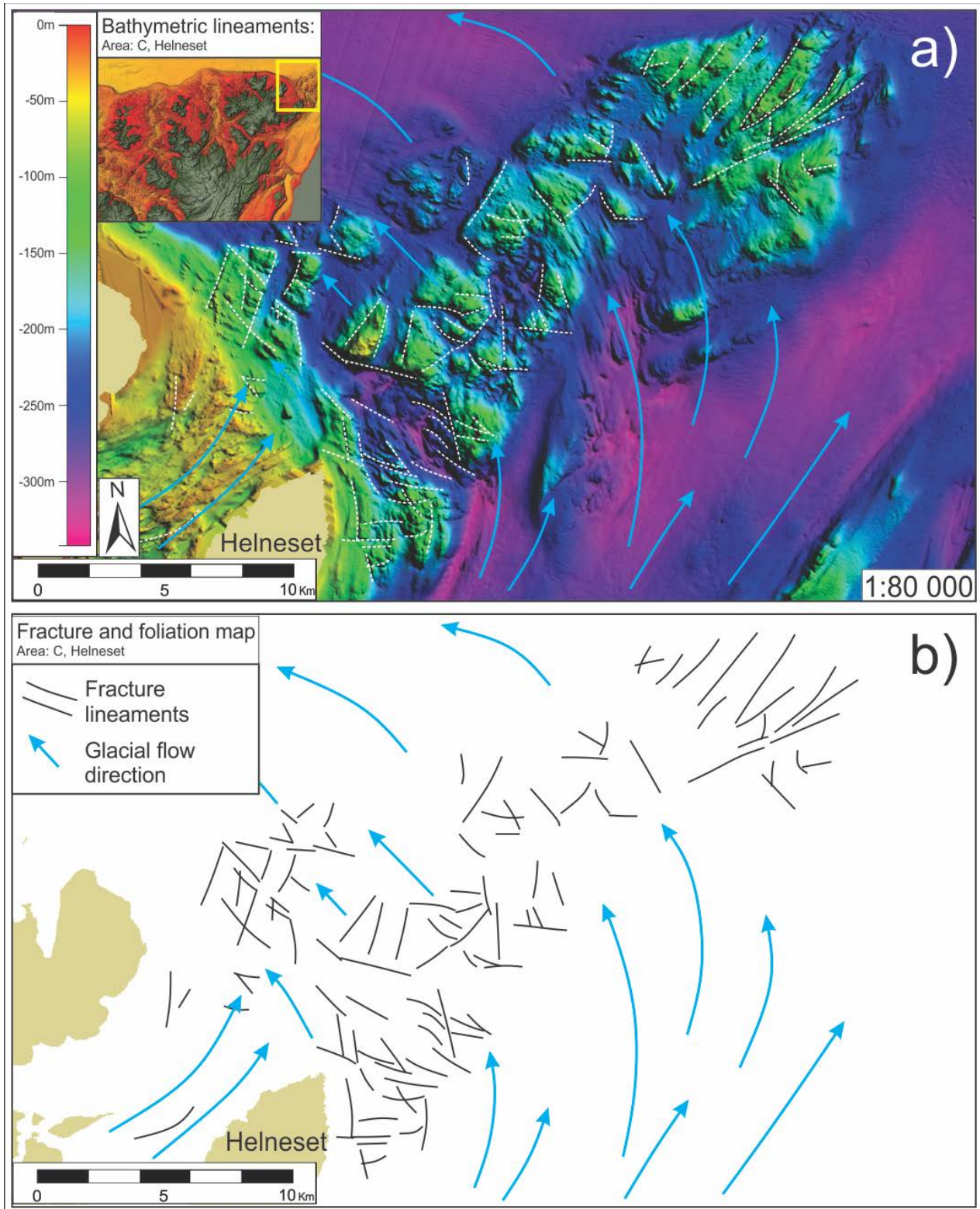
Fig. 4.7 Bathymetric map and interpretation of lineaments in Area C, near Helneset, a) bathymetric surface, white dashed lines indicate lineaments, parallel ridges and troughs indicated by yellow lines b) Interpretation of lineaments. Fault-fracture lineaments interpreted as solid black lines. Glacial flow direction indicated by blue arrows.

4.6   Area D - Snefjord

Parallel ridges and troughs, crosscut by NE-SW, NE-SW and E-W trending channels, characterize the strandflat near Snefjord. Smaller basins, linear channels, flutes and sedimentary deposits characterizes the deeper sections (fig. 4.9). From the extension of Skjarvodden, a NW-SE deep channel splays into NE-SW striking escarpments and lineaments, that continue into Selvika, Bakfjorden and the tip of Skjarvodden. Similar larger channels can be seen in the outlet of Myrfjorden and Snefjord, where the lineaments connects with similar striking onshore lineaments and escarpments (fig. 4.9).

The bathymetric lineaments in this area show three distinct trends (fig. 4.8), where the most dominant are NW-SE and NE-SW, as well as a smaller group of WNW-ESE and E-W striking lineaments. The geometry of the lineaments differs throughout the area, where lineaments on the strandflat near Skjarvodden show a rhombic shape, the lineaments in Snefjord displays a rectangular to sub-rhombic shape, with some cross-cutting lineaments.
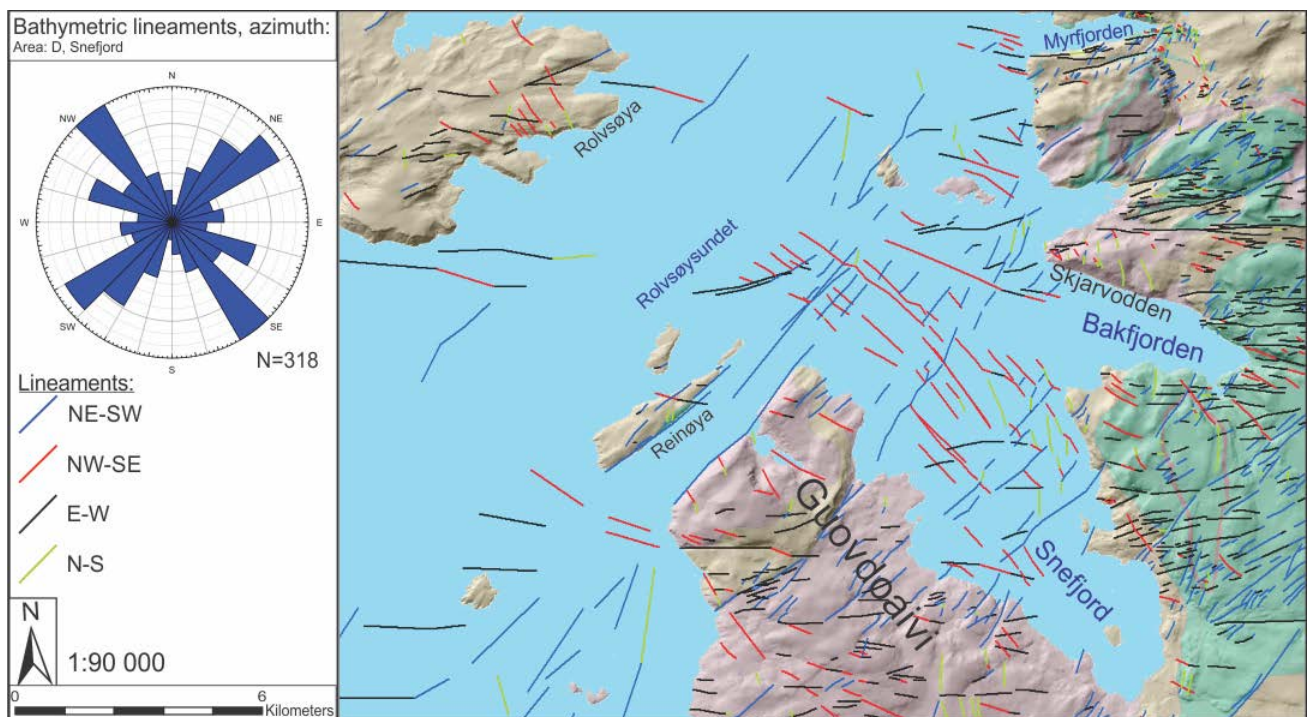
Fig. 4.8, Area D, Snefjord. Distribution of bathymetric lineaments, trend indicated by color. Note the continuation of onshore lineament offshore.
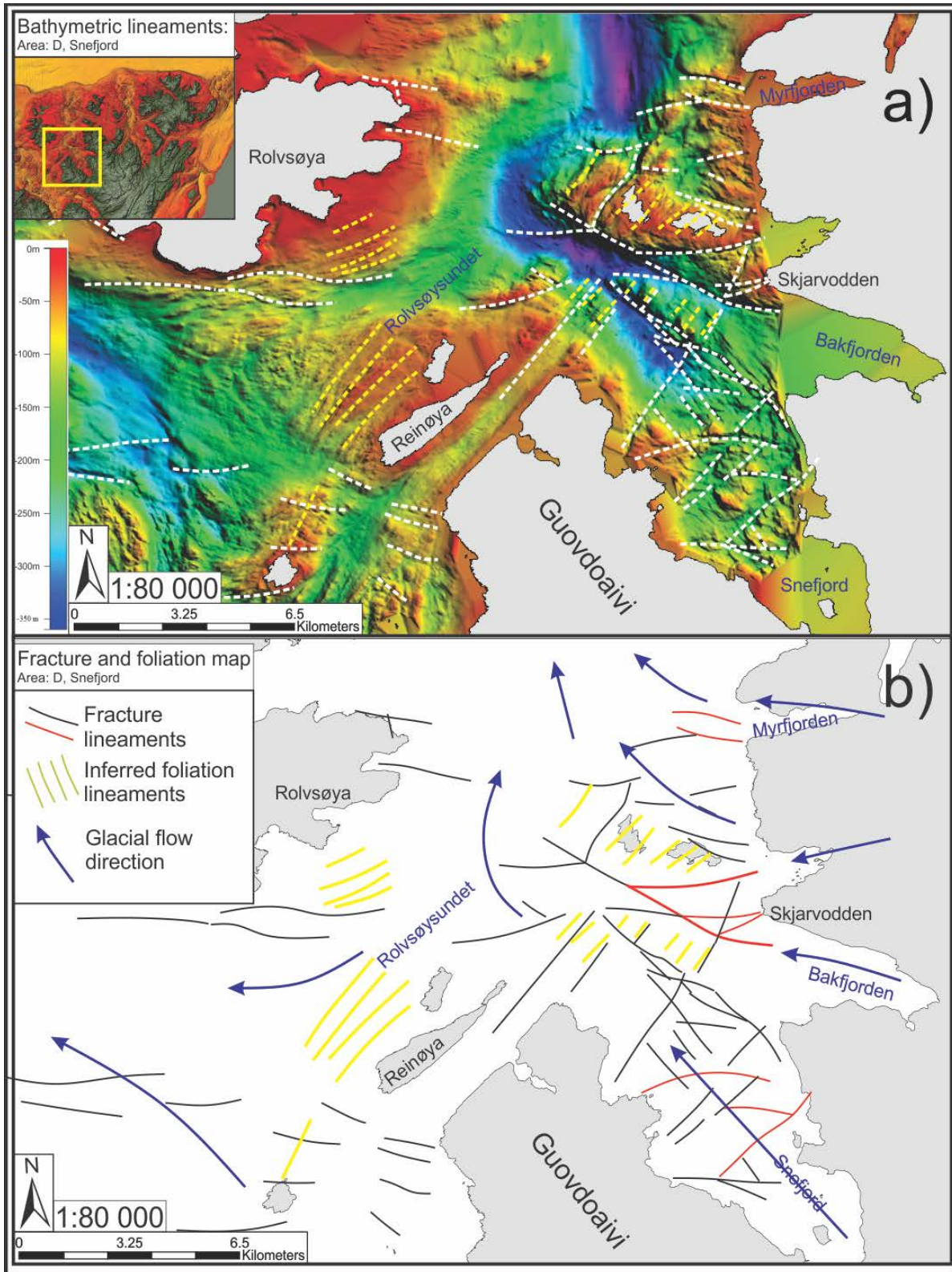
*Fig. 4.9 Bathymetric map and sketch interpretation of area D, Snefjord **a)** bathymetric surface, white dashed lines indicate lineaments, parallel ridges and troughs indicated by yellow lines **b)** sketch of interpreted bathymetry. Fault-fracture lineaments (black & red lines), parallel ridges and troughs (yellow), and is interpreted as foliation in the crystalline bedrock. Note the red lines, indicating a direct continuation of lineaments seen onshore (fig. 4.8).*

4.7 Summary and preliminary interpretation

The interpreted bathymetric lineament show a similar distribution as the lineaments interpreted onshore. The orientation of the lineaments show that there are three major trends: 1) E-W, 2) NE-SW and 3) NW-SE, similar to onshore lineaments directions. The glacial flow direction shows a small amount of influence over the fracture lineaments, but as it is seen from the escarpments and lineaments, the glacial flow direction does not overprint these, but the glacial erosion rather follows pre-existing zones of weakness, rather than carving depressions parallel to the glacial flow direction. As seen by the trends in areas heavily influenced by glacial erosion, e.g. Snefjord and Helneset (fig. 4.3 & 4.7), the lineaments in the immediate proximity to glacial erosional features show trends similar to the dominant fault-fracture trends found offshore in these areas. The shallow submarine plateaus encompassing parallel ridges and troughs are being cut by deeper channels trending NE-SW, E-W and NW-SE, indicating that the parallel ridges and troughs are not linked to fault-fractures (fig. 4.3, 4.5 & 4.9). Deep elongated depressions can be found in the fjords. These are bound by NE-SW and NW-SE trending escarpments, showing glacial features such as flutes and rounded topography near the bottom, indicating that the glacial erosion has followed pre-existing fracture zones (fig. 4.3, 4.5, 4.7 & 4.9).

From these interpretations, the following preliminary interpretations can be drawn:

1) The strandflat encompasses shallow plateaus continuing the landforms seen onshore. These marine plateaus appears as fault-blocs, down faulted in relation to the main topography similar to, but not as dramatic as seen in Lofoten, Vesterålen and Troms (Forthun, 2014; Haraldsvik, 2015; Indrevær et al., 2014; Thorsnes et al., 2009).

2) The study area has experienced glacial activity as erosion and deposition, as seen from the flutes, moraines and scour marks encompassed in the fjord, supporting the glacial flow direction indicated (modified from Barbolla et al., in prep).

3) Parallel ridges and troughs suggest that they represent the bedrock foliation.

4) NE-SW, NW-SE and E-W trending channels, troughs and escarpments follows the same patterns as seen onshore.

5) Depressions bound by NE-SW, NW-SE and E-W trending escarpments are interpreted as glacial erosion in areas with a high fault-fracture frequency, where this makes the area preferentially eroded compared to other areas.

5   Description of Seismic data

5.1   Introduction

2D and 3D seismic data were used to interpret and map structures on the Finnmark platform. The 3D seismic data gives a detailed view of the faults, fault interaction and fault geometry of the intersection between the TFFC and the MFC. This chapter will present 2D and 3D seismic surveys that cover the southwestern Barents Sea from the coast of Magerøy and the northwest Porsanger Peninsula, the Finnmark Platform, the Gjesvær Low (informal term), to the southern parts of the Nordkapp Basin (fig. 5.2). The focus was to compare onshore-offshore fault geometry in the area east of Gjesvær Low, where the TFFC changes orientation and trends NW-SE before terminating on MFC. Previous studies map a basin/graben-like structure in this fault intersection (Roberts, D. et al., 2005).

The aim in this chapter is to map and interpret the 2D seismic lines in order to map fractures, the changes in fracture geometry and the character around this basin. In addition, the presence of TKFZ and its connection to the NW-SE leg of TFFC will be explored, as proposed by Gabrielsen et al. (1989). To accomplish this, the data is presented in following order: 1) Presentation of the database, 2) Overview of the 2D seismic lines interpreted, 3) Interpretation of key 2D seismic lines, 4) interpretation of 3D seismic cube. 5) Summary and preliminary fault map.

5.2 Database

The 2D seismic lines interpreted are selected from the NTNU-Schulmberger Petrel ready database. Even though more 2D seismic lines have been interpreted, this thesis will present the key 2D lines and the 3D survey (fig. 5.1 & 5.2). In addition, the tie line that covers the well-ties is included to support the stratigraphy and the interpretation of seismic reflectors (fig 5.3). The 2D seismic surveys available in this database (NTNU-Schulmberger Petrel ready database) are BSS-01, oriented NE-SW and NE-SW, NPD-FI-84 and NPD-FIØ2-86, oriented N-S and E-W (fig. 5.1). The 3D seismic survey covers the interaction of the NW-SE leg of TFFC and MFC, this survey has a rectangular outline oriented NE-SW (fig. 5.1). The seismic surveys consist of conversional zero-phase 2D and 3D seismic data, and the key lines were chosen due to their placement and orientation with regards to the main structures on the Finnmark Platform and SW Barents Sea (fig. 5.2).
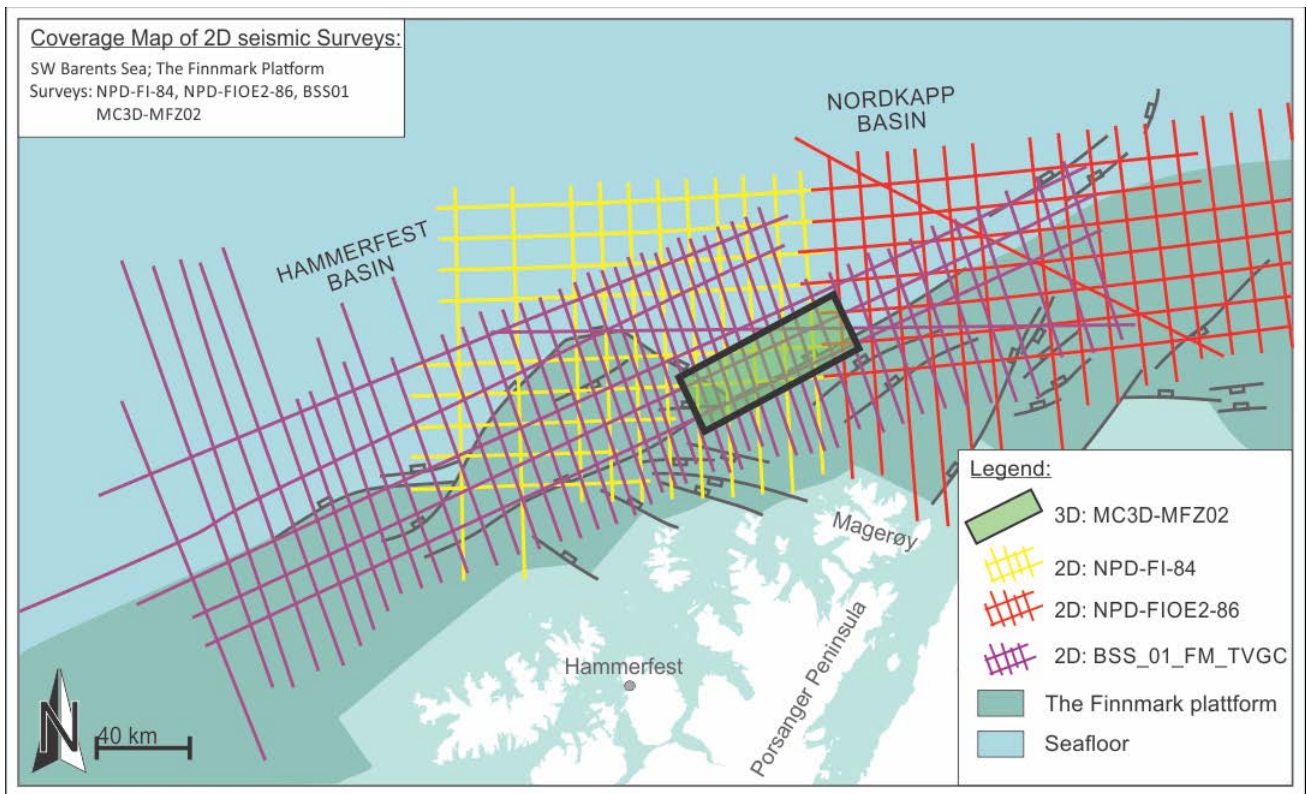
Fig. 5.1, Overview map of seismic data available. The different surveys differentiated by color. 2D seismic surveys NPD-FI-84 (yellow), NPD-FIOE2-86 (red), BSS_01_FM-TVGC (purple), 3D cube MC3D-MFZ02 (black square, green fill). Structural background map modified from Roberts et al., 2005.

Description of Seismic data
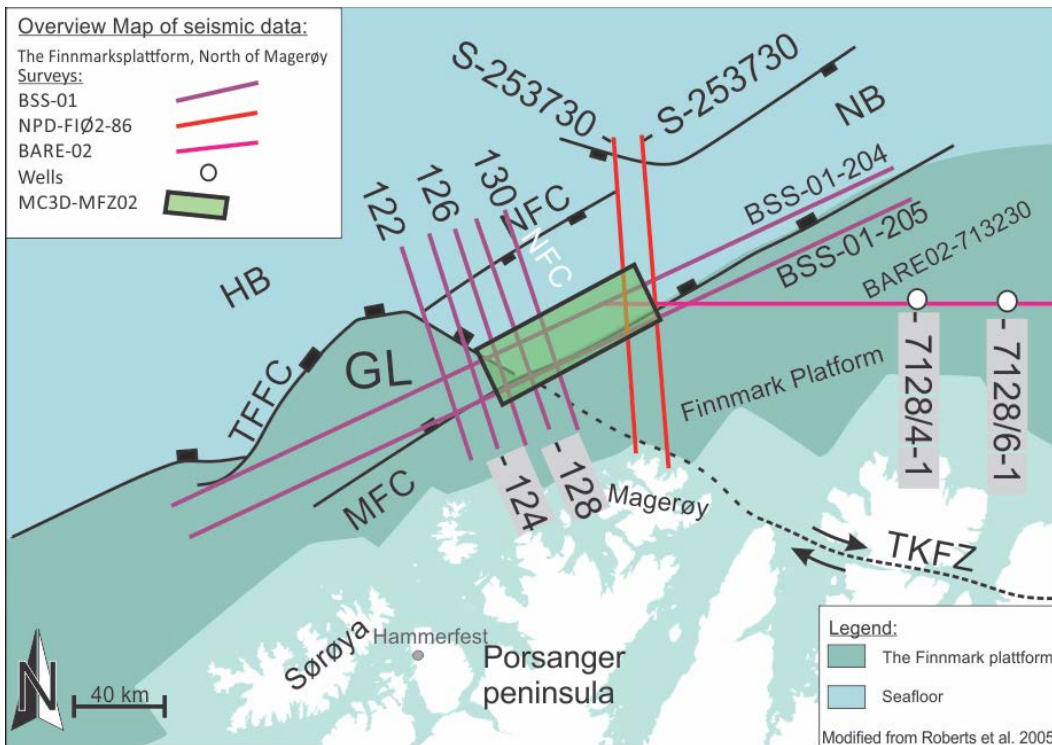
Fig. 5.2 Overview of selected 2D seismic lines and 3D survey. See table 2 for abbreviations. Structural map modified from Roberts & Lippard (2005).

Table 3: Overview of key seismic lines and data interpreted in this thesis

Survey	2D line	Quality	Age of survey/ reprocessed	Survey company	Reprocessed by	Area	NPDID
BSS01	204	Good	2001	Nopec AS		S Barents Sea	*4091*
	205	Good	2001	Nopec AS		S Barents Sea	*4091*
	122	Good	2001	Nopec AS		S Barents Sea	*4091*
	124	Good	2001	Nopec AS		S Barents Sea	*4091*
	126	Good	2001	Nopec AS		S Barents Sea	*4091*
	128	Good	2001	Nopec AS		S Barents Sea	*4091*
	130	Good	2001	Nopec AS		S Barents Sea	*4091*
NPD-FIØ2-86	S-253730	Good	1986	Oljedirektoratet		S Barents Sea	*2859*
	S-260730	Good	1986	Oljedirektoratet		S Barents Sea	*2859*
BARE02	713230	Good	2002	Fugro AS	Nopec As	S-SE Barents Sea	*Not available*
MC3D-MFZ02	3D cube	Very Good	2002	WesternGeco AS		S Barents Sea	*4170*

5.2.1   Seismic Stratigraphy, Lithology and key seismic reflections

The sequences are based on previous research in Lofoten-Troms (e.g. Haraldsvik (2015); Indrevær et al., 2013) (Haraldsvik, 2015; Henningsen, 2016; Indrevær et al., 2013; Lundekvam, 2015) and interpretations of seismic data and well-ties provided by Statoil (Henningsen, 2016). The reflectors (tab. 4) and sequences (tab. 5) are based on data from Larssen et al. (2002) and the shallow drill cores 7128/4-1 & 7128/6-1. The following describes the composition of sediments found in these wells, from base-up.

The well-ties show a Quarzitic basement most likely from the Barents-group in northeastern Finnmark, resulting in sequence 1, S1, and reflector 1, R1. The following sediments are dominated by siliciclastic sediments, changing between sandstone, mudstone and shales. Some areas include coal seams (meter-scale). This sequence is characterized by varying amplitudes, but similar character possibly due to the coal layer (Larssen et al., 2002). After this siliciclastic dominant period, the Barents Sea experienced a regional uplift, leading to a regional inconformity that is possible to identify on most seismic data in the Barents Sea (pers. com. Henningsen). This sequence is noted S1 and the reflector at the top unconformity is noted R2. Following the regional uplift came Late Carboniferous subsidence that lead to continued sediment deposition, dominantly siliciclastic. The upper areas of the platform record shallow reefs, whereas halite and anhydrite are recorded in depressions and basins.

The Early Permian deposits are dominated by limestone deposits, whereas the Late Permian is dominated by chert interfingered with limestone and varying shales, making up sequence 3, S3. These sediments mark a definite seismic reflection that defines the Near Base Triassic reflector, R3. The overlying Triassic sediments are mostly siliciclastic and are dominated by sandstones, mudstones and shales, occasionally organic shale. The deposit originates mostly from the south to east. This defines sequence 3, S3. The Near Base Cretaceous Unconformity represents a regional unconformity in the southwestern Barents Sea. It ranges in age from Late Jurassic to Early Cretaceous. This reflection marks an erosional period tied to uplift the Platform, ridges and banks as well as a subsidence of basin areas. The Base Paleogene reflector and sequence, R5 and S5, are not present in the well ties, but have been tied in via the 2D seismic line BSS01-122 (fig. 5.5). These sediments mainly consist of siliciclastic sediments ranging from sandstone, mudstone and shale. The Upper Regional Unconformity (URU), R6, marks the lower limit of glacial erosion and the following glacial sediments. This sequence is characterized by chaotic reflectors, and records channels, moraines and other glacial features (Larssen et al., 2002). This marks the sequence S6, and the seafloor, R7. The interpreted

reflectors are colored based on their age in accordance with the geologic timescale presented by Gradstein et al. (2012).
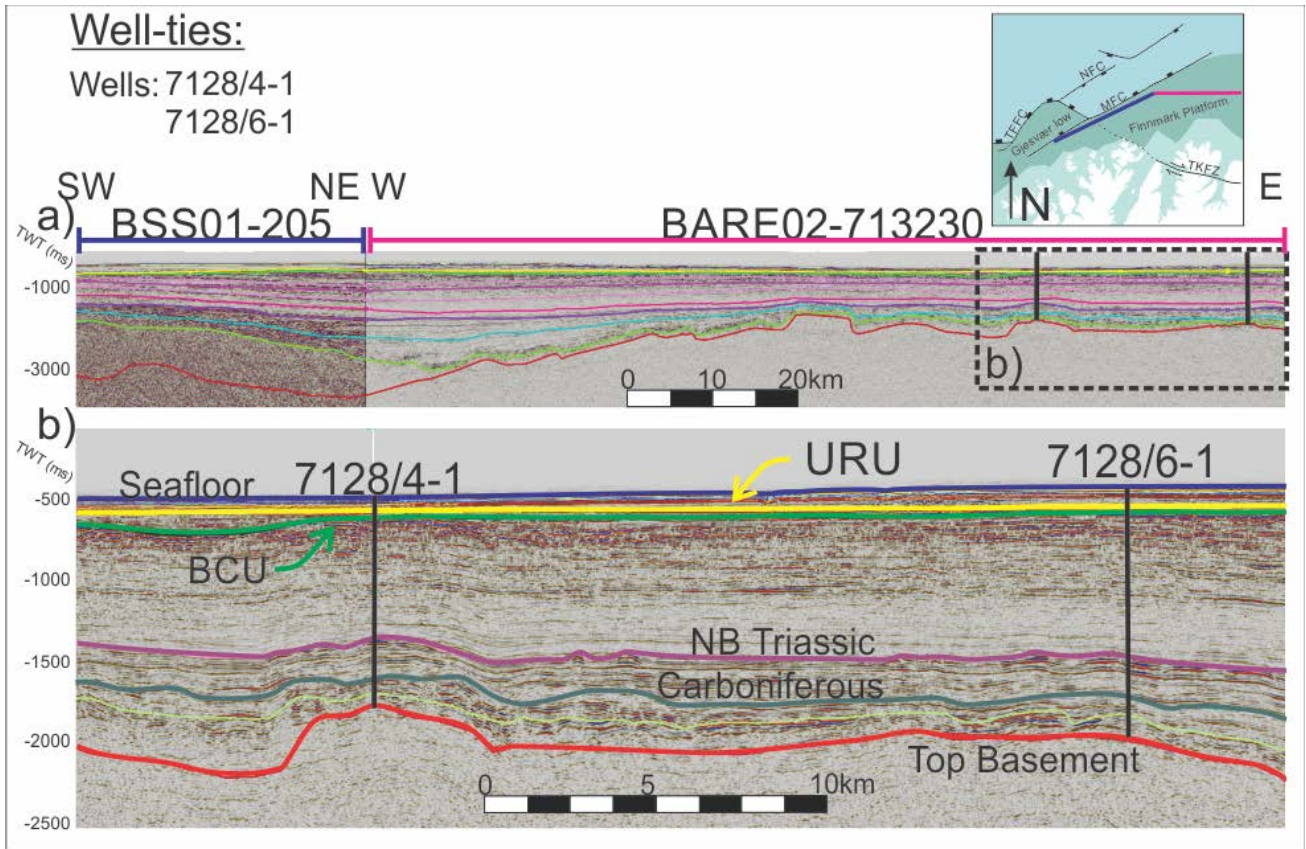
*Fig. 5.3, Well ties for seismic surveys, **a)** Composite line from 2D seismic lines BSS-01-205 and BARE02-713230, also showing wells 7128/4-1 & 7128/6-1, tie in via lines BARE02-713230 (purple) and BSS01-205 (blue). **b)** Interpreted model in the lower section. Reflectors marked by colored lines: R6 blue, R5 yellow, R4 orange, R3 green, R2 purple, R1 red. Light blue and bright green marks intra carboniferous reflectors. Modified from Henningsen (2016).*

Table 4. Seismic sequences in interpreted seismic sections.

Sequence	Abb.	Age (correlated to wells 7128/4-1 & 7128/6-1)
1	S1	Precambrian, top basements interpreted as quarzitic bedrock in tie-in wells.
2	S2	Carboniferous- Devonian
3	S3	Devonian-Late Permian
4	S4	Triassic-Late Jurassic
5	S5	Cretaceous
6	S6	Paleogene
7	S7	Neogene – late quaternary

Description of Seismic data

Table 5. Key seismic reflectors/horizons

Reflection	Abb.	Characteristics	Well ties
1 - Top Basement	R1	Strong continuous reflector, differentiating chaotic well stratified reflectors to the underlying chaotic or transparent reflectors. Difficult to differentiate from R2 in deeper parts of surveys.	7128/4-1 7128/6-1
2- Carboniferous	R2	Strong non-continuous reflectors, marks the boundary between the somewhat random, but some continuous internal reflectors can be traced.	7128/4-1 7128/6-1
3 - Near Base Triassic (NB Triassic)	R3	Strong continuous reflector differentiates lower-lying stratified reflectors (S2) from the less stratified reflectors above, shows on-lap on interpreted faults.	7128/4-1 7128/6-1
4 - Base Cretaceous Unconformity (BCU)	R4	Strong continuous reflector, erosional boundary over lower-lying stratified reflectors, mostly continuous along seismic sections.	7128/4-1 7128/6-1
5 - Paleogene	R5	Continuous strong reflector differentiates the top of strongly stratified cretaceous sediments and the more transparent Paleogene sediments.	Tied in from Hammerfest Basin (pers. com. Henningsen 2016)
6 - Upper Regional Unconformity (URU)	R6	Strong erosional disconformity, marking the erosional boundary of lower-lying sediments, sharply erodes all previous mentioned reflectors.	7128/4-1 7128/6-1
7 - Seafloor	R7	No seismic reflections above this reflector. However, some artefacts are observed above.	7128/4-1 7128/6-1

5.3 Seismic interpretation

Due to the similarities and the short interval of the key seismic sections, the description of seismic 2D lines will be collectively presented, followed by figure interpretation of the 2D seismic lines. Lastly the 3D seismic volume will be described and presented.

5.3.1 2D seismic data

The key seismic lines are oriented 1) NE-SW, 2) SE-NW and 3) N-S. The seismic lines cover structural features offshore in the study area such as the Gjesvær Low, N. Hammerfest Basin, S. Nordkapp Basin, Nysleppen Fault complex (NFC), Troms Finnmark Fault Complex (TFFC), Måsøy Fault Complex (MFC) and the Finnmark Platform (Gabrielsen et al., 1989; Johansen et al., 1994; Roberts, D. et al., 2005; Samuelsberg et al., 2003) (fig 5.2). The seismic lines show several key reflectors and sequences (tab. 5 & 6). The interpreted top basement, R1, and the Precambrian basement, S1, appears in all seismic lines, where it exhibits a sharp reflection above chaotic deeper reflectors at the Finnmark platform, at -600 ms (twt) depth. In the areas north of TFFC and MFC, including Gjesvær Low, N. Hammerfest Basin and S. Nordkapp Basin, R1 is down faulted along TFFC and MFC, from -4 s to -6 s (twt) depth (e.g. fig. 5.5), and becomes difficult to differentiate from the lower chaotic reflectors in S2.

R2, boundary between the lower diffuse random reflections from S2, and the more non-random reflectors of S3. The internal reflectors of S2 is characterized by segmented tilted reflectors (fig. 5.4 e.g. from MFC to Nordkapp Basin). The lower reflections in the sequence shows random/chotic, segmented and rotated reflectors, making it hard to differentiate from S1, that also displays some of these random reflections.

R3 marks the boundary between S3 and S4, and is interpreted as a Triassic erosional upper boundary of S3. S2 shows strong stratification and multiple reflectors in the upper parts of the sequence, to more chaotic and irregular reflectors toward R1. The seismic profiles (fig. 5.5 – 5.11) show a shallow thickness on the Finnmark platform, and a substantially deeper thickness near Gjesvær Low, and north of TFFC and MFC. However, at the boundary between Gjesvær Low and north Hammerfest Basin a horst-like structure truncates the sequence, before thickening on both sides. From the well ties, S2 comprises Devonian to Late Permian sedimentary rocks. S3 ranges from -4.5 s to -2 s (twt).

S4 marks the Triassic to Late Jurassic sediments and is located between R4 and R5. The sequence shows well stratified layers, and parallel reflectors, dipping north. S4 records Triassic to Late Jurassic sediments. The

sequence appears to have a constant thickness north from MFC. The top of the sequence is defined as the Base Cretaceous Unconformity, R4, where the Cretaceous sediments have eroded the upper Triassic reflectors. Parallel reflectors, offset by numerous smaller normal faults and larger faults, such as TFFC and MFC, characterize S4. The intensity of faulting increases near the larger regional faults TFFC and MFC. The reflectors show onlap onto the larger faults, TFFC and MFC. The southern sections show a dip north and an erosional unconformity to where R5 marks the boundary to the chaotic glacial sediments in S6.

S5 records parallel internal reflectors, and is not found on the shallow Finnmark platform. R5 marks the upper boundary, where Cretaceous deposits are eroded by R6. The internal reflectors are generally horizontal, recording onlap onto the larger faults, but show some internal faulting, with minor offset of reflectors, near MFC and TFFC, and onlap and truncation towards the faults.

S6 comprises Paleogene deposits containing horizontal reflectors. S6 is narrow throughout the study area and truncates towards and terminates at TFFC and MFC. In the southeastern parts of the study area, and past MFC in the northeast parts of the study area, S6 has been tied in via the 2D seismic line BSS-01-122 from the Hammerfest Basin (pers. com. Henningsen).

S7 records Quaternary deposits characterized by chotic reflectors, and is constrained by R6 & R7. S7 is seen throughout the study area, where it erodes lower-lying sequences, marking the lower extent of glacial erosion.

Salt-influenced structures are generally not seen on seismic lines from BSS-01, but vertical dome-shaped structures can be seen on 2D seismic lines S-253730-86 and S-260730-86, these domes cut sequences S2-S5 and can be seen in the northeastern areas of the study area towards southern areas of the Nordkapp Basin.

5.3.1.1   2D line BSS-01-204
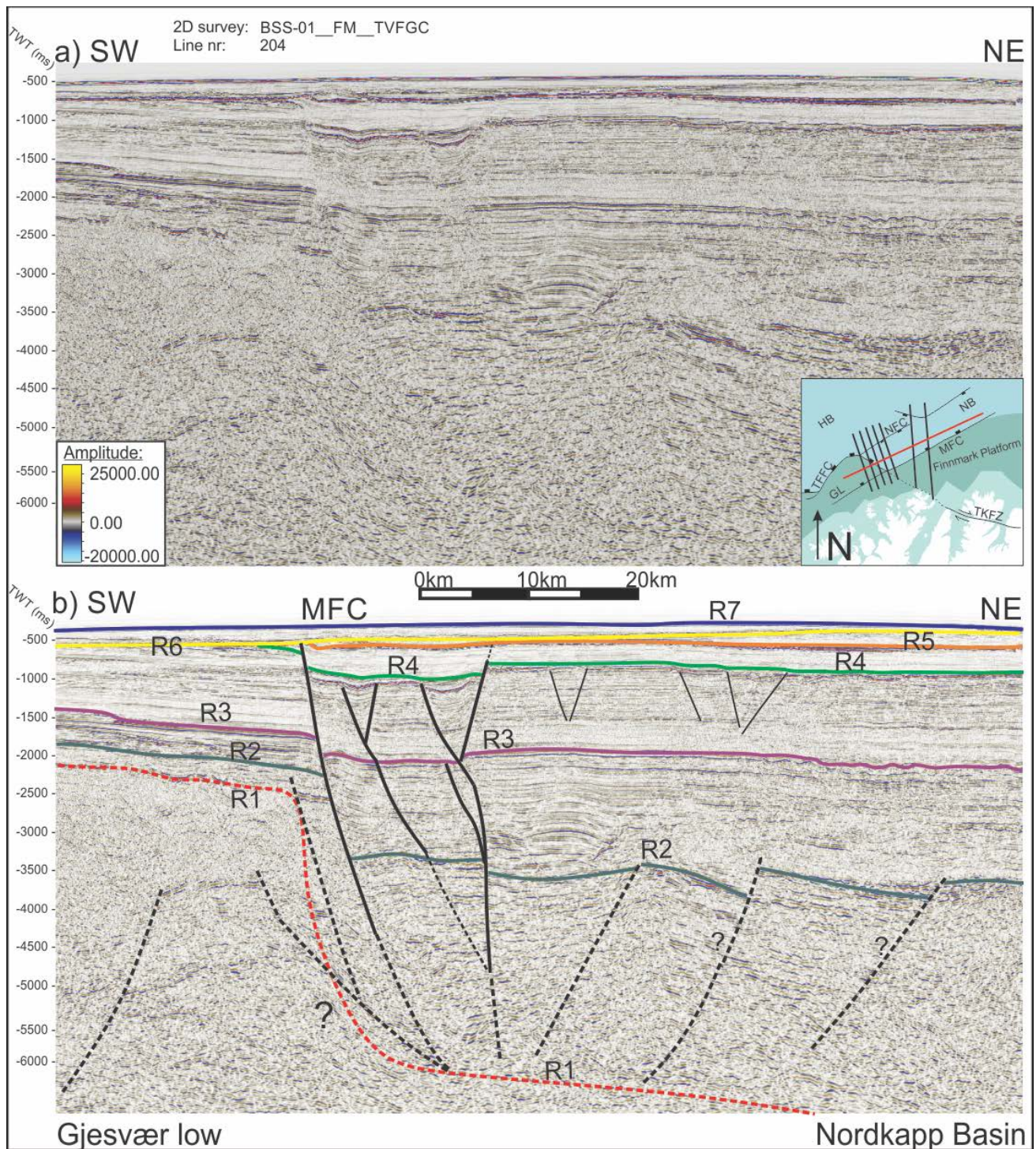
*Fig. 5.4, 2D seismic line, BSS-01-204. **a)** Non- interpreted line. **b)** Sketch interpretation of a). Reflectors marked by colored lines: R7 blue, R6 yellow, R5 orange, R4 green, R3 purple, R2 forest green, R1 red. Faults: primary faults thick black lines, uncertain faults shown as dashed lines, secondary and minor faults shown as thin black lines*

5.3.1.2   2D line BSS-01-122
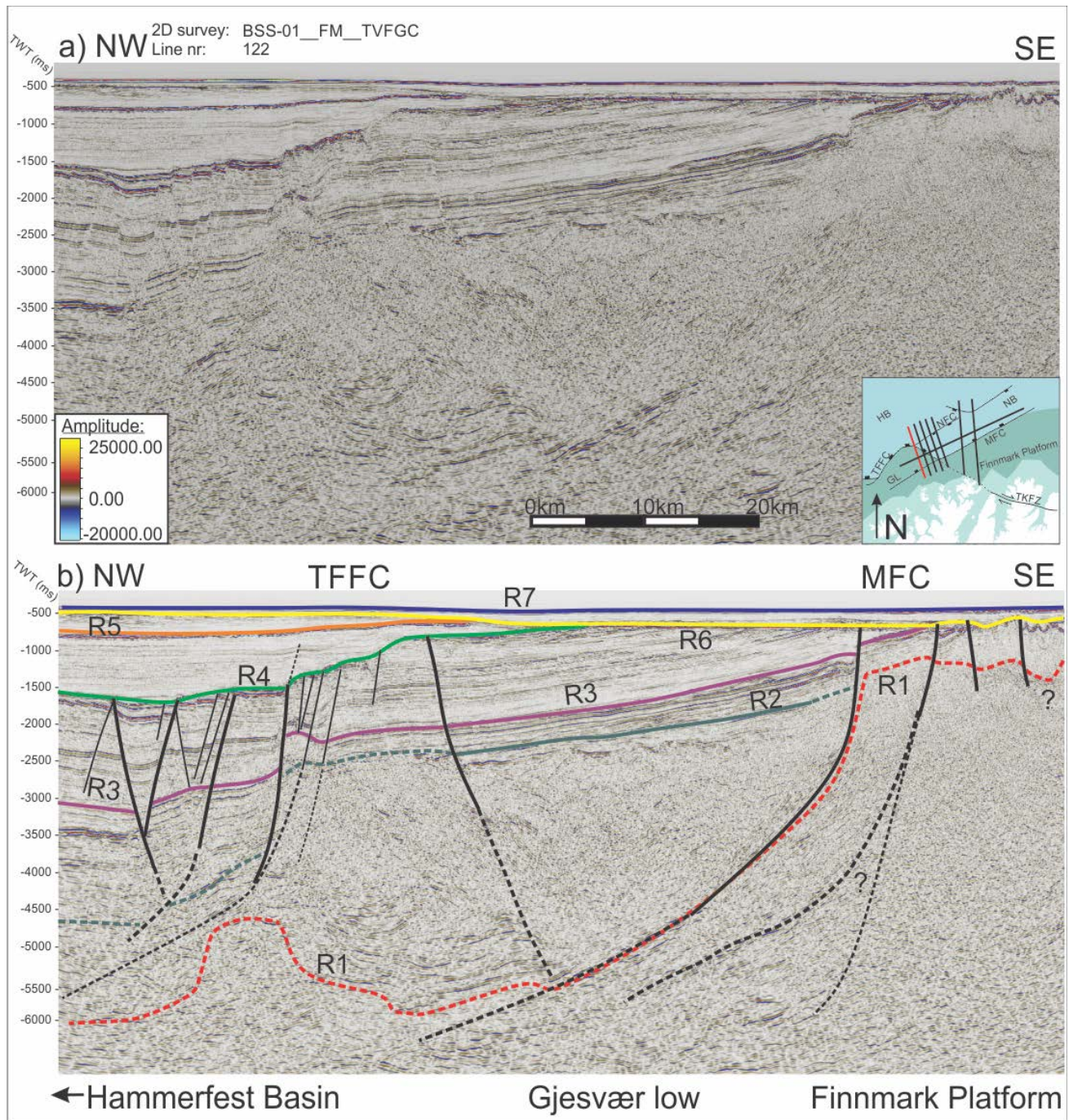
Fig. 5.5, 2D seismic line, BSS-01-122. a) Non- interpreted line. b) Sketch interpretation of a). Reflectors marked by colored lines: R7 blue, R6 yellow, R5 orange, R4 green, R3 purple, R2 forest green, R1 red. Faults: primary faults thick black lines, uncertain faults shown as dashed lines, secondary and minor faults shown as thin black lines

5.3.1.3   2D line BSS-01-124
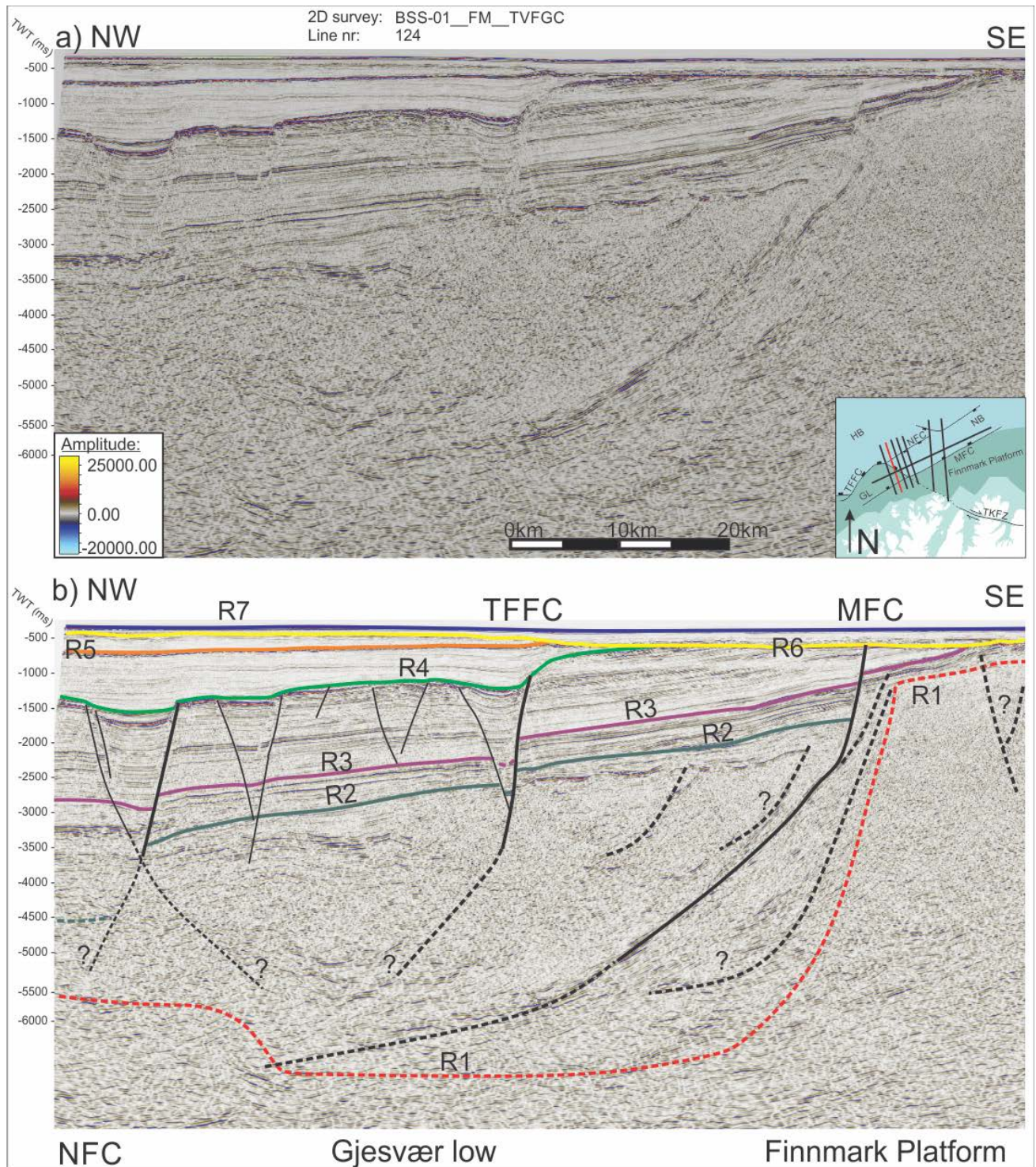
Fig. 5.6 2D seismic line BSS-01-124 a) Non- interpreted line. b) Sketch interpretation of a). Reflectors marked by colored lines: R7 blue, R6 yellow, R5 orange, R4 green, R3 purple, R2 forest green, R1 red. Faults: primary faults thick black lines, uncertain faults dashed lines, secondary and minor faults thin black line.

5.3.1.4   2D line BSS-01-126

*Fig. 5.7, 2D seismic line BSS-01-126. **a)** Non- interpreted line. **b)** Sketch interpretation of a). Reflectors marked by colored lines: R7 blue, R6 yellow, R5 orange, R4 green, R3 purple, R2 forest green, R1 red. Faults: primary faults thick black lines, uncertain faults dashed lines, secondary and minor faults thin black line.*

5.3.1.5   2D line BSS-01-128

*Fig. 5.8 2D seismic line BSS-01-128. **a)** Non- interpreted line. **b)** Sketch interpretation of a). Reflectors marked by colored lines: R7 blue, R6 yellow, R5 orange, R4 green, R3 purple, R2 forest green, R1 red. Faults: primary faults thick black lines, uncertain faults dashed lines, secondary and minor faults thin black line.*

Description of Seismic data

5.3.1.6   2D line BSS-01-130
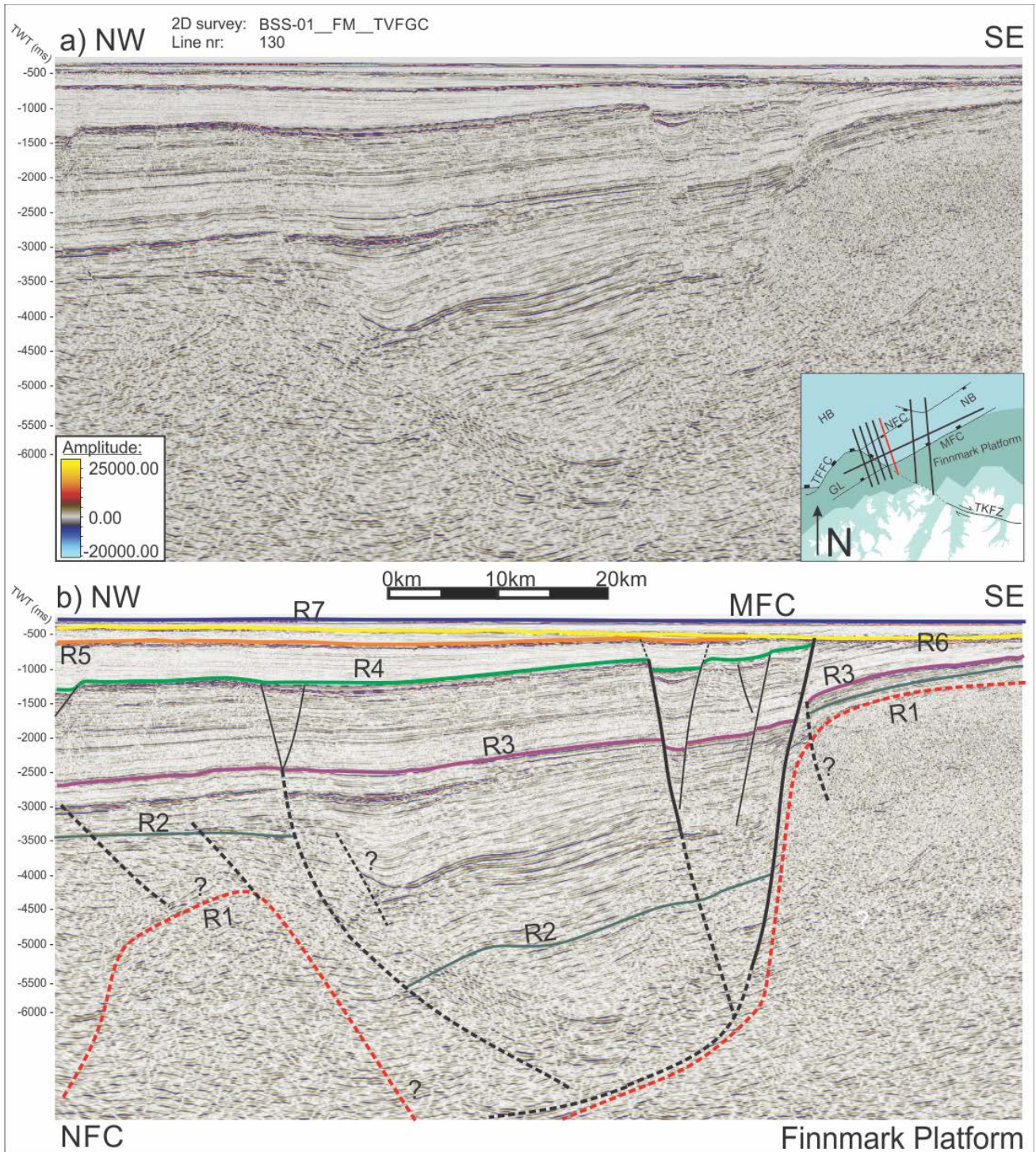
*Fig. 5.9 2D seismic line BSS-01-130. **a)** Non- interpreted line. **b)** Sketch interpretation of a). Reflectors marked by colored lines: R7 blue, R6 yellow, R5 orange, R4 green, R3 purple, R2 forest green, R1 red. Faults: primary faults thick black lines, uncertain faults dashed lines, secondary and minor faults thin black line.*

5.3.1.7   2D line S-253730-86, from survey NPD-FIOE2-86
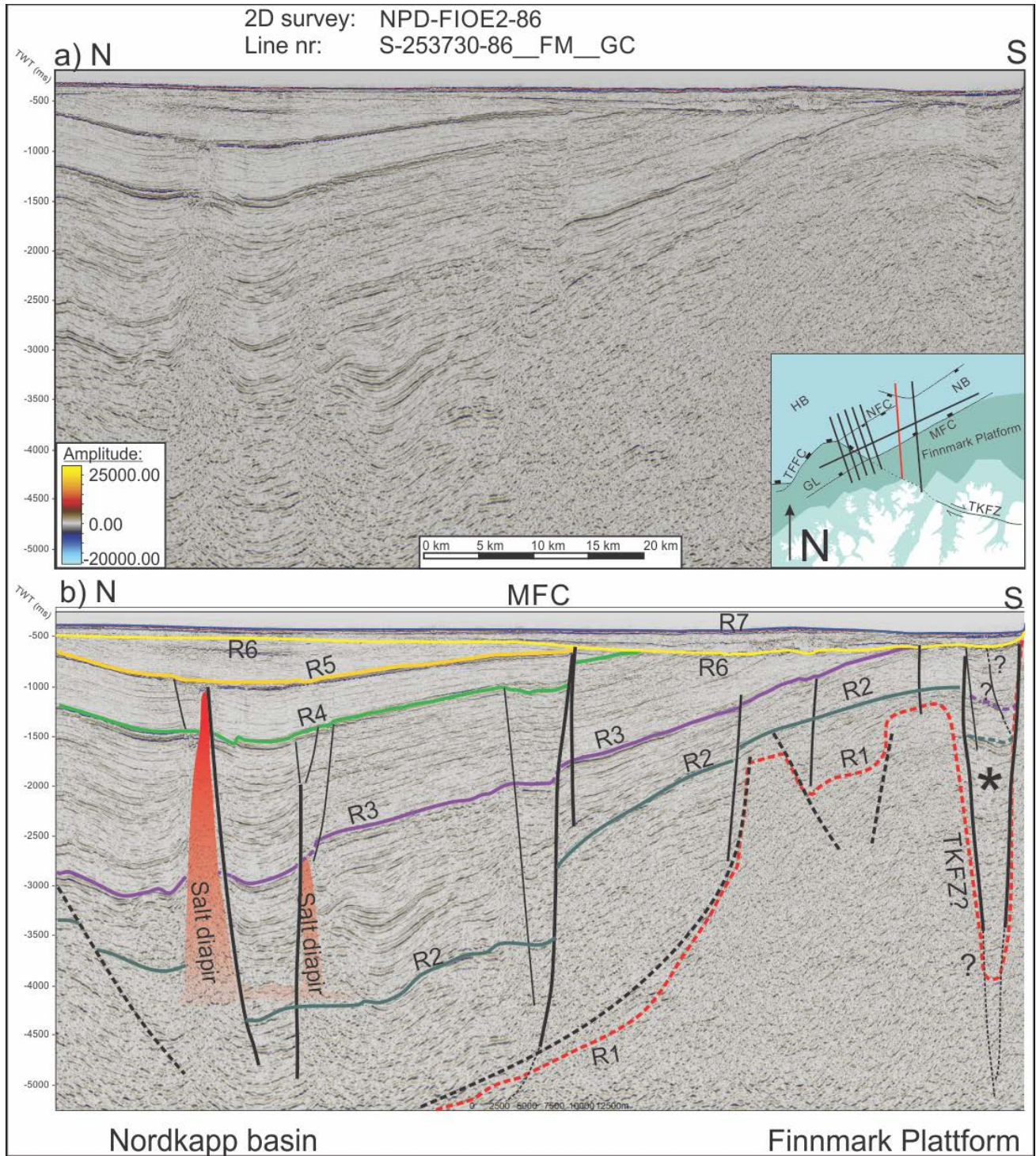
Fig. 5.10, 2D seismic line S-253730-86, from survey NPD-FIØ2-86. **a)** *Non- interpreted line.* **b)** *Sketch interpretation of a). Reflectors marked by colored lines: R7 blue, R6 yellow, R5 orange, R4 green, R3 purple, R2 forest green, R1 red. Faults: primary faults thick black lines, uncertain faults dashed lines, secondary and minor faults thin black line.*

5.3.1.8   2D line S-260730-86, from survey NPD-FIOE2-86
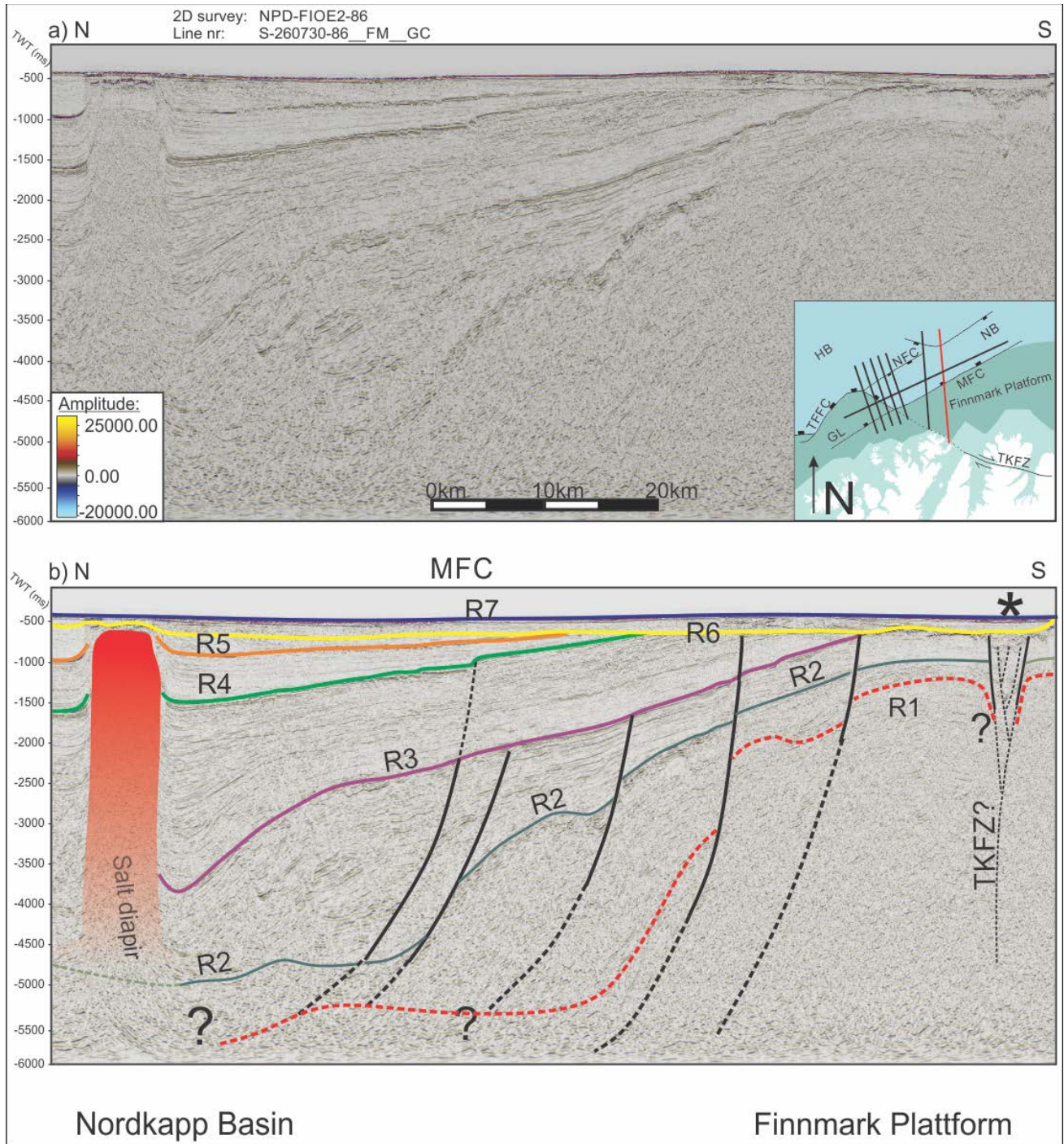
*Fig. 5.11 2D seismic line S-260730-86, from survey NPD-FIØ2-86. **a)** Non- interpreted line. **b)** Sketch interpretation of a). Reflectors marked by colored lines: R7 blue, R6 yellow, R5 orange, R4 green, R3 purple, R2 forest green, R1 red. Faults: primary faults thick black lines, uncertain faults dashed lines, secondary and minor faults thin black line.*

5.3.2   3D seismic data

This chapter will present the 3D data in order to explore the intersection of the NW-SE leg of TFFC and MFC, this is illustrated by using the seismic reflections R3 and R4, as well as three random lines through the cube (fig. 5.12-5.16).

The 3D seismic data consists of the cube MC3D-MFZ02, the resolution of this cube shows excellent quality. The reflectors R3 and R4, presented in chapter 5.1 and 5.2, have been interpreted from the 3D seismic data, these reflectors are both affected by both TFFC and MFC, and the interaction between the two appears clearly on the 3D data. Moreover, the data have been interpreted to highlight the fault interaction of the NW-SE striking leg of TFFC and MFC. In addition, the reflectors R3-R7 have been interpreted; only R3 and R4 (BCU and NB Triassic) show direct fault offset. R5, Paleogene, show onlap onto R4, as well as an apparent infill (fig. 5.14 to 5.16). A small graben structure can be seen bounded by NW-SE striking TFFC and the NE-SW striking MFC, and a NE-SW striking, south dipping fault (fig. 5.12 & 5.13). The western parts of the E-W striking fault curves towards TFFC, while it splays out and terminates before reaching MFC (fig. 5.12 & 5.13).

At the interaction of MFC and TFFC, the latter appears to splay out into several smaller fault segments. Most of these smaller faults display similar trend as TFFC, while others bend and curve to a more E-W trend, parallel to the E-W striking fault. The smaller faults shows a north dip (fig. 5.12 & 5.13).

The hanging wall of both TFFC and MFC, smaller minor faults striking NE-SW, NW-SE and E-W. To the northeast of the surface, north of MFC, minor faults make up polygonal faults below R3; these are not seen on R4 or the reflectors above. Minor faults dipping both north and south continue along the hanging wall of MFC, displaying en echelon, parallel to splaying interaction towards TFFC (fig. 5.12 & 5.13).
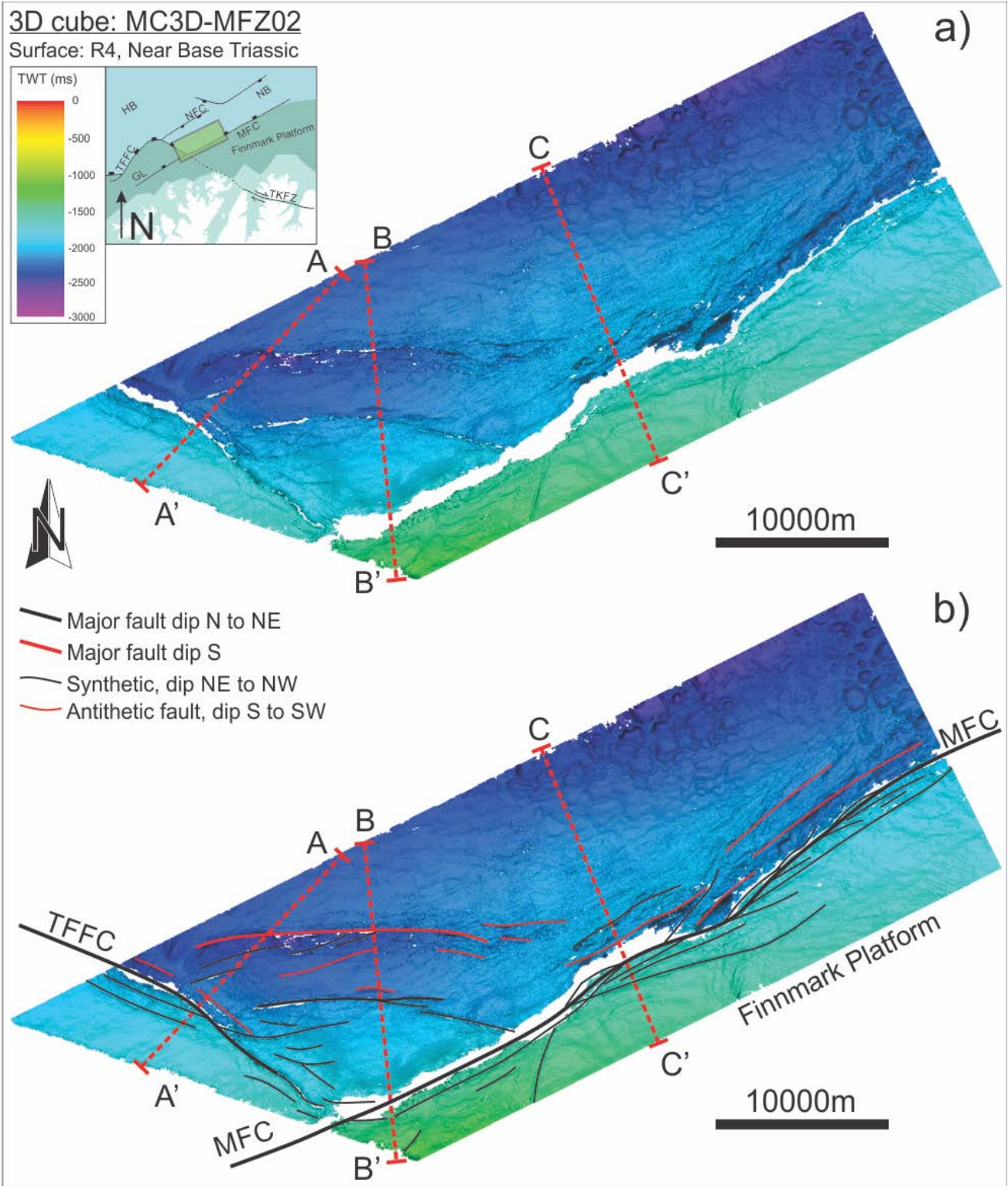
*Figure 5.12. 3D seismic data, non- interpreted seismic horizon and sketch interpretation of R3 (NB Triassic) **a)** Non interpreted horizon, note the gaps in the surface, indicating an escarpment and change of height. **b)** Sketch interpretation of a), Primary/Major faults: TFFC (NW-SE) and MFC (NE-SW) (marked in thick lines) dip NE and NW respectably, secondary faults: synthetic and antithetic faults concerning TFFC and MCF (**Red** SE-SW dip, **Black** NE to NW dip)*
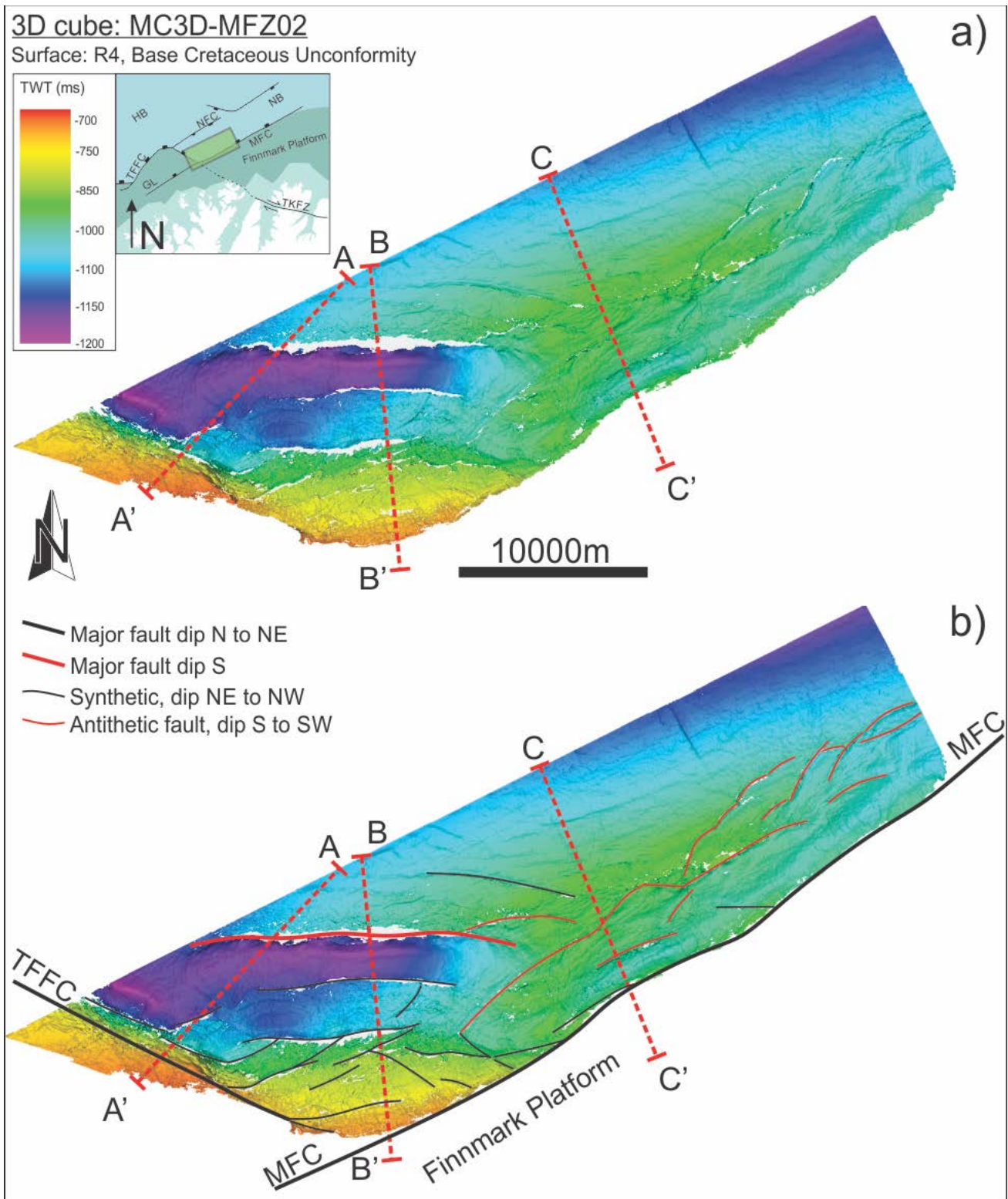
Figure 5.13 3D seismic data, non- interpreted seismic horizon and sketch interpretation of R4 (BCU) **a)** Non interpreted horizon, note the gaps in the surface, indicating an escarpment and change of height. **b)** Sketch interpretation of a), Primary/Major faults: TFFC (NW-SE) and MFC (NE-SW) (marked in thick lines) dip NE and NW respectably, secondary faults: synthetic and antithetic faults concerning TFFC and MCF (**Red** SE-SW dip, **Black** NE to NW dip)
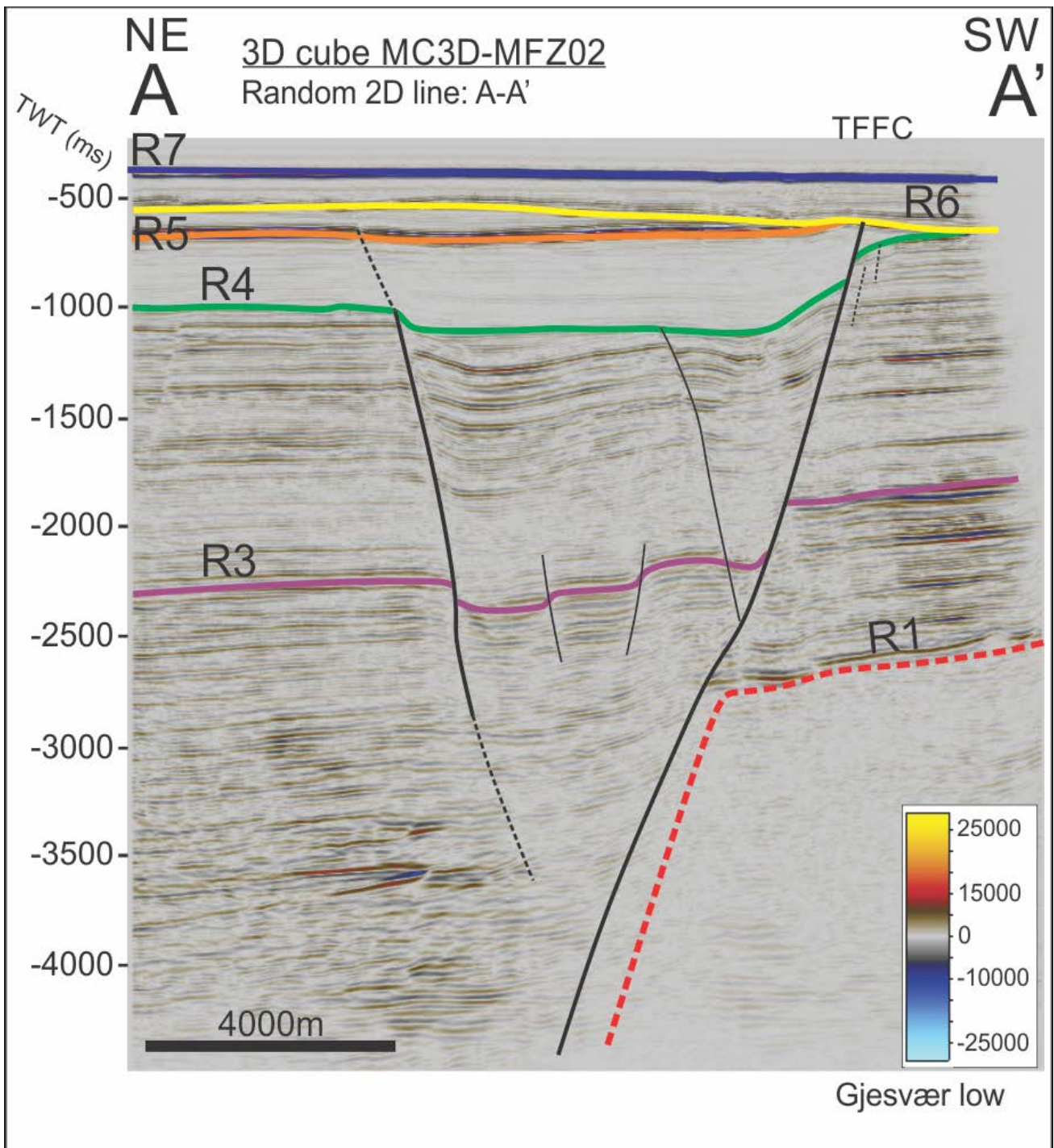
Figure 5.14 Random 2D line from seismic 3D cube, illustrating the NW-SE leg of TFFC. Reflectors marked by colored lines: R7 blue, R6 yellow, R5 orange, R4 green, R3 purple,, R1 red. Faults: primary faults thick black lines, uncertain faults dashed lines, secondary and minor faults thin black line.
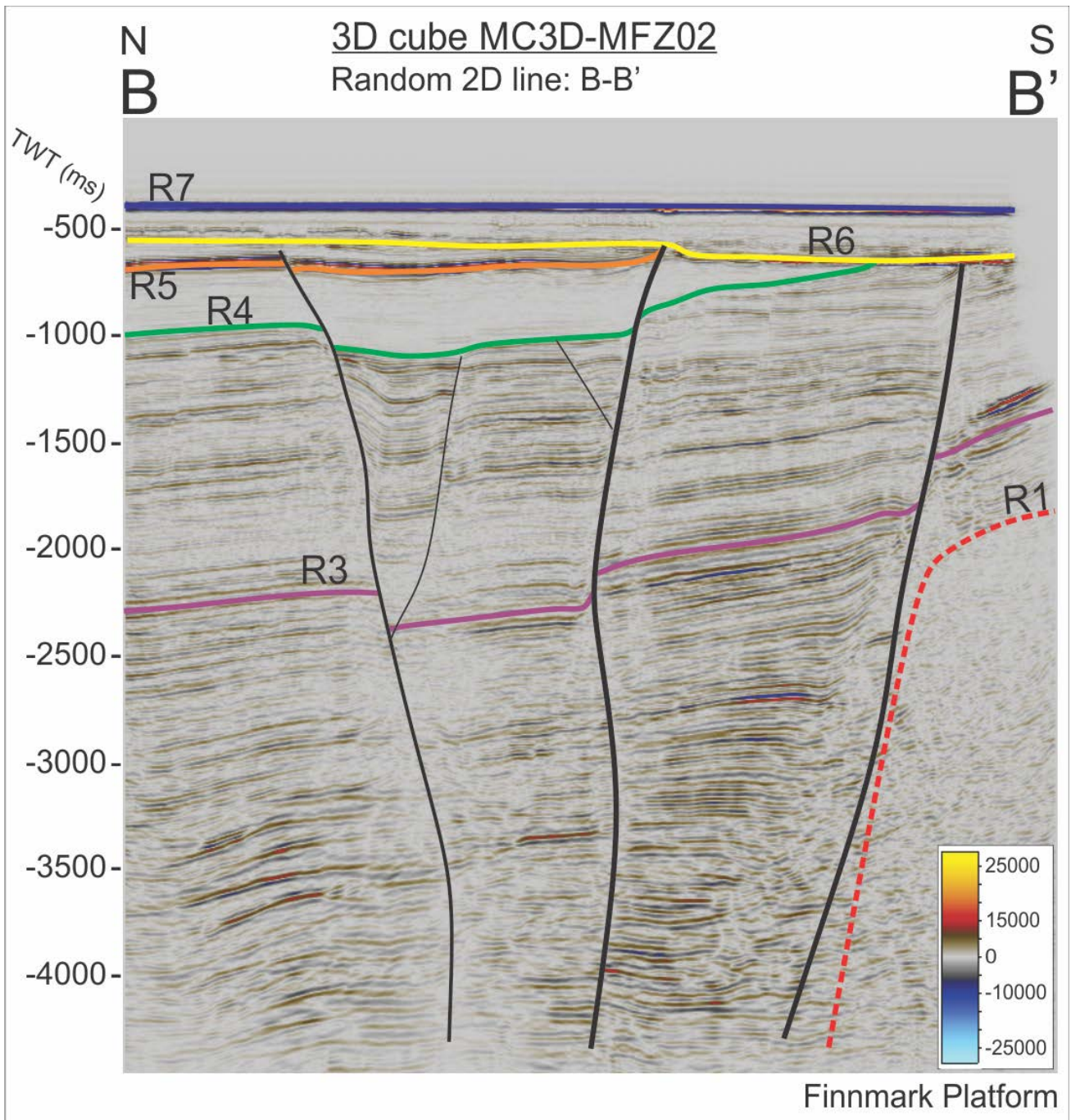
Figure 5.15 Random 2D line from seismic 3D cube, illustrating the interaction of the NW-SE leg of TFFC terminating on MFC. Reflectors marked by colored lines: R7 blue, R6 yellow, R5 orange, R4 green, R3 purple,, R1 red. Faults: primary faults thick black lines, uncertain faults dashed lines, secondary and minor faults thin black line.
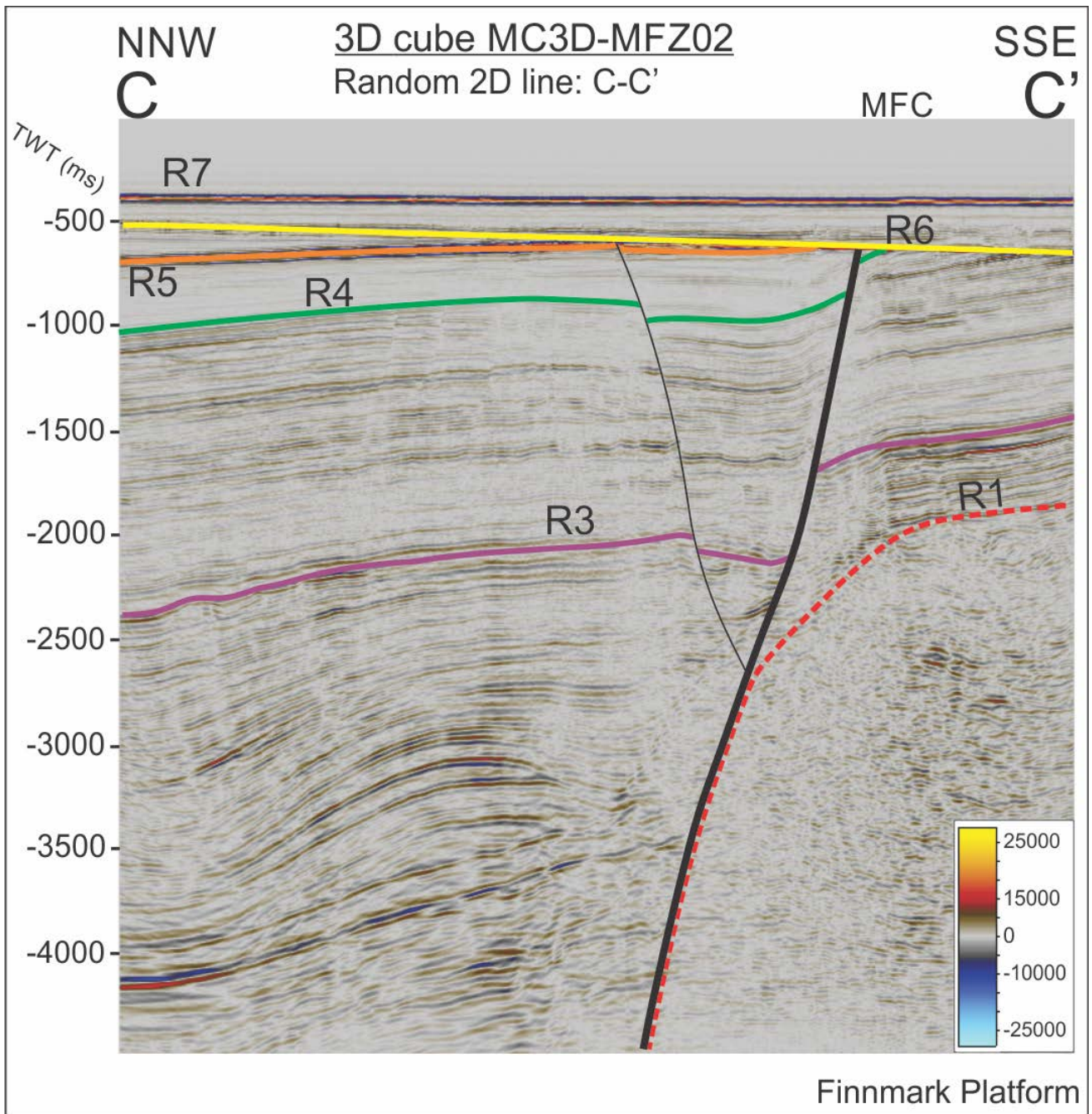
Figure 5.16 Random 2D line from seismic 3D cube, illustrating the MFC. Reflectors marked by colored lines: R7 blue, R6 yellow, R5 orange, R4 green, R3 purple,, R1 red. Faults: primary faults thick black lines, uncertain faults dashed lines, secondary and minor faults thin black line.

5.4   Summary and Preliminary interpretation

This chapter will summarize the previous chapters and propose a fault map synthesized from interpreted seismic data (fig. 5.17).

The Finnmark Platform is seen to extend south from MFC and TFFC, where the basement, S1 & R1, subcrops to URU (fig. 5.4-5.11). The major faults, TFFC & MFC, have a general NE-SW trend. However, TFFC shows a NW-SE striking leg, terminating near MFC. This confirms previous models of the structures of the SW Barents Sea (Indrevær et al., 2013; Roberts, D. et al., 2005). However, the 3D seismic data show a more complex fault geometry and interaction. The interaction show that TFFC splays out into several smaller faults that show a horsetail to anastomosing pattern in map-view, before terminating at MFC.

The larger fault complexes, TFFC, MFC and NFC, generally appear to encompass several fault surfaces striking from ENE-WSW to NNE-SSE, where the NW-SE striking leg of TFFC displays WNW-ESE to NNW-SSE striking faults, as well as minor secondary antithetic and synthetic faults, terminating in larger faults. Late tertiary uplift (Ronnevik et al., 1982) of the Finnmark platform have exaggerated the visible onlap and drag-structures in relation to the TFFC and MFC (fig. 5.4-5.11). Both TFFC and MFC show visible fault offset of top basement to Early Carboniferous sediment sequences and reflectors, indicating that these where active up to Carboniferous, as well as smaller offset in Paleogene indicated by the 3D seismics (fig. 5.14-5.16).

The NE-SW trending leg of TFFC near the North Hammerfest Basin shows segmented faulting and a graben structure towards the Hammerfest Basin (fig. 5.2 & 5.5). Near the Gjesvær Low TFFC appear to form a horst structure, where the Hammerfest Basin and Gjesvær Low as graben structures. The majority of the faults in TFFC dip north, where antithetic faults form the graben structure seen north of the Gjesvær Low (fig. 5.5 & 5.6). TFFC comprises listric faults, with steep dip in the upper sequences, offsetting S2-S4, transitioning to dip more shallowly towards a detachment plane. Towards NFC, TFFC changes trend to NW-SW (fig. 5.7). In these areas, TFFC appears to have several antithetic and synthetic faults offsetting Carboniferous to Late-Jurassic sequences, S2 to S4.

At the interaction of TFFC and MFC, smaller graben-structure is observed (fig. 5.12 & 5.13). This graben-structure shows a displacement of R3-R5, and at the interaction of MFC and TFFC displays a dome like shape. This dome comprises several minor faults, to a larger north-dipping fault that make up the graben structure. The graben structures seen in the intersection of TFFC and MFC can be interpreted as an accommodation

graben, as seen by the doming and minor fault activity at the intersection of TFFC and MFC (fig. 5.13 & 5.14). As well as a lack of E-W striking faults on both the Finnmark Plattform and Gjesvær Low.

Salt diapirism in the southern Nordkapp Basin is the results of the activation of Late Carboniferous halite sediments (fig. 5.10 & 5.11). The narrow salt diapirs seen in 2D seismic line S-253730 can be seen in relation to fault activity offsetting the reflectors R2 to R4 (fig. 5.10). The wider salt diapir in 2D seismic section S-260730 displays a fault-induced origin, but the wider berth might indicate a single fault plane.

Gjesvær Low is bounded by TFFC (fault dipping south) and MFC (north dipping fault), that appear as horst-structures where the Gjesvær Low composes a graben-like structure between the two fault complexes (fig. 5.5 & 5.6). The internal structures of the Gjesvær Low shows chaotic reflectors in S2, but it is possible to make out rotated fault blocks (fig. 5.4-5.6). The overlying sequences, S3-S7, show no influence of these fault structures, and the internal reflectors of these sequences encompasses sub-horizontal north-dipping reflectors. Mostly unaffected by faulting beside TFFC and MFC related faults (fig. 5.5 & 5.6). Towards the northeast of Gjesvær Low these rotated fault blocs seem to disappear and sequences, S1-S5, appear to be affected by both TFFC and MFC.

The 2D seismic lines NPD-FIOE2-86 S-253730-86 and S-260730-86 (fig. 5.10 & 5.11) shows steep vertical faults possibly trending NW-SE, on the southern Finnmark Platform, just north of Magerøy. These fault bound a possible basin-structure, where chaotic reflections possibly represents Carboniferous (R2) and Near Base Triassic (R3) reflectors. The internal minor faults show steep dip, and the fault architecture show antithetic and synthetic smaller faults.
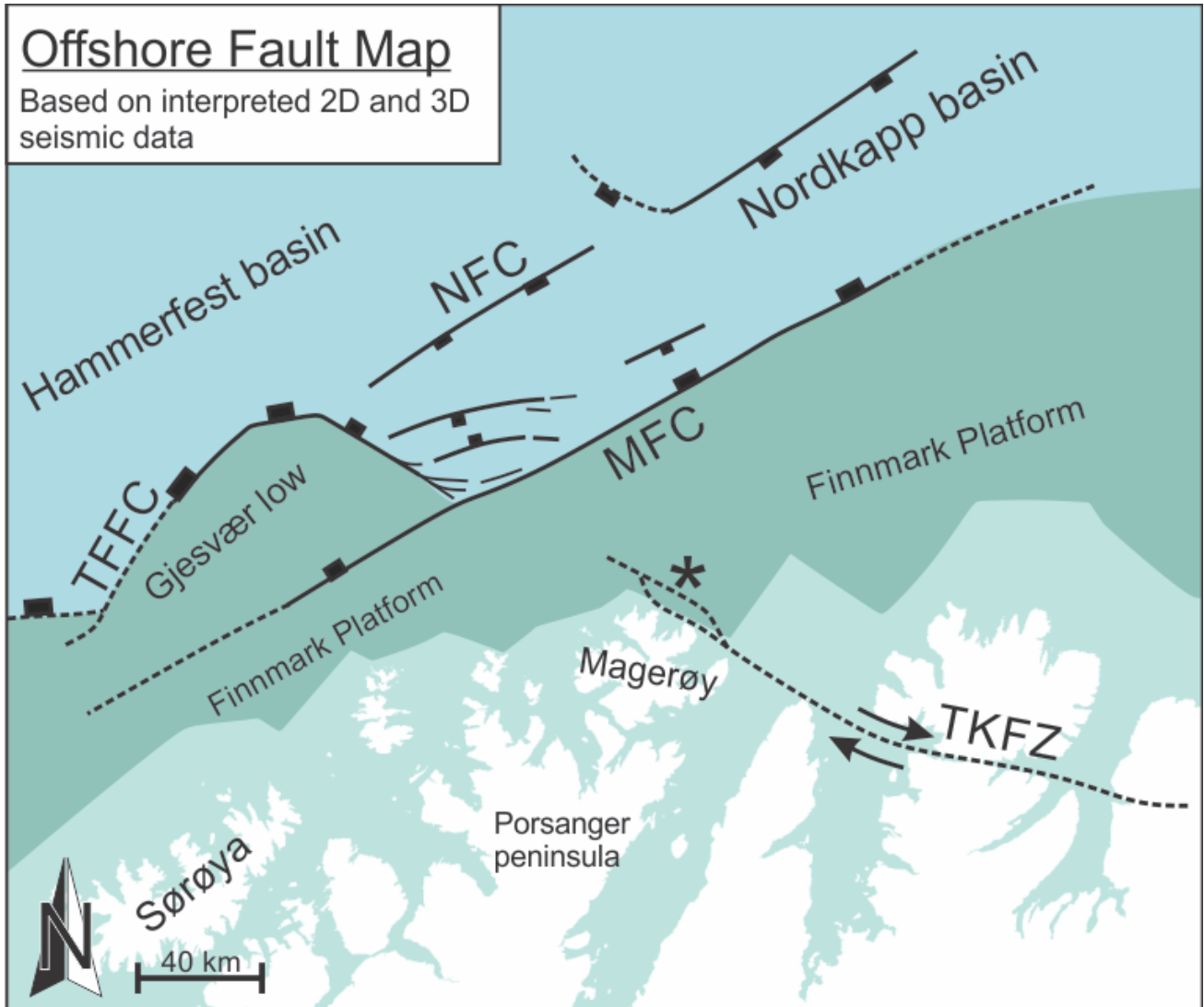
Fig. 5.17 Offshore fault map compiled from interpreted 2D and 3D seismic data. Faults interpreted from seismic data (solid black lines), faults compiled from Roberts (2005) shown as dashed black lines. * indicates the pull-apart-structure interpreted from fig. 5.10 & 5.11

6   Description of magnetic anomaly data

NGU's (2014, www.ngu.no) updated magnetic anomaly maps of northern Finnmark and surrounding offshore areas are valued contributions to understanding the overall fault-fracture architecture of the SW Barents Sea margin. This map (fig. 6.1) outlines linear anomaly patterns that correspond with NW-SE striking fault-fracture lineament patterns and trends that characterize the onshore areas (see chapter 2). The magnetic anomaly data covering the study area (fig. 6.1) show that lineaments described/presented in chapter 2.2 and 2.3. continue offshore. The magnetometric data shows NE-SW and NW-SE trending linear positive anomalies on Magerøy and east to Nordkinn Peninsula. The NE-SW trending lineaments are due to magnetic minerals in sedimentary units found in the area (Roberts, D. et al., 2012). The NW-SE trending anomalies follows the similar pattern as TKFZ (Beckinsale et al., 1976; Herrevold et al., 2009), and are seen to cut through Sværholdt Peninsula and Magerøy before terminating in a large positive anomaly west of Magerøy. These NW-SE trending anomalies follow the path of several Carboniferous dolerite dykes on Magerøy (Lippard et al., 1997).

Figure 6.1, Magnetic filtrated anomaly map and sketch interpretation. **a)** *Magnetic anomaly map of northwest Finnmark, note the red positive linear anomalies northwest on the map.* **b)** *Sketch interpretation of Magnetic anomaly map on Bathymetric and Topographic map. (NW-SE trending positive anomalies as solid* red *lines). c) Area where NW-SE and NE-SW trending anomalies crosscut in a rhombic pattern. Modified from NGU.*

7 Discussion

7.1 Introduction

The main goal of this thesis is to map, describe and analyze onshore fractures, faults and lineaments found in the study area in West-Finnmark, and to compare these with faults and major basin-boundary faults offshore on the nearby Finnmark Platform and the southwestern parts of the Nordkapp basin (chap. 1.2) (Gernigon, L. et al., 2014; Koyi et al., 1993; Roberts, D. et al., 2005). This was done through structural fieldwork and interpretation of DEM, aerial images, bathymetric, seismic and magnetic anomaly data. The results are presented in the chapters 3-6 and their implications will be discussed in the following chapter.

7.2 Discussion of the validity of digital data and methods

Results obtained from DEM, bathymetric data, aerial photos, seismic data and magnetic anomaly data will never give a truly accurate description of the geologic features, mainly because of the inaccuracy of the method used to gather and process the data. The common denominator for these data types is that they are remote sensing data, meaning that they are gathered from afar by electronic instruments. Therefore, in this chapter, the digital methods used to gather, interpret and analyze structural features will be briefly discussed.

DEM and bathymetry data, collected by Statens Kartverk and the MAREANO survey collected by the Norwegian Hydrographic Service respectably, is data collected by reflecting energy off surfaces, by laser and sound respectably. The data used have a resolution of 5x5m for the DEM and 25x25m for the bathymetry. This means that features smaller than this scale will not show on the models presented. In order to compare major features observed on the bathymetry with similar onshore features aerial images together with DEM have been used to increase the accuracy and the resolution. However, there are no such alternative for the bathymetric data. So only features larger than 25x25m appears on bathymetric data, and have been mapped accordingly.

Fault-fracture lineaments have been interpreted from aerial photos, DEM- and bathymetric data in order to calculate the azimuth (trend). This process used the Polyline tool in ArcGIS. If the polyline (i.e. lineament) is curved, ArcGIS construct the line from multiple small straight line segments. The program (see chapter 2.2) then calculates the trend for each small segment. However, this affects the results in a rose-plot because the sum of each segment will have a higher weight in the rose-plot than a similar straight line. However, due to

the large numbers of measurements in the database, the error is not thought to be significant to the overall distribution.

Seismic data are inherently inaccurate compared to aerial images, DEM and bathymetric data. The vertical and horizontal resolution is dependent on the frequency and resolution of the survey gathering the data. For the 2D seismic data the horizontal and vertical resolution can be as low as 50m, depending on the survey and the collection method (pers. com. Henningsen, 2016). Compared to 2D seismic, the 3D seismic data has a higher resolution, mainly due to shooting geometry and 3D spatial relations used in the processing sequences. Hence, geologic features can be difficult to differentiate, and in some cases smaller features such as faults and smaller reflections cannot be differentiated from larger ones. To accommodate for this, the outline and throw of faults were used to identify and interpret faults. In addition, the focus has been on large-scale faults and fault-related structures, so very high vertical and horizontal resolution of the seismic data is not crucial for the regional interpretation of faults, as the interaction of TFFC and MFC is covered by 3D seismic data.

Overall, there are several challenges using digital methods and data, as there are multiple sources of errors and corresponding uncertainties. However, in the scope of this thesis, the digital methods and data used are considered sufficiently accurate.

7.3 Discussion of the onshore data

The following chapter will discuss the onshore regional fault-fracture patterns, fault-fracture interaction, relative age and fault-fracture evolution.

7.3.1 Regional fault-fracture patterns

This study has shown that the dominant linear features observed from DEM and aerial images can be interpreted as brittle faults and fractures with a varied geometry throughout the study area. The key difference between glacial and fault-fracture lineaments is both the geometry and relief. Tectonic lineaments, e.g. fault-fracture and foliation appears as a sharp, jagged contrast to the surrounding landscape, displayed as gullies, fractures, ridges and cracks (fig. 2.2) . Glacial lineaments on the other hand, appear as more gentle lineaments, having more rounded erosional patterns (e.g. fjords, u-valleys, rounded linear depressions), and striae and scratches from scouring in smaller scale. At larger scale, glaciers leave behind linear sedimentary deposits such as flutes, eskers and drumlins (Nichols, 2009). Glacial lineaments and fault-fracture lineaments are not mutually exclusive, as glacial erosion often preferentially erodes pre-existing weakness zones such as bedding, foliation, faults, fractures and softer lithologies (Jansson et al., 2005; Nichols, 2009; Olvmo et al., 2002). These glacial lineaments can be mistaken as fault-fracture lineaments, but is avoided by not interpreting lineaments in areas covered by talus and/or vegetation, by employing aerial images in addition to DEM (see chap. 2). However, there is some overlap between glacial lineaments and large-scale fault-fracture lineaments (fig. 4.1), where larger depressions are oriented parallel with the glacial flow direction (e.g. in Snefjord).

The geometry of lineaments ranges from chaotic, parallel and rhombic to anastomosing patterns (e.g. fig. 3.2, 3.3, 3.9, 3.13 and 3.22). The geometry and attitudes of linear features, fjords and sounds vary a lot along the studied transect of northwest Porsanger Peninsula, and can be seen as a typical wedge to anastomosing geometry near the narrower fjord mouths (Myrfjord, Bakfjorden), while more open fjords (Snefjord) show rhombic geometries (fig. 3.1-3-3). The orientation of such landscape elements shows the results of three dominant fault-fracture trends on the Porsanger Peninsula: NE-SW, NW-SE and E-W trends, and two dominant trends on Magerøy WNW-ESE to E-W and ENE-WSW (chap. 3.5). In addition, subsidiary N-S trending lineaments appear in the extension of the more dominant trend direction (fig. 3.2 & 3.3). On Magerøy, both the N-S and E-W trending lineaments can be seen as an extension to both the NE-SW and NW-SE trends trough the study area. By contrast, on the northwestern Porsanger Peninsula the E-W trending

lineaments appear as a more dominant trend than the NW-SE trending lineaments. Both the lineament distribution displayed in rose plots and the geometric patterns seen in maps, fig. 3.2 & 3.3, show that Magerøy dominantly encompasses E-W (WNW-ESE to ENE-WSW) trending lineaments, while northwest Porsanger peninsula show dominantly NE-SW and E-W trending lineaments, supporting the rose plot distribution. At smaller scale, the lineaments show a variation in orientation (fig. 3.3), where the lineaments are in line with the shape of the landscape. Wedge and anastomosing geometries can be seen in fjords near wedge-shaped peninsulas, such as Selvika and Bakfjorden (fig. 3.8 & 3.9). Rhombic patterns can be seen on the inland areas and more open fjord mouths and larger rounded peninsulas, e.g. Snefjord, Lillefjord, Gjesvær and the inland areas on northwestern Porsanger Peninsula (fig. 3.2, 3.3, 3.13, 3.17 & 3.22).
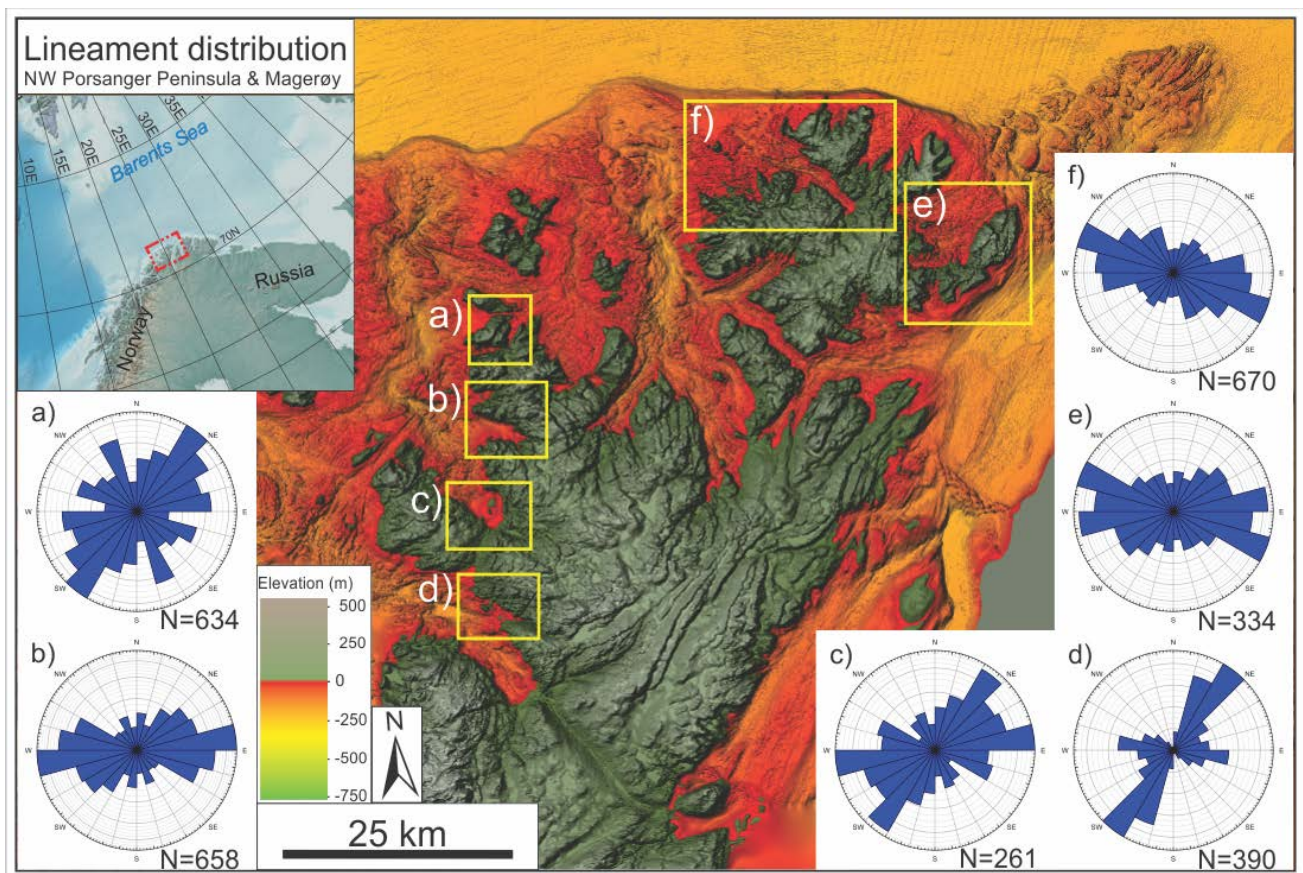
Figure 7.1 Distribution of lineament trends at areas (yellow squares) in northwest Porsanger Peninsula and Magerøy a) Area 1, Havøysund. b) Area 2, Bakfjorden. c) Area 3, Snefjord. d) Area 4, Lillefjord. e) Area 5, Honningsvåg. f) Area 6, Gjesvær

The regional lineament trends and fault-fracture strikes vary throughout the study area. For example, in a traverse from north to south in the Porsanger peninsula (Localities 1 to 6; fig. 3.3, 3.5, 3.9, 3.12, 3.13 & 3.17), the landscape and lineament patterns change character (ch. 3.4). The fault-fracture lineaments on northwest Porsanger Peninsula shows a variance in trend, where the dominant trend orientation changes from north to

south along the coast of the northwestern parts of the peninsula. Magerøy also shows a variation from this, where the dominant lineament trends are NW-SE to E-W, and trends vary over the island (fig. 3.2, 3.18, 3.21 & 7.1).In more detail, Havøysund (area 1) displays a dominance of NE-SW to ENE-WSW trending lineaments and fractures (fig. 3.4, 3.5 & 7.1). Bakfjorden (area 2) shows mainly E-W trending lineaments (fig. 3.9 & 7.1). Snefjord (area 3) shows dominantly NE-SW and E-W trending lineaments (fig. 3.13 & 7.1). Lillefjord (area 4) displays mainly NNE-SSW and E-W trending lineaments (fig. 3.17 & 7.1). Honningsvåg (area 5) shows WNW-ESE to ENE-WSW trending lineaments (fig. 3.19 & 7.1). Lastly, Gjesvær shows WNW-ESE trending lineaments (fig. 3.22 & 7.1).

Field observations and structural data show a direct correlation between meso-scale fractures observed in the field and the lineaments interpreted from DEM and aerial images (e.g. fig. 3.15, 3.23 & 3.24). From the outcrops studied, the lineaments largely follow the same strike orientations as faults observed (e.g. fig. 3.15). In addition, the rose plots and stereonets show similar trends, both regionally and locally. All these observations support an overlap between landscape patterns, regional lineaments, and meso-scale faults and fracture systems.

7.3.2   Fault and fracture geometry

Observations from fieldwork show that the northwestern Porsanger peninsula has three dominant fault-fracture strikes: 1) NE-SW, 2) NW-SE and 3) E-W. Magerøy on the other hand record predominantly E-W (WNW-ESE to ENE-WSW) striking fractures.

The faults and fractures observed in meso-scale along these dominant orientations differ throughout the study area, display unique characteristics in outcrops. Most of the fractures have a planar geometry (ex. fig. 3.7 & 3.11) but some become listric downwards, where splaying (fig. 3.10) and apparent conjugate fault sets are present (fig. 3.25, stereo plot). Conjugate faults have not been directly observed, but NE-SW and some NW-SE and E-W trending faults may interact to produce a conjugate geometry. NW-SE and E-W striking faults however, mostly show a planar geometry and steep dips to the north (fig. 3.25), while oppositely dipping faults may have formed synchronously as conjugate strike-slip dominated faults. Alternatively, the oppositely dipping faults are antithetic relative to the larger and dominant synthetic fault structures (ref. fig. 3.10 & 3.11). These antithetic faults generally show less vertical offset than the main synthetic fault surface. Furthermore, the antithetic faults generally have a listric geometry splaying into the more planar synthetic

faults. This is faulting most likely due to space-problems along the fault surface, where the antithetic faulting in the hanging wall accommodated by splay faulting and block rotation.

7.3.3 Kinematic data

Field observations and orientation data (chapter 3) show that all the dominant fault trends show both dip-slip and oblique-slip moments. However, the kinematic data on northwest Porsanger Peninsula shows that the NW-SE to N-S striking faults and fractures display a dominant normal dip-slip and normal oblique-slip shear (fig. 3.25), whereas faults in Magerøya display dominantly normal-oblique to strike-slip shear (fig. 3.26). Comparing the two data sets, it is apparent that the three main fault orientations identified do not share the same kinematic characters and sense of shear. The few (16) measurements of fault kinematic data from Magerøya indicate that all or most of the studied fault trends have a shear component, whereas northwest Porsanger Peninsula encompasses more measurements where the dominant sense of shear is normal dip-slip. This may suggest that the study area have undergone several events of faulting with different kinematic characters and senses of shear. The strike-slip character of the NW-SE trending faults in Magerøya can tentatively be linked to the TKFZ, which was formed in the Neoproterozoic as a dextral strike-slip fault and later, reactivated in Caledonian and post-Caledonian times (Herrevold et al., 2009). One possibility is that the NW-SE trending brittle faults reflect Carboniferous transtensional reactivation of the TKFZ (see discussion below). The NE-SW trending normal faults, on the other hand, may be onshore faults formed during rifting and opening of the North Atlantic Ocean due to NW-SE tensional stress. These two tectonic events might explain the variance of the kinematics and shear senses observed throughout the study area. As the stipulated trajectory of TKFZ lies north of Magerøy (fig. 1.1), it is natural to assume that this area has experienced a higher degree of strike-slip movements since it lies closer to TKFZ, and thus may be part of the damage zone. As indicated by the magnetic anomaly data (fig. 6.1), TKFZ splays out into several NW-SE to E-W striking linear anomalies that terminates east of and at Magerøy. These data suggest that Magerøya might be the "end-zone" where TKFZ terminates by splaying out onto the Finnmark Platform, the fjords and sounds, and that the high frequency of NW-SE striking faults may be linked to this wide "end zone". In addition, most NW-SE striking fault-fracture lineaments on northeast Porsanger Peninsula appear as smaller segments cut by the NE-SW, E-W and N-S striking fault-fracture lineaments (fig. 3.3). This is not seen on Magerøy, where NW-SE to E-W striking lineaments appear to be the dominant strike (fig. 3.2), where the NE-SW striking fault-fracture lineaments are cut by NW-SE to E-W striking faults.

7.3.4 Fault rocks

The study area records several faults with a core zone defined by fault gouge and cataclasitic rock (fig. 3.11, 3.14, 3.15 & 3.24). The faults recording fault rocks on the northwest Porsanger peninsula generally strike NE-SW to ENE-WSW and dip 50° to 75° NW, e.g. near Snefjord and Bakfjorden (fig. 3.14 & 3.15). These faults rocks record grey to dark red fault gouge, with crushed clasts of host rock. The red color of the fault gouges is most likely due to precipitation of iron hydroxides and oxides (fig. 3.14). In addition, one of the studied fault zones (fig. 3.15) shows zonation with an internal transition from cataclasitic fault rock to a fault gouge, indicating two stages of deformation or reactivation of the fault. Cataclasitic fault rocks are also found on steep NW-SE striking faults in Magerøya (fig. 3.24), but these faults lack the gouge overprint. Most of the faults in the studied area comprise slickensides surfaces with precipitated chlorite (see chapter 3.4).

The presence of gouge, cataclasites and secondary chlorite on fault surfaces, indicate that the faults formed by cataclastic deformation in the frictional regime at shallow to moderate depth in the crust (Twiss et al., 1994), corresponding with data, e.g. from western Troms (Indrevær et al., 2014).

7.3.5 Fault timing and interaction

In order to establish the relative timing between the various fault trends, crosscutting relationships must be considered. Such relationships are not commonly observed in the study area. However, there are a few examples of crosscutting relationships of lineaments in map scale, and fractures and faults in outcrop scale. At Skjarvodden a NW-SE striking fault clearly cross-cuts an E-W striking fault (fig. 3.11), whereas Selvika records a NE-SW striking fault cutting a NW-SE striking fault (fig. 3.10). This suggest that the NE-SW striking faults are relatively younger than the NW-SE striking faults. Similar interpretations can be inferred from DEM and aerial photographs showing that NE-SW and E-W striking lineaments offset and/or truncate W-SE striking lineaments on northwestern Porsanger Peninsula (fig. 3.1 & 3.3). By contrast, however, NW-SE to E-W striking faults also seem to offset NE-SW striking faults in several places on Magerøya (fig 3.1 & 3.2).

Antithetic and synthetic fault-fracture geometry can be seen in small scale at most localities, where Skjarvodden and Selvika has excellent examples of antithetic fractures (Fig. 3.10). WNW-ESE striking, ENE dipping faults show antithetic fractures interacting with the main fault plane, and terminating into the main fracture as well as several fractures continuing through the main faults surface (fig. 3.10 & 3.11). This indicates that these antithetic faults terminates at a larger fault surface not seen. In addition, several splaying geometries are found in most areas, where steeply dipping or antithetic faults curve and terminates

into the main fault plane (fig. 3.6, 3.10, 3.11, 3.20 & 3.24). These faults and fractures show that there is a wide range of fault-interaction, where steep faults curve and trends towards main fault surfaces. This is seen in smaller scale near faults with fault rock, where several smaller fractures to joints can be seen to terminate into the larger fault (fig. 3.15 & 3.24). However, these smaller fractures show little to no offset of the host rock, but show distinct fracturing and in some cases mineralization of calcite and chlorite (fig. 3.15 & 3.24).

The way faults terminate or merge into each other can also be used to discuss the relative timing and kinematic relationships between them. In the study area, N-S and E-W striking faults usually splay out from the NW-SE striking (TKFZ) faults. This can be explained by dextral movement along the TKFZ, and the formation of subsidiary NE-SW striking normal oblique-slip to strike-slip faults. However, this does not account for the normal oblique-slip found on some NE-SW striking faults. If this where the case, the NE-SW striking faults would display normal dip-slip, and not normal-oblique shear. However, this can also be explained by scissor faults or rotational fault block (Twiss et al., 1994), where the rotation leads an uneven distribution of shear along the fault surface from the fulcrum point of the fault. This can be affirmed by the many escarpments that displays tilting and rotation (fig. 3.4, 3.7, 3.8 & 3.11), although this tilting is barely noticeable compared to for example, tilting of fault blocks in Lofoten (Eig et al., 2011). This suggests that the measured fault and fractures themselves have been rotated in situ as part of a larger fault-block.

7.3.6   Synthesis of onshore data

Three dominant fault/fracture strikes and lineament trends are seen through the study area on the northwestern Porsanger Peninsula: 1) NE-SW, 2) NW-SE and 3) E-W. However, these are not constant as it is seen in the areas from Havøysund to Lillefjord, where there are several variations in the distributions of the dominant fault strike and lineament trend (chap. 3.4 & fig 3.3). Magerøy shows predominantly E-W (WNW-ESE to ENE-WSW) trending lineaments. However, these lineaments also varies along the island (fig. 3.2), there are several subsidiary trends as well as a variation in fault and fracture strike throughout the island. The kinematic data shows that faults on northwestern Porsanger Peninsula striking NE-SW dominantly show normal dip-slip, NW-SE dominantly show normal dip-slip and oblique-slip, while E-W show normal dip-slip (fig. 3.25), possibly a result of tensional strain from the opening of the North Atlantic Margin. On the other hand, the kinematic data of faults on Magerøy on show strike-slip to normal oblique-slip in all strike directions (fig. 3.26), and is most likely the result of dextral transtensional stress from TKFZ. The normal oblique-slip shear sense seen on NE-SW and E-W striking faults are most likely due to scissor faulting, where larger fault-block have had a uneven rotational component in addition to the normal faulting leading to a rotation of fractures and their kinematic indicators.

7.4   Discussion of the offshore data

7.4.1   Discussion of the bathymetric data

The bathymetric data show that the strandflat comprises features such as parallel ridges, troughs, channels, deep depressions and fjords (chapter 4: fig. 4.1-4.9). The parallel ridges and troughs can be interpreted as bed-rock foliation that is apparently crosscut by NE-SW, NW-SE and E-W trending channels. These features are seen in on plateaus near Hjelmsøy, Gjesvær and Snefjord. These are submerged plateaus of the same type of bedrock as found onshore (fig. 4.3, 4.5 & 4.9). The crosscutting channels have been interpreted as fault-fracture lineaments, as they mark features that are easily eroded (weak zones) and crosscut the foliation. These fault-fracture lineaments follow the same trends/distribution as the fault-fracture lineaments onshore (fig. 4.2, 4.4, 4.6 & 4.8). Regionally, the bathymetric data show glacial features where the glacial flow direction and erosion is thought to influence the fjords, sounds and the strandflat as an erosional agent, predominantly eroding weakness-zones, e.g. faults and fracture zones. Comparing the onshore and offshore lineament trends, distribution and maps (fig. 4.1-4.9), it is apparent that the onshore fault-fracture lineaments continue offshore. This is especially seen on the strandflat where fault-fracture lineaments are easy to distinguish from foliation related lineaments (chap. 4.7). In addition, in fjords and sounds it is possible to trace multiple fault-fracture lineaments that link to these depressions, because the bathymetric images show sediments, and not jagged and exposed rock. This indicates that the fjords, sounds and depressions are zones of high fracturing, allowing a higher glacial erosion than the surrounding areas (fig. 4.1). The depressions are generally bound by NE-SW, NW-SE and E-W trending escarpments, forming rhombic to parallel geometries (fig. 4.1, 4.3, 4.5 & 4.7). In addition, these depressions are elongated, following the glacial flow direction, where the base is generally characterized by rounded topography. This allows for a tentative interpretation, that some of these depressions are minor pull-apart basins, while the elongated depressions are a results of glacial erosion in high density fracture zones (fig. 4.1, 4.3, 4.5 & 4.7).

7.4.2   Seismic data

The 2D seismic sections interpreted in this work show that the regional offshore fault complexes, i.e. the TFFC, MFC and NFC, as well as smaller faults, follow a major NE-SW trend (fig. 5.17). This major Nordkapp Basin trend changes to a more NW-SE oriented leg around the Gjesvær Low on the Finnmark Platform, where the main fault splays out in smaller faults before interacting with the MFC (fig. 5.17). The TKFZ is not directly observed on the seismic data, but is thought to be present and having affected the basin architectures (fig. 5.4-5.11). Previous research (Herrevold et al., 2009; Johnson et al., 1978; Townsend, 1987) has proposed that the NW-SE trending TKFZ appears as segments extending into the southwest and western Barents Sea, appearing as NW-SE trending segments. The NW-SE leg of the TFFC e.g. near the Gjesvær Low, has previously been interpreted as one of these segments (Herrevold et al., 2009; Johnson et al., 1978; Townsend, 1987). However, the seismic data show no signs of strike-slip fault offset of the Finnmark Platform, MFC or TFFC (fig. 5.4-5.11). In addition, the NW-SE leg of TFFC shows a listric geometry, not the steep to near-vertical faults one would expect from a major strike-slip fault (Hsiao et al., 2004; Okay, Aral I. et al., 1999). The seismic data from the Finnmark Platform indicate the presence of a possible NW-SE oriented basin-like structure north of Magerøy, near Nordkapp and Helneset (fig. 5.10 & 5.11), bounded by steep faults. The internal reflectors show possible Carboniferous and Triassic reflectors, indicating that this basin was formed prior to the Middle Triassic. The internal configuration of minor faults indicates a possible negative flower-structure (Okay, Aral I. et al., 1999; Okay, A. I. et al., 2000) (fig. 5.10 & 5.11). However, this structure does not appear on other seismic sections further west or east, indicating that this a feature constrained to the local area. In addition, the 2D seismic lines further to the east show no sign of dextral offset. This may be explained by a possibly overprint by the MFC and TFFC at a later age, or that the TKFZ terminates before reaching MFC. This supports previous findings (Gabrielsen et al., 1989). However, since this structure only appears on two 2D seismic lines, the extent and shape of this basin cannot be determined without new seismic data of this area.

The analyzed 3D seismic data outline the geometries of the main faults north of Magerøya, more specifically the interaction of the NW-SE trend of TKFZ and MFC. The 3D seismic data show that TFFC have a listric fault geometry, as indicated by 2D seismic data (fig. 5.4, 5.6 & 5.7), random lines through the 3D seismic data also suggest the same (fig. 5.14-5.16). In addition, neither MFC nor the Finnmark platform shows any dextral offset. This suggests that MFC and TFFC overprints TKFZ, if it is present. The 3D data also indicate the presence of an accommodation-graben at the interaction of the NW-SE leg of TFFC and MFC (fig. 5.12 & 5.13). This graben seems to be a localized graben that dies out just north of the MFC and northeast of

Gjesvær low, since neither the TFFC nor the MFC displays any signs of E-W striking faults in the continuation of this graben-structure. In addition, the 3D seismic data displays quite clearly the fault-fracture geometry of minor faults (fig. 5.12 & 5.13). These surfaces record minor faults with anastomosing, parallel, conjugate to rhombic geometries, indicating that the fault geometry changes with relation to the major faults.

7.5   Magnetic data

The magnetic anomaly survey displays several linear positive anomalies trough the study area. However, the positive NW-SE trending linear anomalies seen on and near Magerøy, Sværholdt Peninsula and Nordkinn Peninsula are especially interesting (fig. 6.1). These linear anomalies have the same trend as the proposed path of TKFZ (Beckinsale et al., 1976; Herrevold et al., 2009; Johnson et al., 1978; Roberts, D. et al., 2005). In addition, the carboniferous dolerite dykes seen on Magerøy (the Magerøy dykes) follow this trend. The magnetic data shows that these are possibly related to TKFZ.

The previous mentioned fault rocks (chap. 7.3.4), recording red to dark brown fault gouge, does not appear as linear anomalies on the magnetic anomaly data, indicating that this fault does not have magnetic mineralization and are different from the NW-SE striking faults seen on the on Magerøy.

Besides the NW-SE trending anomalies northeast in the study area the magnetic anomaly data does not record any other major linear anomalies. Neither the NE-SW nor the NW-SE trending anomaly, suggest that the brittle faults and fractures in the study area comprise enough magnetic minerals to appear as magnetic anomalies.

7.6 Onshore-offshore fault comparative synthesis

This study have describe onshore lineaments, faults and fractures in western Finnmark and compared them with offshore faults and major basin-boundary faults offshore on the nearby Finnmark Platform and the southwestern parts of the Nordkapp basin. These data, based on structural fieldwork, DEM, bathymetric, seismic and magnetic data show that the interpreted lineaments (brittle faults and fractures) continue and can be directly correlated from the onshore to the offshore areas. The onshore-offshore correlation is well illustrated by major NE-SW, E-W and NW-SE trending escarpments and fault-fracture lineaments traced from onshore to the shallow strandflat offshore, where they continue and terminates or intersects with similar lineaments. In addition, the onshore areas of Helneset and a few areas on Magerøy display linear magnetic anomalies that correlate directly with the field-results. The NW-SE trending linear anomalies are perfectly parallel with NW-SE trending carboniferous dykes and the TKFZ (Lippard et al., 1997). The study area is located where the TKFZ is suggested to die/splay out along the strike (Herrevold et al., 2009; Johnson et al., 1978; Roberts, D. et al., 2005). This is supported by the magnetic data, as there is not a single linear anomaly where the TKFZ is stipulated to be. Instead, there are multiple linear anomalies cutting the Sværholdt peninsula and Magerøya (fig. 6.1). This strongly suggest that TKFZ does not appear as a single strike-slip fault in the study-area, similar to the Varanger peninsula (Johnson et al., 1978), but rather appears as several fault segments. The only signs of strike-slip faulting on the Finnmark Platform is the NW-SE oriented pull-apart feature inferred from the seismic interpretation just north of Magerøya (fig. 5.10 & 5.11). This indicates the presence of strike-slip faults and possible negative flower structures on the nearby Finnmark Platform. The onshore data also show a higher frequency of NW-SE to E-W striking faults with normal oblique-slip to strike-slip with dextral and sinistral sense of shear faults on Magerøy than on the northwestern Porsanger Peninsula (fig. 3.10 & 3.11).

The NE-SW and E-W trending lineaments, faults and fractures can be compared with the NE-SW to E-W trending MFC in the Nordkapp Basin and the TFFC that marks the boundary between the Finnmark platform and the Hammerfest Basin (see Chapter 1.3.4). In this study, there has not been observed any major NE-SW striking fault zones, but rather a collection of multiple, parallel, oblique and orthogonal faults striking E-W to NE-SW and locally, N-S, allowing a comparison with similar features onshore. Features, such as smaller rhombic shaped pull-apart basins and rhombic geometry of fault-fracture lineaments, both offshore and onshore indicate that the dominant fault/fracture geometries are similar to the larger basin-bounding faults found on in the southwestern Barents Sea. Indicating that these are possible coeval (fig. 3.2, 3.3 &7.1)

The seismic data indicate larger fault structures offshore display different throw along the fault surfaces (fig. 5.12 & 5.13). This apparent scissor faulting can explain why some of the E-W and NE-SW striking faults onshore northwestern Porsanger Peninsula display oblique-slip character. In addition, the seismic data indicate that several larger fault-bounded structures exist both in the basement and Carboniferous units on the Finnmark Platform and these may be interpreted as rotated fault blocks.

Most of the fjords in the study area may have been localized parallel to high-density fracture zones, or the core zones of major faults, as indicated by the large amount of fault-fracture lineaments terminating towards the fjords, and the large amount of fracturing seen on the bathymetric data (fig. 4.3, 4.5 & 4.9). The landscape itself, also indicates that there are several hidden larger faults in western Finnmark, which have affected the landscape, similar to tectonically induced landscapes in Lofoten and western Troms (Eig et al., 2011; Indrevær et al., 2014; Thorsnes et al., 2009), as seen by e.g. gently tilted paleosurfaces and steep escarpments (fig. 4.9).

8   Conclusion

This thesis concludes that there is a link between the offshore and onshore fault/fracture systems based on the following:

The onshore data shows three dominant fault strike and lineaments trends throughout the study area. The lineaments on Porsanger Peninsula show NE-SW and E-W trends, while Magerøy has NW-SE to E-W trending lineaments. The dominant fracture strikes on Porsanger Peninsula are 1) NE-SW, 2) NW-SE and 3) E-W. Magerøy on the other hand records predominantly E-W (WNW-ESE to ENE-WSW) striking fractures. On the Porsanger Peninsula the NE-SW and E-W striking fractures record normal dip-slip to oblique-slip, while all strike orientations on Magerøy record strike-slip to normal oblique-slip. Overall, the dominant fracture and lineaments orientation show a direct relationship, where there are similar variations in strike and trend distribution on the northwestern Porsanger Peninsula and Magerøy.

The bathymetric data indicate that the strandflat in the area record foliation and fault-fracture lineaments that display similar trends(NE-SW, NW-SE and E-W) as the onshore fault-fracture lineaments as well as linkage with onshore lineaments. The bathymetric data also reveal smaller rhombic shaped pull-apart basins with the same orientation. The fjords and sounds are localized in high-density fracture zones. These basins, fjords, and sounds are bounded by escarpments trending in the dominant fault and fracture orientations.

The seismic data shows that TFFC and MFC have listric geometries, where the NW-SE leg of TFFC possibly overprints older segments of TKFZ. TKFZ does not offset TFFC and MFC, but north of Magerøy a possible negative flower-structure indicate that TKFZ have affected the Finnmark Platform, but not the NE-SW trending fault complexes.

Magnetic anomaly data illustrates that the NE-SW trending carboniferous dykes on Magerøy are parallel to the assumed orientation of TKFZ, showing that TKFZ appears as several segments cutting Magerøy, Sværholdt Peninsula and Nordkinn Peninsula. The data also shows a small positive anomaly north of Magerøy parallel to the negative flower structure, supporting that this is a NW-SE trending feature, most likely a segment of TKFZ.

9 References

Andersen, T. B. (1981). The structure of the Magerøy Nappe, Finnmark, North Norway. *Norges Geologiske Undersøkelse, 363*, 1-23.

Andreassen, K. (2009). Marine Geophysics: Lecture notes for GEO-3123. *University of Tromsø*, 106.

Andreassen, K., Laberg, J. S., & Vorren, T. O. (2008). Seafloor geomorphology of the SW Barents Sea and its glaci-dynamic implications. *Geomorphology, 97*(1), 157-177.

Beckinsale, R., Reading, H., & Rex, D. (1976). Potassium-argon ages for basic dykes from East Finnmark: stratigraphical and structural implications. *Scottish Journal of Geology, 12*(1), 51-65.

Bergh, S. G., Eig, K., Kløvjan, O. S., Henningsen, T., Olesen, O., & Hansen, J.-A. (2007). The Lofoten-Vesterålen continental margin: a multiphase Mesozoic-Palaeogene rifted shelf as shown by offshore-onshore brittle fault-fracture analysis. *Norwegian Journal of Geology/Norsk Geologisk Forening, 87*, 29-58.

Bryhni, I., Ramberg, I. B., Nøttvedt, A., Solli, A., Nordgulen, Ø., forening, N. g., & Undersøkelse, N. G. (2006). *Landet blir til: Norges geologi*: Norsk geologisk forening

Eig, K., & Bergh, S. G. (2011). Late Cretaceous–Cenozoic fracturing in Lofoten, North Norway: Tectonic significance, fracture mechanisms and controlling factors. *Tectonophysics, 499*(1), 190-205.

Faleide, J. I., Tsikalas, F., Breivik, A. J., Mjelde, R., Ritzmann, O., Engen, O., . . . Eldholm, O. (2008). Structure and evolution of the continental margin off Norway and the Barents Sea. *Episodes, 31*(1), 82-91.

Forthun, T. (2014). *Onshore-offshore correlation in the Andfjorden area and the structural controls on the opening and evolution of the Mesozoic sedimentary basins on Andøya and Andfjorden, northern Norway.* Unpublished master thesis, University of Tromsø. 114

Gabrielsen, R. H., & Braathen, A. (2014). Models of fracture lineaments—Joint swarms, fracture corridors and faults in crystalline rocks, and their genetic relations. *Tectonophysics, 628*, 26-44.

Gabrielsen, R. H., Braathen, A., Dehls, J., & Roberts, D. (2002). Tectonic lineaments of Norway. *Norsk Geologisk Tidsskrift, 82*(3), 153-174.

Gabrielsen, R. H., & Færseth, R. B. (1989). The inner shelf of North Cape, Norway and its implications for the Barents Shelf-Finnmark Caledonide boundary. A comment. *Norsk Geologisk Tidsskrift, 69*, 57-62.

Gabrielsen, R. H., Faerseth, R. B., & Jensen, L. N. (1990). *Structural Elements of the Norwegian Continental Shelf. Pt. 1. The Barents Sea Region* (Vol. 6). Norm Petrol. Direct. Bull.: Norwegian Petroleum Directorate

References

Gayer, R., Rice, A., Roberts, D., Townsend, C., & Welbon, A. (1987). Restoration of the Caledonian Baltoscandian margin from balanced cross-sections: the problem of excess continental crust. *Transactions of the Royal Society of Edinburgh: Earth Sciences, 78*(03), 197-217.

Gernigon, L., & Brönner, M. (2012). Late Palaeozoic architecture and evolution of the southwestern Barents Sea: insights from a new generation of aeromagnetic data. *Journal of the Geological Society, 169*(4), 449-459.

Gernigon, L., Brönner, M., Roberts, D., Olesen, O., Nasuti, A., & Yamasaki, T. (2014). Crustal and basin evolution of the southwestern Barents Sea: From Caledonian orogeny to continental breakup. *Tectonics, 33*(4), 347-373.

Gradstein, F. M., Ogg, G., & Schmitz, M. (2012). *The Geologic Time Scale 2012 2-Volume Set*: elsevier

Hans, W. s. A. (1924). [The Strandflat and Isostasy. Videnskapsselskapets Skrifter. 1. Matnaturv. Klasse 1921. No 11., Fridtjof Nansen]. *Geografiska Annaler, 6*, 199-207.

Haraldsvik, K. (2015). *Analyse av mesozoiske forkastninger og asymmetriske landskap i et profil over Lofotryggen ved Leknes, Vestvågøy.*, Unpublished master thesis, University of Tromsø.   108

Henningsen, T. (2016). Unpublished Seismic interpretations, seismic surveys BSS01, NPD-FIØ-86 and BARE02. In S. interpretation (Ed.), *Correldraw*. Harstad: Statoil ASA.

Herrevold, T., Gabrielsen, R. H., & Roberts, D. (2009). Structural geology of the southeastern part of the Trollfjorden-Komagelva Fault Zone, Varanger Peninsula, Finnmark, North Norway. *Norwegian Journal of Geology/Norsk Geologisk Forening, 89*(4).

Holtedahl, H. (1998). The Norwegian strandflat-a geomorphological puzzle. *Norsk Geologisk Tidsskrift, 78*(1), 47-66.

Hsiao, L.-Y., Graham, S. A., & Tilander, N. (2004). Seismic reflection imaging of a major strike-slip fault zone in a rift system: Paleogene structure and evolution of the Tan-Lu fault system, Liaodong Bay, Bohai, offshore China. *AAPG Bulletin, 88*(1), 71-97.

Indrevær, K., & Bergh, S. G. (2014). Linking onshore-offshore basement rock architecture and brittle faults on the submerged strandflat along the SW Barents Sea margin, using high-resolution (5 x 5 m) bathymetry data. *Norwegian Journal of Geology, 94*, 1-34.

Indrevær, K., Bergh, S. G., Koehl, J.-B., Hansen, J.-A., Schermer, E. R., & Ingebrigtsen, A. (2013). Post-Caledonian brittle fault zones on the hyperextended SW Barents Sea margin: New insights into onshore and offshore margin architecture. *Norwegian Journal of Geology, 93*(3-4).

Jakobsson, M., Mayer, L., Coakley, B., Dowdeswell, J. A., Forbes, S., Fridman, B., . . . Rebesco, M. (2012). The international bathymetric chart of the Arctic Ocean (IBCAO) version 3.0. *Geophysical Research Letters, 39*(12).

References

Jansson, K. N., & Glasser, N. F. (2005). Using Landsat 7 ETM+ imagery and Digital Terrain Models for mapping glacial lineaments on former ice sheet beds. *International Journal of Remote Sensing, 26*(18), 3931-3941.

Johansen, S. E., Henningsen, T., Rundhovde, E., Sæther, B. M., Fichler, C., & Rueslåtten, H. G. (1994). Continuation of the Caledonides north of Norway: seismic reflectors within the basement beneath the southern Barents Sea. *Marine and Petroleum Geology, 11*(2), 190-201.

Johnson, H., Levell, B., & Siedlecki, S. (1978). Late Precambrian sedimentary rocks in East Finnmark, north Norway and their relationship to the Trollf jord-Komagelv fault. *Journal of the Geological Society, 135*(5), 517-533.

Kirkland, C. L., Daly, J. S., & Whitehouse, M. J. (2008). Basement–cover relationships of the Kalak Nappe Complex, Arctic Norwegian Caledonides and constraints on Neoproterozoic terrane assembly in the North Atlantic region. *Precambrian Research, 160*(3-4), 245-276.

Koyi, H., Talbot, C. J., & Tørudbakken, B. O. (1993). Salt diapirs of the southwest Nordkapp Basin: analogue modelling. *Tectonophysics, 228*(3-4), 167-187.

Larssen, G., Elvebakk, G., Henriksen, L. B., Kristensen, S., Nilsson, I., Samuelsberg, T., . . Worsley, D. (2002). Upper Palaeozoic lithostratigraphy of the Southern Norwegian Barents Sea. *Norwegian Petroleum Directorate Bulletin, 9*, 76.

Lippard, S. J., & Prestvik, T. (1997). Carboniferous dolerite dykes on Magerøy: new age determination and tectonic significance. *Norsk Geologisk Tidsskrift, 77*(3), 159-163.

Lundekvam. (2015). *Land sokkel korrelasjon av sprø mesozoiske og paleozoiske forkastninger i et profil over Vestfjordbassenget, Vestvågøya og ribbebassenget.*, Unpublished master thesis, University of Tromsø. 92

Nansen, F. (1922). *The strandflat and isostasy* (Vol. 2): Skrifter, Vitenskapsselskapet i Kristiania, Matematisk-Naturvitenskapelig Klasse.313

Neuendorf, K. K. (2005). *Glossary of geology*. Springer Science & Business Media

Nichols, G. (2009). *Sedimentology and stratigraphy* (Fourth Edition ed.). Upper Saddle River, New Jersey, Pearson Prentice Hall, : John Wiley & Sons

O'leary, D., Friedman, J., & Pohn, H. (1976). Lineament, linear, lineation: some proposed new standards for old terms. *Geological Society of America Bulletin, 87*(10), 1463-1469.

Okay, A. I., Demirbağ, E., Kurt, H., Okay, N., & Kuşçu, İ. (1999). An active, deep marine strike-slip basin along the North Anatolian fault in Turkey. *Tectonics, 18*(1), 129-147.

107

References

Okay, A. I., Kaşlılar-Özcan, A., İmren, C., Boztepe-Güney, A., Demirbağ, E., & Kuşçu, İ. (2000). Active faults and evolving strike-slip basins in the Marmara Sea, northwest Turkey: a multichannel seismic reflection study. *Tectonophysics, 321*(2), 189-218.

Olesen, O., Ebbing, J., Lundin, E., Mauring, E., Skilbrei, J., Torsvik, T., . . . Sand, M. (2007). An improved tectonic model for the Eocene opening of the Norwegian–Greenland Sea: Use of modern magnetic data. *Marine and Petroleum Geology, 24*(1), 53-66.

Olesen, O., Kierulf, H. P., Brönner, M., Dalsegg, E., Fredin, O., & Solbakk, T. (2013). Deep weathering, neotectonics and strandflat formation in Nordland, northern Norway. *Norwegian J. Geol, 93*(3-4), 189-213.

Olvmo, M., & Johansson, M. (2002). The significance of rock structure, lithology and pre-glacial deep weathering for the shape of intermediate-scale glacial erosional landforms. *Earth Surface Processes and Landforms, 27*(3), 251-268.

Osmundsen, P. T., & Redfield, T. (2011). Crustal taper and topography at passive continental margins. *Terra Nova, 23*(6), 349-361.

Ramsay, D., Sturt, B., Jansen, Ø., Andersen, T., & Sinha-Roy, S. (1985). The tectonostratigraphy of western Porsangerhalvøya, Finnmark, north Norway. *The Caledonide Orogen: Scandinavia and related areas. Edited by DG Gee and BA Sturt. John Wiley, Chichester, UK*, 611-619.

Reusch, H. (1894). The Norwegian Coast Plain. A New Feature of the Geography of Norway. *The Journal of Geology, 2*(4), 347-349.

Reynolds, J. M. (2011). *An introduction to applied and environmental geophysics*: John Wiley & Sons

Rice, A. (1990). Possible basement rocks in the Kalak Nappe Complex on Sørøy, Finnmark, N. Norway. *Norsk Geologisk Tidsskrift, 70*, 159-172.

Robb, L. (2013). *Introduction to ore-forming processes*: John Wiley & Sons

Roberts, D. (Cartographer). (1981). Geologic map, scale 1:250 000, Nordkapp & Honningsvåg

Roberts, D., & Lippard, S. J. (2005). Inferred Mesozoic faulting in Finnmark: current status and offshore links. *Norges geologiske undersøkelse Bulletin, 443*, 55-60.

Roberts, D., Mitchell, D., & Andersen, T. (1991). A post-Caledonian dolerite dyke from Magerøy, North Norway: age and geochemistry. *Norsk Geologisk Tidsskrift, Vol. 71*, 289-294.

Roberts, D., & Siedlecka, A. (2012). Provenance and sediment routing of Neoproterozoic formations on the Varanger, Nordkinn, Rybachi and Sredni peninsulas, North Norway and Northwest Russia: a review. *Norges geologiske undersokelse Bulleti, 452*, 1-19.

References

Roberts, R., Corfu, F., Torsvik, T., Hetherington, C., & Ashwal, L. (2010). Age of alkaline rocks in the Seiland Igneous Province, Northern Norway. *Journal of the Geological Society, 167*(1), 71-81.

Ronnevik, H., Beskow, B., & Jacobsen, H. P. (1982). Structural and stratigraphic evolution of the Barents Sea.

Samuelsberg, T. J., Elvebakk, G., & Stemmerik, L. (2003). Late Palaeozoic evolution of the Finnmark Platform, southern Norwegian Barents Sea. *Norwegian Journal of Geology/Norsk Geologisk Forening, 83*(4).

Skogseid, J., Planke, S., Faleide, J. I., Pedersen, T., Eldholm, O., & Neverdal, F. (2000). NE Atlantic continental rifting and volcanic margin formation. *Geological Society, London, Special Publications, 167*(1), 295-326.

Smelror, M., Petrov, O., Larssen, G. B., & Werner, S. (2009). *Geological history of the Barents Sea* (M. Smelror, O. Petrov, G. B. Larssen, & S. Werner Eds.). Trondheim, Norway: Geological Survey of Norway.1-135

Sturt, B., Pringle, I., & Ramsay, D. (1978). The Finnmarkian phase of the Caledonian orogeny. *Journal of the Geological Society, 135*(6), 597-610.

Sturt, B., Pringle, I., & Roberts, D. (1975). Caledonian nappe sequence of Finnmark, northern Norway, and the timing of orogenic deformation and metamorphism. *Geological Society of America Bulletin, 86*(5), 710-718.

Sundvoll, B., & Roberts, D. (2003). A likely Early Ordovician age for the regional, penetrative cleavage in the Gaissa Nappe Complex, northern Norway. *Norges Geologiske Undersøkelse, 441*, 51-60.

Thorsnes, T., Erikstad, L., Dolan, M. F., & Bellec, V. K. (2009). Submarine landscapes along the Lofoten–Vesterålen–Senja margin, northern Norway. *Norwegian Journal of Geology, 89*(1), 5-16.

Townsend, C. (1987). The inner shelf of North Cape, Norway and its implications for the Barents Shelf-Finnmark Caledonide boundary. *Nor. Geol. Tidsskr, 67*(2), 151-153.

Twiss, R. J., & Moores, E. M. (1994). *Structural Geology by RJ . WH Freeman & Co., , .* San Francisco: W. H. Freeman and Company.532

Veeken, P. P. (2006). *Seismic stratigraphy, basin analysis and reservoir characterisation* (Vol. 37): Elsevier.509

Vollmer, F. W. (2015). *Orient 3: a new integrated software program for orientation data analysis, kinematic analysis, spherical projections, and Schmidt plots.* Paper presented at the Geological Society of America Abstracts with Programs.

Vorren, T. O., Strass, I. F., & Lind-Hansen, O. W. (1978). Late Quaternary sediments and stratigraphy on the continental shelf off Troms and west Finnmark, northern Norway. *Quaternary Research, 10*(3), 340-365.

References

Wellman, H., & Wilson, A. (1965). Salt weathering, a neglected geological erosive agent in coastal and arid environments. *Nature, 205* (1965)*, pp. 1097–1098.

Winsborrow, M. C., Andreassen, K., Corner, G. D., & Laberg, J. S. (2010). Deglaciation of a marine-based ice sheet: Late Weichselian palaeo-ice dynamics and retreat in the southern Barents Sea reconstructed from onshore and offshore glacial geomorphology. *Quaternary Science Reviews, 29*(3), 424-442.

Appendix A: Python coding

Python programming code for calculating the azimuth of interpreted lineament lines in ArcGIS, using the Field Calculator in ArcMAP 10.5, the values calculated are ΔX, ΔY, Sector and Azimuth. The scrips are written in Python programming language, implementing the formula 1, presented in chapter 2.2, # indicates a comment to the code.

Code 1, Scrip for calculating ΔX (delta value of east coordinates, x1, x2)

```python
def  deltax(x1,x2):
  if (x2>x1):
    return x2-x1
  else:
    return x1-x2
```

Code 2, Scrip for calculating ΔY (delta value of north coordinates, y1, y2)

```python
def  deltay(y1,y2):
  if (y2>y1):
    return y2-y1
  else:
    return y1-y2
```

Code 3, Script to calculate Sector

```python
def sector(deltax,deltay):
#sector = where in the circle the angle is, 0-90=1, 90-180=2,180-270=3,270-360=4
#degrees 0-90
  if (deltax > 0 and deltay > 0):
     return 1
#degrees 90-180
  elif (deltax > 0 and deltay < 0):
    return 2
#degrees 180-270
  elif (deltax < 0 and deltay < 0):
    return 3
#degrees 270-360
  elif (deltax < 0 and deltay > 0):
    return 4
```

Code 4, Scrip for calculating Azimuth of lines

```python
def azimuth(deltax,deltay,sector):
#sector( 0-90 degree =1, 90-180degree =2, 180-270 degree =3, 270-360degree =4)
  #if deltax = 0 the funtion wont work, but the azimuth=0 (north-south)
  if (deltax == 0):
    return 0
  #if deltay = 0 the fuction wont work, but the azimuth=180 (east-west)
  elif(deltay == 0):
    return 180
  else:
  #degree 0-90
    if (sector == 1):
      return (math.degrees(math.atan(math.fabs(deltax)/math.fabs(deltay))))
    #degree 90-180
    elif (sector == 2):
      return (180-math.degrees(math.atan(math.fabs(deltax)/math.fabs(deltay))))
    #degree 180-270
    elif (sector == 3):
      return (180+math.degrees(math.atan(math.fabs(deltax)/math.fabs(deltay))))
    #degree 270-360
    elif (sector == 4):
      return (360-math.degrees(math.atan(math.fabs(deltax)/math.fabs(deltay))))
```

Appendix B: Field Measurements

Measurements collected during fieldwork, Fracture & Fault data presented by Strike and Dip. Kinematic fault data are presented by Strike, Dip, Plunge, Type (u-up or d-down), Trend and Fault kinematics

Table 6, field data consisting of strike and dip, organized by locality.

Loc_1A

Strike	Dip
95	62
140	80
95	62
140	80
355	87
160	90
80	70
30	86
320	74
60	50
356	68
290	70
92	60
100	80
196	68
310	80
90	86
40	62
286	78
34	90
20	74
234	71
290	78
272	62
18	64
18	70
86	84
130	60
150	82
135	58
120	64
100	68

Loc_1B

Strike	Dip
140	80
94	62
120	35
30	40
340	70
63	85
246	57
70	84
60	80
58	89
270	80
268	75
9	47
120	35
30	40
340	70
63	85
246	57
246	57
324	70
347	77
20	40

Loc_1C

Strike	Dip
190	80
270	80
270	45
10	88
190	88
178	88
160	78
190	80
146	86
150	82
334	84
190	80
188	89
194	80
330	70
200	88
100	70
145	80
110	70
174	76
340	78
90	80
335	80
135	78

Loc_2A

Strike	Dip
296	80
45	51
48	50
39	53
46	59
300	54
312	69
304	69
298	76
320	80
358	78
310	86
315	80
320	88

Loc_2B

Strike	Dip
60	80
325	80
280	70
321	77
285	63
67	70
320	80
240	55
162	66
160	82
210	90
150	75
54	83
340	80
309	39
320	68
320	83
290	36
240	76
320	84
280	70
321	77
340	70
150	78
317	85
320	80
320	70
330	52
240	60
318	75
140	80
240	50
238	78
270	70
130	88
68	62
320	76
160	82
92	85
270	40
220	80
160	80
330	45
225	

Loc_2C

Strike	Dip
26	80
90	60
275	60
332	70
200	60
90	50
90	70
260	70
270	80
30	80
300	50
300	40
230	80
280	60
280	88
80	80
310	80
340	85
280	78
310	20
298	50
100	55
280	60
160	60
100	70
290	52
264	52
252	50
258	50
248	50
114	85
258	85
110	57
274	40
110	62
95	49
332	49
92	58
110	43
206	70
250	64
254	64
307	52
317	50
309	
258	
248	

Loc_2D

Strike	Dip
310	80
80	60
160	70
94	60
245	55
310	62
245	55
150	70
80	55
70	80
205	65
310	40

Loc_3A

Strike	Dip
254	75
331	62
66	72
245	78
260	60
329	66
220	60
240	51
233	65
320	65
320	73
12	90
346	78
66	50
360	70
240	60
311	88
260	60
220	60
227	64
200	60
210	60
310	54
30	50
276	60
261	80
48	56
30	72
320	78
316	70
32	60
320	65
40	70
80	84
310	

Loc_3B

Strike	Dip
95	84
68	50
164	50
54	45
90	60
60	50
60	80
68	54
60	90
66	70
300	55
320	70
348	80
320	75
290	80
314	86
300	70
223	56
228	80
300	74
312	70
74	64
70	86
300	80
314	80
310	56
228	70
310	

Loc_3C

Strike	Dip
356	80
120	88
4	80
354	74
358	80
2	70
268	70
251	84
276	52
238	80
250	70
2	86
220	48
219	58

Appendix B: Field Measurements

Loc_6B

Strike	Dip
70	68
105	70
80	68
65	54
312	80
50	75
134	68
325	88
290	82
134	68
110	58
326	88
110	68
100	60
95	70
320	80
82	70
280	85
72	60
60	70
68	74
70	80
76	68

Loc_6A

Strike	Dip
105	75
103	72
102	72
110	68
320	95
318	54
315	40
155	68
122	60
145	60
110	80
296	80
300	70
300	80
30	10
110	80

Loc_5C

Strike	Dip
115	80
105	85
110	70
70	70
110	80
114	72
100	68
70	78
230	60
220	72
80	78
79	74
85	70
30	80
70	80
115	85
105	70
110	70
70	80
114	72
100	68
70	78
230	60
220	72

Loc_5B

Strike	Dip
25	80
315	54
285	65
280	61
310	70

Loc_5A

Strike	Dip
35	70
60	82
240	88
230	70
260	75
244	73
255	68
303	58

Loc_4B

Strike	Dip
16	80
30	75
20	80
200	40
234	60
286	75
110	80

Loc_4A

Strike	Dip
50	80
258	80
290	65
110	90
304	76
295	80
358	64
352	65
55	65
360	70
260	50
12	80
14	78
258	66
22	90
19	88
3	70
352	50
20	60
40	65
325	72
30	50
352	50
310	70
30	76
148	85
180	90
20	50

9.1.1 Kinematic fault data from Magerøy and Porsanger Peninsula:

Table 7, Kinematic data

loc_1A

Strike	Dip	Plunge	Type	Trend	Fault kinematics
30	40	-25	d	175	Fa-N-sin
58	89	64	d	149	Fa-N-dex
60	80	42	d	214	Fa-N-dex
63	85	56	d	52	Fa-N-dex
70	84	50	d	153	Fa-N-dex
120	35	-10	d	184	Fa-N-sin
246	57	24	d	109	Fa-N-sin
268	75	-63	d	56	Fa-N-dex
270	80	-45	d	279	Fa-N-dex
340	70	-20	d	189	Fa-N-dex

loc_1B

Strike	Dip	Plunge	Type	Trend	Fault kinematics
18	64	64	d	108	Fa-N
18	70	-69	d	127	Fa-un-slip
86	84	82	d	134	Fa-N-sin
95	62	-60	d	208	Fa-N-dex
100	68	-68	d	190	Fa-N-dex
120	64	-62	d	233	Fa-N-dex
130	60	60	d	220	Fa-N
135	58	50	d	183	Fa-N-sin
140	80	76	d	185	Fa-N-sin
150	82	60	d	164	Fa-N-sin
272	62	62	d	2	Fa-N

loc_1C

Strike	Dip	Plunge	Type	Trend	Fault kinematics
10	88	-20	d	189	Fa-N-dex
80	80	70	d	109	Fa-N-sin
90	80	-78	d	214	Fa-N-dex
135	78	-70	d	279	Fa-N-dex
160	78	62	d	184	Fa-N-sin
174	88	30	d	175	Fa-N-sin
300	60	-58	d	52	Fa-N-dex
335	80	-31	d	149	Fa-N-dex
340	78	-30	d	153	Fa-N-dex

loc_2A

Strike	Dip	Plunge	Type	Trend	Fault kinematics
296	80	-37	d	108	Fa-N-dex
45	51	-47	d	165	Fa-N-dex
48	50	50	d	138	Fa-N
39	53	-48	d	162	Fa-N-dex
46	59	54	d	102	Fa-N-sin
312	69	68	d	24	Fa-N-sin
304	69	-68	d	52	Fa-N-dex
298	76	70	d	341	Fa-N-sin

Appendix B: Field Measurements

loc_2B

Strike	Dip	Plunge	Type	Trend	Fault kinematics
160	82	46	d	168	Fa-N-sin
270	65	64	d	343	Fa-N-sin
220	40	38	d	289	Fa-N-sin
330	80	75	d	11	Fa-N-sin
225	45	-45	d	315	Fa-N-dex
160	80	40	d	169	Fa-N-sin
330	52	52	d	60	Fa-N
332	80	64	d	353	Fa-N-sin
294	46	44	d	3	Fa-N-sin
309	33	23	d	350	Fa-N-sin
330	68	38	d	348	Fa-N-sin
150	78	-31	d	323	Fa-N-dex
320	84	23	d	323	Fa-N-sin
130	88	80	d	141	Fa-N-sin
240	65	-62	d	359	Fa-N-dex

loc_2C

Strike	Dip	Plunge	Type	Trend	Fault kinematics
110	85	-48	d	284	Fa-N-dex
274	45	45	d	4	Fa-N
95	57	56	d	169	Fa-N-sin
332	40	32	d	20	Fa-N-sin
92	62	62	d	182	Fa-N
110	49	45	d	170	Fa-N-sin
206	49	46	d	270	Fa-N-sin
250	58	52	d	303	Fa-N-sin
254	43	36	d	305	Fa-N-sin
307	70	65	d	358	Fa-N-sin
317	64	64	d	47	Fa-N
309	64	62	d	16	Fa-N-sin
258	52	2	d	260	Fa-N-sin
248	50	20	d	266	Fa-N-sin

loc_2D

Strike	Dip	Plunge	Type	Trend	Fault kinematics
NO_DATA					

loc_3A

Strike	Dip	Plunge	Type	Trend	Fault kinematics
254	75	72	d	310	Fa-N-sin
331	62	58	d	29	Fa-N-sin
329	66	24	d	340	Fa-N-sin
240	51	-31	d	31	Fa-N-dex
316	78	65	d	343	Fa-N-sin
30	54	54	d	120	Fa-N
276	50	41	d	323	Fa-N-sin
261	60	-58	d	13	Fa-N-dex

loc_3B

Strike	Dip	Plunge	Type	Trend	Fault kinematics
60	55	-48	d	189	Fa-N-dex
30	54	54	d	120	Fa-N
22	50	50	d	112	Fa-N

loc_3C

Strike	Dip	Plunge	Type	Trend	Fault kinematics
268	70	60	d	307	Fa-N-sin
2	70	-23	d	173	Fa-N-dex
276	52	50	d	345	Fa-N-sin
250	70	-68	d	6	Fa-N-dex

loc_4A

Strike	Dip	Plunge	Type	Trend	Fault kinematics
NO_DATA					

Appendix B: Field Measurements

loc_4B

Strike	Dip	Plunge	Type	Trend	Fault kinematics
NO_DATA					

loc_5A

Strike	Dip	Plunge	Type	Trend	Fault kinematics
240	88	25	d	241	Fa-N-sin
230	70	20	d	238	Fa-N-sin
260	75	15	d	264	Fa-N-sin
244	73	22	d	251	Fa-N-sin
255	68	18	d	263	Fa-N-sin
303	58	-6	d	119	Fa-N-dex

loc_5B

Strike	Dip	Plunge	Type	Trend	Fault kinematics
280	61	-35	d	77	Fa-N-dex
285	65	-30	d	89	Fa-N-dex
315	54	54	d	45	Fa-N

loc_5C

Strike	Dip	Plunge	Type	Trend	Fault kinematics
80	78	-40	d	250	Fa-N-dex
79	78	-39	d	249	Fa-N-dex

loc_6A

Strike	Dip	Plunge	Type	Trend	Fault kinematics
300	70	70	d	30	Fa-N

loc_6B

Strike	Dip	Plunge	Type	Trend	Fault kinematics
280	85	80	d	310	Fa-N-sin
110	68	58	d	150	Fa-N-sin
65	70	70	d	155	Fa-N
70	68	65	d	130	Fa-N-sin